
Three-dimensional Microscopic Topology of the Human Placental Villous Tree Reveals Relationships with Placental Function in Health and Obstetric Disease

Eva Maria Häußner



München 2016

Three-dimensional Microscopic Topology of the Human Placental Villous Tree Reveals Relationships with Placental Function in Health and Obstetric Disease

Eva Maria Häußner

Dissertation
der Fakultät für Biologie der
Ludwig-Maximilians-Universität München
zur Erlangung des akademischen Grades
Doktor der Naturwissenschaften
(Dr. rer. nat.)

vorgelegt von
Eva Maria Häußner

München, den 11.05.2016

Erstgutachter: PD Dr. Annette Müller-Taubenberger

Zweitgutachter: Prof. Dr. Elisabeth Weiß

Dekan: Prof. Dr. Heinrich Leonhardt

Promotionsgesuch eingereicht am: 11.05.2016

Tag der mündlichen Prüfung: 06.09.2016

Eidesstattliche Erklärung

Ich versichere hiermit an Eides statt, dass die vorgelegte Dissertation von mir selbständig und ohne unerlaubte Hilfe angefertigt wurde.

Des Weiteren erkläre ich, dass die hier vorgelegte Dissertation nicht in gleicher oder in ähnlicher Form bei einer anderen Stelle zur Erlangung eines akademischen Grades eingereicht wurde.

.....
München, den

.....
Unterschrift, Eva Häußner

Ort der Durchführung

Der experimentelle Teil dieser Dissertation wurde von Mai 2011 bis Dezember 2015 im Labor unter Anleitung von Herrn Prof. Dr. Hans-Georg Frank am Lehrstuhl von Herrn Prof. Dr. Christoph Schmitz in der Anatomischen Anstalt (Lehrstuhl II / Neuroanatomie) der Ludwig-Maximilians-Universität München ausgeführt.

Dem Storch gegenüber haben die Frösche beschränkte Souveränität.

David Frost

Contents

Glossary	ix
Summary	x
1 Introduction	1
1.1 Relevance of the present study	1
1.1.1 Clinically normal pregnancies and <i>in utero</i> programming of adult disease	1
1.1.2 Incidences and consequences of obstetric disease	1
1.1.3 A perspective on the current status of placental research	3
1.2 Approaches to quantitative macroscopy of the human placenta	4
1.2.1 Essential macroscopic features of the human placenta	4
1.2.2 Standard gross morphological placental measures	4
1.2.3 A perspective: Shape analysis in biology and its application to the human placenta	6
1.3 From the macroscopic to the microscopic scale: What are the difficulties? . .	7
1.4 The unifying concept of ischemic placental disease	9
1.5 Constituents of the mature human placental villous tree	11
1.5.1 Developmental pathology of the branching pattern of the villous tree .	15
1.5.2 The challenge underlying microscopic analysis of human placental villous trees	16
1.6 The lack of animal models of the functional microscopic anatomy of the human placenta	18
2 Aim of this thesis	21
3 Abstracts of publications	22
3.1 Publication I	22
3.2 Publication II	39
3.3 Publication III	54
3.4 Publication IV	76

4 Discussion	90
4.1 A perspective: The interpretation of placental shape	90
4.2 Defining the progress achieved by the novel and advanced 3D microscopic analysis of villous trees	93
4.3 The relevance of 3D microscopic analysis of branching patterns	98
4.4 Adaptation of the villous tree to rheological issues	100
Bibliography	103
List of Figures	117
Appendix	118
Acknowledgment	120
Curriculum Vitae	121

Glossary

2D	two-dimensional
3D	three-dimensional
ADHD	attention deficit hyperactivity disorder
BW	birth weight
HT	high tortuosity; value exceeding 1.2
IUGR	intrauterine growth retardation
IVF	in-vitro fertilization
IVS	intervillous space
LT	low tortuosity; value below 1.2
PE	preeclampsia
PlGF	placental growth factor
PVS	perivascular sheath
PW	placental weight
PW/BW	feto-placental weight ratio; placental weight divided by birth weight
VEGF	vascular endothelial growth factor

Summary

The newborn and placenta become accessible at birth and are witnesses of the intrauterine phase of early human life. Although obstetric imaging methods and neonatology have significantly improved the clinical management of pregnancies in recent decades, the analysis of the placenta at birth and the functional understanding of placental structure have not kept pace with these developments. The increasing understanding of the widespread occurrence and impact of prenatal programming and the rising incidence of obstetric diseases (e.g. intrauterine growth retardation (IUGR)) are current challenges in the field of placental research.

The primarily epidemiological research in prenatal programming relies on birth records that contain macroscopic data related to placentas and newborns. These epidemiological studies indicate that the conditions of intrauterine life are reflected by the macroscopic placental morphology and correspond to the long-term postnatal health outcomes of the children. These correlations are well known for placental size (which is typically represented by the placental weight) and placental form (such as the diameter). However, the placental shape, which may be a factor independent of placental size, has not been analyzed previously because appropriate opportunities to determine the placental shape absolutely independently of the placental size were lacking. One important task of the present study was to implement and validate a geometric morphometric approach to the size-independent analysis of the placental shape (**Publication I**). This approach could be used to elucidate the possible interplay between the placental shape and the uterine habitat.

To date, no direct correlation between macroscopic data and the microscopic features of placentas from different courses of pregnancies (clinically normal and, for example, IUGR) has confirmed the expected relationship between macroscopic and microscopic structural features. Particularly with regard to the developmental aspects of the villous tree, the microscopic placental structure, the expected relationships with, e.g., placental thickness or diameter have not been confirmed. Because conventional (two-dimensional (2D), section-

based) histological methods may have limited abilities to characterize the three-dimensional (3D) microscopic structure, the present study implemented a novel microscopic approach for placental 3D structural analysis. The main feto-maternal exchange area of the placenta is a tree-like, highly branched structure with a complex 3D architecture. It is likely that variations in placental function in health and disease are reflected by specific 3D aspects of this tree-structure. The strategy used for the 3D analysis of the villous trees was adapted from that used to investigate a similar tree-like microscopic structure: the dendrite tree (**Publication II**). Furthermore, the hypothesis that current 2D histology techniques are observer dependent and have limited access to 3D structure was confirmed in a cross-validation study comparing the novel 3D technique with conventional placental section histology (**Publication III**). Analyzing villous trees from clinically normal and IUGR pregnancies revealed previously unknown differences in the 3D architectures of villous trees (**Publication IV**).

This advanced microscopic study of the 3D structure of villous trees in health and disease provides new insights that further our understanding of the mechanisms underlying prenatal programming and the development of symptoms of IUGR as a late consequence of ischemic placental disease.

1 Introduction

1.1 Relevance of the present study

1.1.1 Clinically normal pregnancies and *in utero* programming of adult disease

The course of pregnancy and fetal development have long-lasting effects on the postnatal life of children [1–4]. A British epidemiologist, David Barker, first demonstrated correlations between discrete variations in pregnancy outcome and the life-long health risk of children, which have since become widely accepted and known as "Barker Hypothesis" or the "Prenatal Programming Hypothesis" [1–4]. Many major disease burdens faced by modern societies have been shown to include prenatally acquired risk factors. The important postnatally occurring diseases that may be associated with prenatal programming are metabolic diseases (e.g. cardiovascular disease [1,5], type II diabetes mellitus [6,7], obesity [8–10], hypertension [11]), cancer [12], or neuropsychiatric disease (e.g. autism [13], schizophrenia [14], and ADHD [15]). Some of these studies focused on pregnancies which were clinically normal [5,16].

Because the effect of prenatal programming extends throughout the population of clinically normal pregnancies, clinically normal is not necessarily a synonym for optimal. Thus, the following question arises: If the more severe long-term risks associated with obstetric disease may be merely the tip of the iceberg, what is the total incidence of prenatal programming in humans [17–19]?

1.1.2 Incidences and consequences of obstetric disease

Pregnancies complicated by obstetric diseases are the major cause of iatrogenic preterm delivery and result in higher incidences of neonatal and maternal health issues [20,21]. In the 21st century, the incidence of pregnancies complicated by obstetric diseases has consistently increased in the first world, mainly because of social issues, such as the advanced age of

the mother [22], increased stress [23], and the higher incidence of obesity [24]. Currently, primiparous women are, on average, older than they were during the first half of the 20th century [25]. As the mother's age has increased, the incidences of the two most important obstetric diseases—*intrauterine growth retardation* (IUGR) and *preeclampsia* (PE)—have also increased, thus challenging the existing diagnostic and medical capabilities [17–19, 26]. These two obstetric diseases (IUGR and PE) not only have substantial co-morbidities [20, 21, 27, 28] but are also linked to a common pathogenetic hypothesis: the unifying concept of *ischemic placental disease* [29].

In general, IUGR (which is mainly characterized by fetal symptoms) is defined by a fetal growth curve that starts normally but decreases to below the 10th percentile after the 20th week of gestation and is usually determined by ultrasound observations of fetal growth marks [20, 21, 27, 28]. Detailed clinical monitoring and iatrogenic preterm delivery are often required to avoid fatal consequences [20, 21, 27, 28].

In contrast to IUGR, *preeclampsia* (which is mainly characterized by maternal symptoms) is defined by elevated arterial blood pressure, sub-arterial edema, elevated proteinuria, and very dangerous *eclampsia*, which is a type of epileptic reaction of the brain [20, 21, 27, 28]. The co-morbidity of IUGR and PE leads to simultaneous fetal and maternal symptoms, substantially complicating the clinical situation [30]. Severe syndromes of obstetric diseases, including IUGR and PE, can compromise children's postnatal development, as was known long before the first report of the "Barker Hypothesis" [31–34]. Indeed, epidemiological research in prenatal programming enabled a broader and more detailed understanding of the magnitude of the array of postnatal risks associated with human pregnancies. Syndromes such as IUGR and PE (or combinations thereof) affect up to 5-10% of all pregnancies to variable degrees [21, 35] and confirm that prenatal development is not a marginal factor of life-long human health.

Such life-long health risks associated with obvious pregnancy complications, such as IUGR and PE, include *schizophrenia* [36] and *type II diabetes mellitus* [37, 38]; furthermore, the diseases themselves (IUGR and PE) have higher incidences than the latter two diseases (*schizophrenia* has a worldwide incidence of 0.8% (according to a WHO report from 2001, [39]), and *type II diabetes mellitus* has a worldwide incidence of 6.6% (according to the Deutsches Zentrum für Diabetesforschung report of 2010, [40, 41])). These are only two other diseases that attract significant medical attention. Thus, medically, a deeper understanding of the prenatal risk factors and improvement of their classification based on findings at the time of birth, e.g., by examining the placenta, are urgently needed.

1.1.3 A perspective on the current status of placental research

Recently, the US National Institute of Child Health and Human Development (NICHD) launched the *The Human Placenta Project* with the central argument that "The human placenta is the least understood human organ" [42]. The *Human Placenta Project* is a worldwide collaborative effort aiming to improve the understanding of the role of the placenta in health and disease [42–45]. This research initiative was launched to better answer urgent questions relating to the health challenges associated with prenatal programming and the constantly increasing incidence of obstetric diseases [46, 47].

These circumstances and the comparative uniqueness of human placentation (see the chapter 1.6 below) and its complications justify the need for intensified research on the functional macroscopic and microscopic architectures of this fetal organ in humans [42–45]. Many areas of placental research include specific deficits, supporting the necessity of the NICHD's initiative. However, although morphological research on the human placenta is an important sub-discipline of placental research, this field is complicated by many challenges, including the following:

- None of the currently routinely determined macroscopic parameters of the human placenta enables inter-placental comparison of macroscopic features that are independent of gestational age and placental size (see the chapter 1.2).
- The macroscopic anatomy of the human placenta correlates with postnatal health issues, but to date, its histology has not been shown to be sufficient to identify the underlying microscopic correlates of prenatal programming (see the chapter 1.3).
- The postulated causes of obstetric disease are events occurring early in pregnancy, but clinical disease manifestation occurs weeks to months later (see the chapter 1.4). Quantitative structural correlates of disease manifestation in late pregnancy have not yet been reliably identified by microscopic developmental pathology (see the chapter 1.5).
- Animal models of human placentation are severely compromised by substantial structural and physiological species differences (see chapter 1.6).

1.2 Approaches to quantitative macroscopy of the human placenta

1.2.1 Essential macroscopic features of the human placenta

The human placenta (placental disk, *chorion fundosum*) is a circular or oval disk with a maternal side and a fetal side [20, 27]. The fetal side, which contains the chorionic plate, includes the umbilical cord insertion (central or lateral) and large fetal vessels spreading to and from the umbilical cord insertion point at the placental surface. The chorionic plate is covered with the amniotic epithelium and extends laterally into the membranes (*chorion laeve*).

The maternal side is the attachment side in the uterus, which includes the basal plate, and contains a pattern of sulci that separate larger units. These units, the cotyledons, contain at least one feto-maternal perfusion unit [20, 27].

The placenta contains two intensively interdigitating blood circulations. The feto-placental circulation is connected to the fetal vessels of the umbilical cord. The utero-placental circulation is the maternal counterpart of the feto-placental circulation and is supplied by uterine arteries and veins. The utero-placental circulation opens freely into the intervillous space, which is a cleft-like space around the placental/fetal villous tree. The fetal blood always stays inside the fetal capillary network of the villous tree. Therefore, the surface of the villous tree separates the two placental circulations.

The arborization of the villous tree spans the distance between the chorionic plate and the basal plate and is surrounded by the intervillous space [20]. The villous tree is covered with a specialized cell layer, the trophoblast, which is the epithelial feto-maternal exchange surface of the villous tree [20, 48].

1.2.2 Standard gross morphological placental measures

Epidemiological research in prenatal programming utilizes a small set of the gross morphological parameters of placentas at birth. These placental parameter sets comprise (i) scalar measurements (such as placental diameters, thickness, roundness, volume, and/or surface area; Figure 1.1) and/or (ii) non-scalar measurements (such as weight).

Gross morphological scalar parameters (e.g., diameter and surface area, summarized as the placental size) of the placenta correlate with non-scalar parameters, such as the placenta weight [27, 50–53] or birth weight [54]. These elementary relations seem to be generally

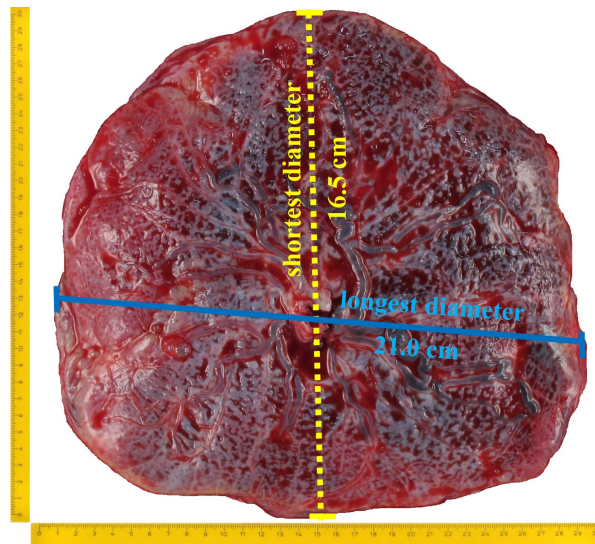


Figure 1.1 Standard gross morphological placental measures used in many epidemiological studies. The scalar measurements of human placentas mainly consist of diameters (shortest diameter: yellow; longest diameter: blue), and thicknesses (measured by ultrasound relative to the chorionic surface). The derived parameters—volume, surface area and roundness—are usually calculated using these basic measures [49]. The photograph was taken in the lab of the department of anatomy II.

applicable rules and are generally maintained, even in obstetric disease (e.g., IUGR and gestational diabetes mellitus) [55–58].

However, the scalar measures of the placenta are form parameters because they not only reflect size but also indicate the shape, e.g., the diameters depend on the placental size and the degree of approximation of the placental disk to an ideal circle. Adding to the confusion, to date, placental research has not used the term shape as a technical term, instead borrowing it from colloquial language. Some of the form parameters were thus referred to as shape parameters in the literature [59,60]. In contrast, the scientific discipline of geometric morphometry interprets "shape" and "size" as two fully independent parameters that both contribute to the property "form" [61–65].

Here, form is a geometric morphometric technical term that describes an object considered in its whole space (e.g., its volume and thickness) [61–65]. Correspondingly, shape is understood as a geometric morphometric technical term reflecting the size-independent features of a given structure (e.g., placental appearances) and are considered to be incorruptible [61–65]. The present study uses the technical language of geometric morphometry throughout.

Because of how they are defined, the placental size (e.g., the diameter or thickness) and weight can be combined into a form parameter (size/weight dependent), and the placental

shape (size/weight independent) can be considered as an independent descriptor. Placental shape could be an important biological determinant of placental function and/or a consequence of early placentation. This is supported by the observation that placental appearance (determined by form parameters) was found to be highly variable, irrespective of the placental size [59,60]. In addition, a link between "placental shape" (actually: placental form, see above) variability and obstetric diseases [59,60,66,67] has been postulated.

To date, morphometric studies of the human placenta have not utilized a method to clearly distinguish the placental form (reflecting the weight and size) and shape (independent of size). Mathematically, it is important to calculate the shape as the pure shape (a separate entity) without considering the influence of the placental weight (the form parameter). Thus, how estimates of the placental shape can be determined independent of the placental weight remains unclear.

Nevertheless, only analyzing the shape as an independent morphological factor would facilitate identifying the specific contributions and roles of weight and shape regarding the various morphometric placental parameters that can be measured at birth. Reliable interpretations of these parameters based on both fundamental measurements of placental morphology, namely, placental shape and placental weight/size, will be required. Unlike placental morphometry, shape analysis is well established in other areas of biology, e.g., paleoanthropology. Shape analysis is essentially an application of geometric morphometry and has contributed substantially to the advancement of paleoanthropological knowledge [68–71]. Extending these approaches to placental research thus represents a promising strategy and is an important objective of the present work.

1.2.3 A perspective: Shape analysis in biology and its application to the human placenta

In paleoanthropology, the evolutionary distance separating different species can be determined by analyses of the variabilities of shapes and forms [68–71].

A straightforward example of the application of geometric morphometry is the analysis of human faces [61]. Every human face has a similar oval/round appearance (form/size-included), but their shape properties vary independently of the form/size parameters and can be used to identify (sub-)populations.

Typically, shape analysis relies on landmarks (in a human face, these include the position and distance between the eyes or the position and broadness of the nose), which may characterize different populations [61–65]. After obtaining the coordinates of such land-

1.3 From the macroscopic to the microscopic scale: What are the difficulties?

marks, the first calculative step of shape analysis is the Procrustes analysis. The Procrustes analysis superimposes all landmarks in the population by translation, rotation and scaling to determine a population-wide best fit of shape. Then, the deviation of each individual shape from the best fit, determined by principal component analysis, indicates shape and form variability. The variability patterns found by shape analysis can then be used to discriminate between, e.g., two or more species, offspring, adults, different genders, and subpopulations. One strength of geometric morphometry is that the two aspects of shape and form variability can be determined independently [61–65].

In paleoanthropology, geometric morphometry can, for example, be used to discriminate among different ape species (e.g., chimpanzees (*Pan*) versus gibbons (*Hylobatidae*)) and specific steps of human evolution (e.g., *Homo neanderthalensis* versus *Homo sapiens*) [68–71]. Extending this approach to placental morphometry depends on defining appropriate landmarks of placental structure. For this purpose, the point of the insertion of the umbilical cord and the outer rim of the placental disk are promising features (Figure 1.2).

1.3 From the macroscopic to the microscopic scale: What are the difficulties?

The placenta and its microarchitecture, especially the villous tree, are sensitive fetal organs of high functional relevance that, when examined at the microscopic scale, should exhibit signs of the pathogenetic processes underlying prenatal programming and obstetric diseases during critical periods of intrauterine life. David Barker, the first researcher who pursued epidemiological studies on prenatal programming, used placental and neonatal measures to correlate life-long health with the results of the intrauterine human life [72, 73].

David Barker initiated the field using the historical birth records (with neonatal parameters such as birth weight, head circumference, abdominal circumference, and length and placental parameters of placenta weight, diameter, thickness, and the insertion of the umbilical cord) of large birth cohorts (several thousand births) and correlated these data with the postnatal health status of the same persons decades after their births [1–4]. Regarding the placental data, it was hoped that the purely macroscopic measurements in birth records could be used to reveal the microscopic placental anatomic parameters that underly various macroscopic parameters, such as placental thickness or diameter.

It was expected that novel microscopic parameters would improve the power of risk assessment regarding postnatal health issues during perinatal medical assessments. However,

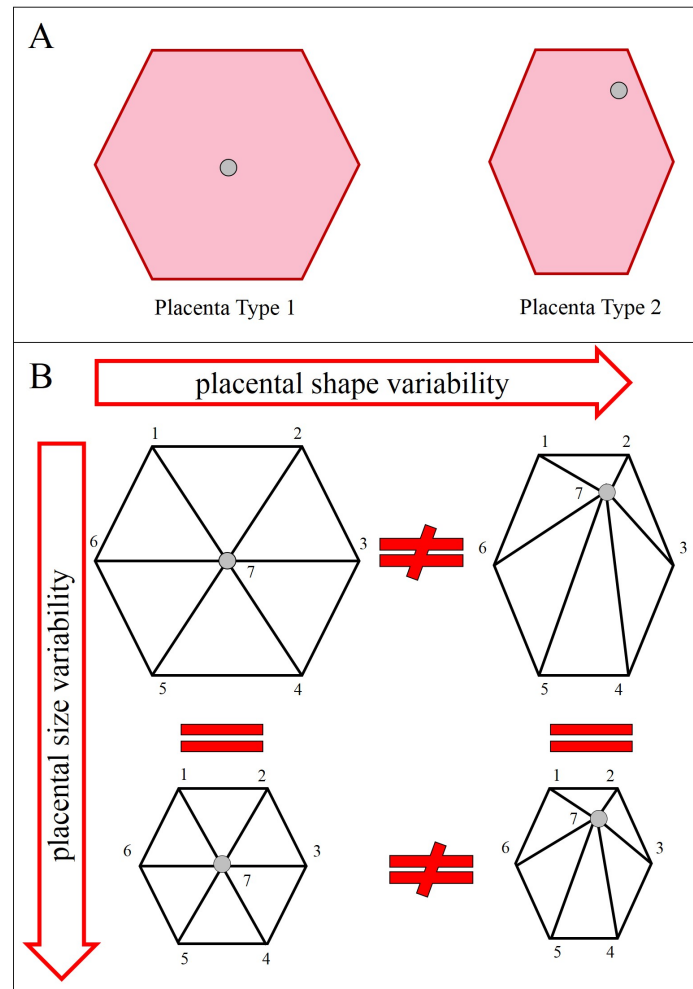


Figure 1.2 Geometric morphometric analysis in placental research. (A) shows two schematic morphological placental appearances: one round type (Placenta Type 1) and one oval type (Placenta Type 2). The umbilical cord is indicated as a gray point. (B) explains the differences in shape and form variability. For clarification, the two placental types are indicated according to landmarks on the outer rim of the placenta (1-6) and the umbilical cord (7). The landmarks are connected in a wireframe. The shape variability between the round type and the oval type (in the upper part of the box) is shown. The size variabilities of the round type (left side) and oval type (right side) are symbolized and are expressed in terms of the form variability.

from the mid-1980s until 2010, the progress in this field was disappointing.

Conventional histology of the human placenta was unable to provide additional information on prenatal programming, and even decades after David Barker's initial studies, no reliable method has been developed to correlate macroscopic parameters with quantitative histological parameters or specific histological findings with postnatal outcomes. This is

illustrated by a short conversation between experts in placental microscopic morphology and David Barker, which was reported in a book published in 2011. The following quote was taken from the book [74] describing the *The Placenta and Human Developmental Programming* conference, which was held in Cambridge (UK). The participants included the epidemiologist Dr. Barker, original author of the prenatal programming concept, and Drs. Robert Pijnenborg, Graham Burton, and Robert Boyd, all experienced placenta researchers and morphologists ¹. After an initial lecture by Dr. Barker (entitled “The maternal and placental origins of chronic disease”), the discussion (page 13) starts with the following comments on the macroscopic diameters of placentas and their microscopic morphologies:

Dr. Bagby: Is there any information on the histology of the placenta in terms of those diameters?

Dr. Pijnenborg: I would add to this: can the placental diameter be translated to the number of spiral arteries?

Dr. Barker: I have no idea.

Dr. Boyd: Do you have any idea, Robert? (to Robert Pijnenborg)

Dr. Pijnenborg: No. [...]

It is possible that current histological analysis methods are simply not sensitive enough to reveal the potentially discrete changes in the placental microarchitecture that are associated with prenatal programming [75]. Thus, the following question arises: Could these same histological methods have been sensitive enough to identify all relevant changes in pathological pregnancies complicated by obstetric disease?

1.4 The unifying concept of ischemic placental disease

The early pregnancy (1st trimester) plays a major role in ischemic placental disease (Figure 1.3). In early pregnancy, the spiral arteries in the uterine tissue are remodeled and dilated by invading fetal trophoblast cells [76–80]. This physiological process occurs in the junctional zone of the basal plate during the histiotrophic phase of early placentation (i.e., during the 1st trimester) and ensures sufficient maternal blood supply during the following hematotrophic phase of fetal nutrition after the first trimester (during the 2nd and 3rd trimesters) [76, 77, 81–83]. The unifying concept of ischemic placental disease is

¹ Among others, Dr. Boyd was, until 1995, an editor of the scientific journal *Placenta* and has deep insight into the field of placenta research. Dr. Burton is the current editor of the journal *Placenta*, and Dr. Pijnenborg is an expert on the placental bed and physiological changes in spiral arteries and has recently published a book on these topics.

widely accepted and implies that insufficient physiological remodeling of the spiral arteries (during the 1st trimester) leads to later symptomatic manifestation (in approximately the 3rd trimester) of ischemic placental diseases, such as IUGR, PE or a combination thereof (Figure 1.3) [28, 76, 77, 84–86]. Obstetric syndromes usually become symptomatic beyond the 20th week of gestation, peaking in the third trimester [21]. Thus, between the beginning of potential pathological mismatch (insufficiently remodeling of spiral arteries) and the occurrence of clinical symptoms, the time delay spans the whole second trimester.

The manifestation of clinically symptomatic ischemic placental disease is expected to be structurally mediated by the developmental pathology of the functional microarchitecture of the human placenta (Figure 1.3). The most important structure involved in fetomaternal exchange during pregnancy is the placental villous tree.

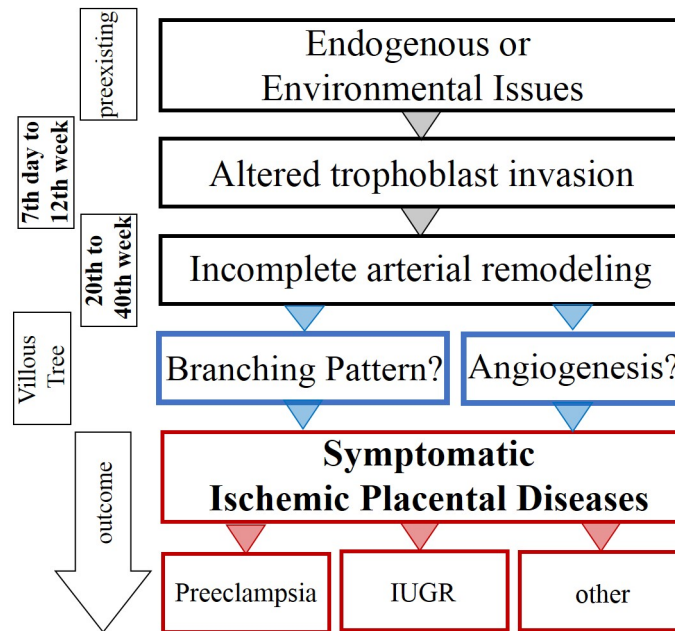


Figure 1.3 The current concept of ischemic placental disease and the pathogenesis of obstetric disease. Hypothetical endogenous (e.g., genetic, immunologic, or endocrine) or environmental (e.g., uterine cesarean section scars) issues lead to disturbances in placentation. Disturbed placentation caused by insufficient invasion of the trophoblast leads to insufficient remodeling of the maternal uterine spiral arteries and could, e.g., lead to altered rheology because of undilated spiral arteries [86]. These conditions should influence the development of the placental villous tree (unknown mechanisms). Steps in blue are still poorly supported by data (modified of [29]).

The placental villous tree is the only postnatal accessible "witness" of the conditions during gestation [29]. Because the villous tree of human placentas exists on a microscopic scale, analyzing the villous tree requires appropriate microscopic technology. Thus, for microscopic analysis of the villous tree to detect alterations of the villous tree resulting from different condition during gestation, conventional histology relies on tissue sections. These analyses are based on two main areas of placental histopathology: general histopathology and developmental histopathology.

General histopathology is a sub-discipline focused on general aspects, such as inflammation (e.g., villitis or chorioamnionitis) [87,88], tumors (e.g., moles or choriocarcinoma) [89], or coagulation disorders (e.g., infection or aberrant fibrinoid deposition) [20,90]. Developmental histopathology mainly relates to mismatches of placental maturation and gestational age [20]. Aberrant maturation patterns are distinguished by changes in angiogenesis, which also define changes in the branching pattern of the villous tree. This is a main research focus in placental pathology in obstetric diseases.

Some general pathological findings (e.g., villous infarction, villitis or fibrosis) [91] occur at higher incidences in placentas complicated by obstetric diseases. These observations indicate that the placentas are modified by pathogenetic processes, but their occurrence alone is a qualitative observation that does not support diagnostic certainty. Indeed, all of these observations can also be made in the placentas of clinically normal pregnancies.

To date, correlations between quantitative microscopic aspects of the developmental pathology of the villous tree with the occurrence and/or severity of clinical symptoms have not been sufficiently or consistently observed, despite substantial efforts. Thus, the following question must be asked: Why has microscopic analysis of the placental villous tree been unable to establish firm and quantitatively reproducible links with disease severity?

1.5 Constituents of the mature human placental villous tree

The villous tree is a complex 3D structure of the human placenta [92–101]. Analogous to a (botanical) tree, which includes a trunk, branches, and leaves, the villous tree consists of villous types known as stem villi, mature intermediate villi (intermediate villi) and terminal villi (Figure 1.4).

Each villous type is named according to its expected position on the villous tree. This nomenclature was derived by comparing scanning electron microscopy images with his-

tological sections of other (similar but not identical) villous trees. The stromal elements (e.g., fibrous tissue, extracellular material, and vessels) were used to classify the villous sections into categories named according to different villous types. Each villous type was allocated to a position in the tree and labeled accordingly. This cross-matching of stroma and the topological positions of villi was unavoidably indirect because scanning electron microscopy and section histology are incompatible methods that cannot be applied to the same sample [101]. At the time this nomenclature was established, this indirect type of linking was the only available method of connecting 2D histology with 3D position.

The classification of villous stroma in 2D determined the positions of each villous type on the tree in 3D and remains the current gold standard in placental microscopic analyses of villous trees [101]. Analyzing the stromal structure of a villous section is performed to define villi as "terminal villi" (in a terminal position), "intermediate villi" (in a preterminal position) and various classes of stem villi, which are differentiated by the caliber of the sectioned villus. Using this type of association, a skilled examiner can be expected to reliably allocate villous sections to positions on the villous tree and to imagine a type of virtual 3D tree in his mind (Figure 1.4) [20,100,101].

Stem villi are characterized by fetal vessels with the so-called perivascular sheath (PVS), a myofibroblast-rich contractile perivascular stroma outside of the vessel media. The PVS is a structure that occurs exclusively in stem villi [96,102–104]. Stem villi form the backbone of the mature villous tree at term. Based on stem villi, the most peripheral parts of the villous tree arise: the intermediate villi and the multiply branched terminal villi. The peripheral part of the villous tree is considered the most important part, especially for fetomaternal gas exchange, because of its large and functionally relevant surface [98,105]. Intermediate villi and terminal villi are characterized by a dense capillary network with few stromal components (Figure 1.5) [20,98]. However, the histological classification of the most peripheral part of the villous tree is especially challenging. The differences in stromal architecture between the smallest stem villi, intermediate villi and terminal villi are quite small and must be identified by skilled examiners.

Only few remnants of the immature villous tree of the placenta that arises before the 20th week of gestation remains at term (Figure 1.4). These villous types are immature intermediate villi, which are the precursor villi of stem villi, and very few mesenchymal villi. These two villous types are responsible for the branching of the immature villous tree. Mesenchymal villi are small sprout-like protrusions and contain loose stroma with almost no capillaries covered by a heavily proliferating trophoblast layer [106]. Immature

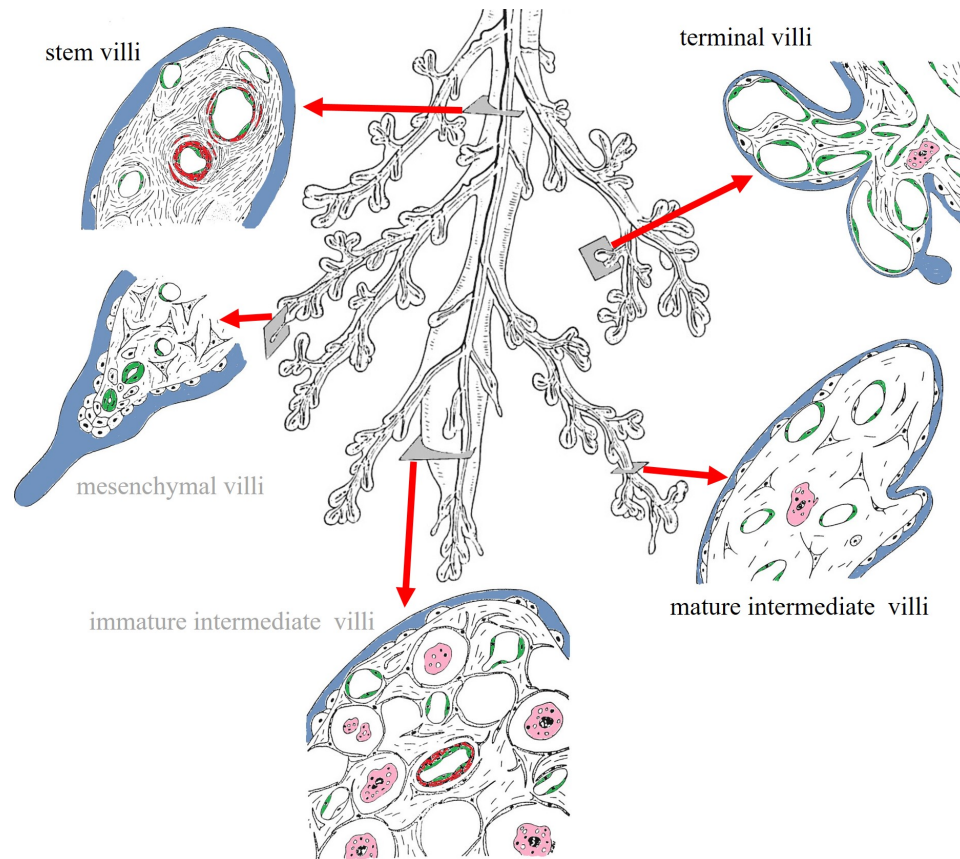


Figure 1.4 Allocation of villous sections to tree position according to stromal classification. The villous tree at term mainly consists of stem villi, (mature) intermediate villi, and terminal villi. Mesenchymal and immature intermediate villi (indicated in gray) occur rarely in term placentas. The center of the figure shows an idealized villous tree containing all villous types. Syncytiotrophoblast (blue), endothelial cells (green), Hofbauer cells in stromal channels (pink), and cells in the arterial media and the contractile perivascular sheath (red) of the stem villus are shown. The red arrows indicate the hypothetical distribution of cross-sections (gray plains) on an idealized villous tree (modified from [28]).

intermediate villi can reach enormous diameters and are characterized by large fluid-filled stromal channels containing macrophages (Hofbauer cells) [107, 108]. They also contain central vessels and a dense sub-trophoblast capillary network. In the immature placenta of the first trimester, the surface of the immature intermediate villi is the main exchange area because terminal villi do not exist yet.

The present study will focus on the most peripheral part of the mature villous trees of placentas at birth. The preexisting villous types of the immature villous tree, the immature intermediate villi and mesenchymal villi [106] that exist during the first trimester, will not

be addressed.

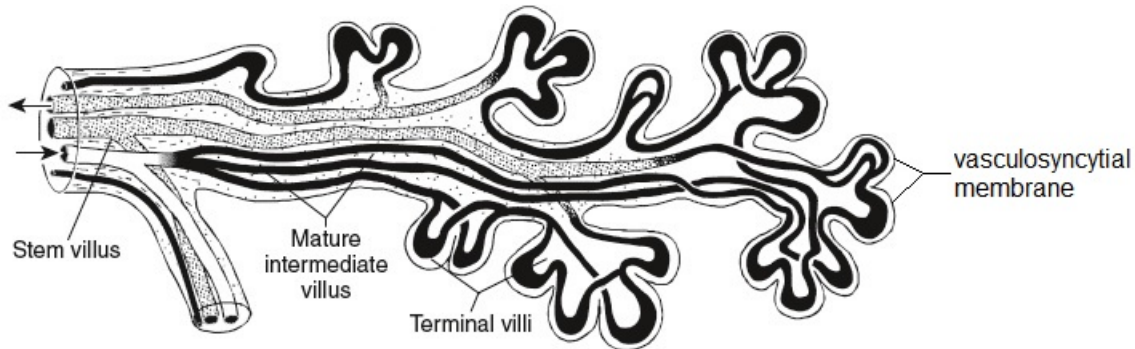


Figure 1.5 Fetal capillaries in the peripheral part of the villous tree. The fetal capillary system of the villous tree includes afferent (clear capillary) and efferent (dotted capillary) vessels. The fetal blood circulation in villous vessels begins with the two umbilical cord arteries (*Arteriae umbilicales*) and ends in the umbilical cord vein (*Vena umbilicalis*) to the fetus. In the villous tree, from stem villi (small lines) to mature intermediate villi (small dots) to terminal villi (white area), the capillaries increase in density and have thinner vessel walls. In the terminal villi, the vessel density increases because of the existence of long sinusoidal loops (black capillary) close to the trophoblast layer, especially in locations with vasculosyncytial membranes (modified from [20]).

The whole villous tree is covered by a specialized cell layer, the trophoblast, which is part of the blood-placenta barrier and enables feto-maternal exchange [20]. The trophoblast is generally two layered and consists of an inner layer (fetal, basal) known as the cytotrophoblast and an outer layer (maternal, apical) known as the syncytiotrophoblast. The syncytiotrophoblast is the only cell layer in direct contact with maternal blood. The villous tree at term consists mainly of syncytiotrophoblast because the cytotrophoblast layer becomes increasingly inconsistent during pregnancy [109]. The epithelium transforms as the pregnancy progresses into a mono-layered form dominated by the syncytiotrophoblast [20, 27]. The trophoblast can become flattened at the surfaces of terminal and intermediate villi. These areas are called vasculosyncytial membranes and are the main sites of gas exchange in term placentas (Figure 1.5) [28].

1.5.1 Developmental pathology of the branching pattern of the villous tree

Developmental pathology of the placental villous tree describes its degree of maturity and identifies both possible mismatches between maturity and gestational age and maldevelopment [93,94]. The main correlate of the maturity or maldevelopment of the villous tree is found in the villous branching pattern (Figure 1.6).

Villous branching serves as the main mechanism of surface enlargement of fetomaternal exchange and increases as the fetus grows, especially during the third trimester. The current concept of villous branching (Figure 1.6) and its consequences relate to the angiogenic processes of the capillary network (development and differentiation of a capillary network) inside the villous tree [92–94]. It is assumed that developmental pathology of the villous tree is an important outcome of early events associated with ischemic placental disease [20,29]. It is assumed that structural aberrations of villous trees are potential consequences of e.g. unremodeled spiral arteries, and are likely an essential correlate of the pathological course of pregnancies (Figure 1.3).

Substantial hyperbranching of the peripheral capillaries in human term placentas of chronically and severely anemic mothers was reported previously [110] and inspired hope that such analyses would reveal the changes in the villous tree that accompany symptomatic manifestations of ischemic placental disease.

Current microscopic assessments of the developmental pathology of the villous tree based on 2D histological analyses of villous sections are guided by the principles outlined above. In this strategy, villous types are determined from 2D sections of villous trees. The distribution of villous types (stem villi, intermediate villi, and terminal villi [for further information, see the previous chapter 1.5]) and their expected deviations from "normal" should determine the degree of developmental pathology [20].

Although these analyses are sensitive enough to demonstrate the developmental adaptation of villous trees in extremely anemic mothers [110], in more discrete pathological cases, such as IUGR and/or PE or even prenatal programming, their sensitivity is likely insufficient [75]. Certainly, it is also possible that no changes occur in the villous trees of pregnancies complicated by obstetric diseases; in this case, the clinical symptoms would arise via completely different and so far unknown mechanisms. However, it is more likely (and must be excluded) that no parameters or changes exist that could not be revealed (qualitatively or quantitatively) by the available analysis methods for placental villous trees.

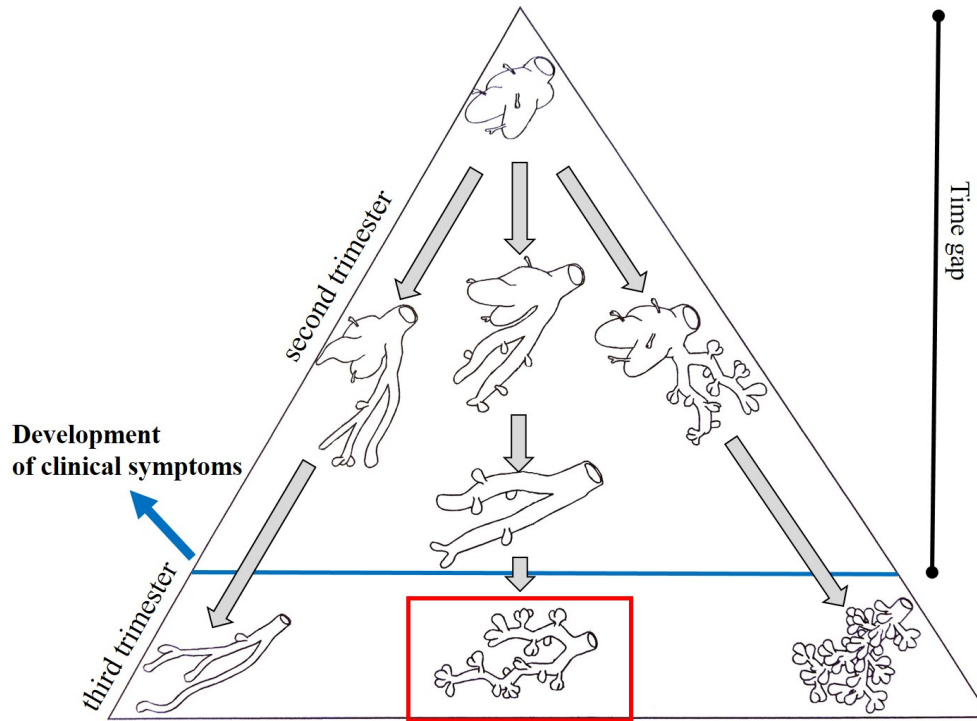


Figure 1.6 An illustration of the proposed types of maldevelopment of the villous tree. Scheme of villous maturation in the second and third trimesters, indicated using a blue line. The red box delineates the endpoint of normal placental development. Pathological hyperbranching, such as, e.g., in severe maternal anemia, is shown to the right of the red box, and pathological hypobranching, such as, e.g., in terminal villus deficiency, is shown to the left of the red box. The time gap between the potential origin and occurrence in complicated pregnancies is marked (modified from [20]).

1.5.2 The challenge underlying microscopic analysis of human placental villous trees

Analogous to other human organs, it can be expected that histological examinations of placental tissue and analysis of the villous tree will provide results that facilitate describing placental developmental pathology in more depth than clinical symptoms alone. A better understanding of the mechanisms leading to the symptoms of IUGR is a major objective of histological assessment to reduce the fraction of "idiopathic", i.e., not explainable, IUGR [20, 21, 27, 28].

Currently, the stromal classification of villous types is believed to be observer independent (though possibly dependent on a certain level of examiner skill) and reliable. Additionally,

such microscopic classifications based on 2D histology are believed to allow for a valid assessment of the 3D villous tree structure [111,112]. To date, no technique for the objective and quantitative validation of the reliability and reproducibility of 2D placental histology and the strength of its link to the 3D structure of villous trees have been established (Figure 1.7). The development of novel and supplementary approaches to the direct 3D microscopic assessment of villous trees would thus be helpful but is challenging.

In neuroscience, similar challenges were associated with the 3D analysis of the dendrite trees of neurons. Currently, the direct microscopic analysis of dendrite trees in 3D is well established and has become a standard method that has substantially contributed to recent progress in this field [113–115]. This advanced microscopic technique has been used for the quantitative morphological and functional 3D reconstruction of neuronal dendritic trees [116,117]. Computer-assisted camera lucida technique has revolutionized the understanding of neuronal density and the 3D connectivity of dendritic trees. Moreover, mathematical analyses, such as Sholl analysis [118], have been used to reveal the dynamical system of dendritic branching [119,120].

This progress would not have been possible using 2D sections of neural tissue alone. The approach to 3D microscopic dendrite analysis was established as a computer-assisted 3D camera lucida technique [116,121,122]. Placental villous trees are biologic 3D tree structures and can be regarded as analogous to dendrite trees with respect to their basic 3D tree construction (Figure 1.7). Thus, it should be possible to transfer and apply this novel 3D microscopic technology to the microscopic assessment of placental villous trees.

As its central objective, the present study defines the transfer of such computer-assisted camera lucida techniques to the 3D analysis of villous trees of the human placenta. The main issues affecting the transfer process are as follows: (i) Dendritic trees are structures with an extended cellular scale and are substantially smaller than the tree structures at the multi-tissue level (stroma, endothelium, and trophoblast) found in the placenta. (ii) Dendritic trees have different functions than villous trees and might require adapted analysis procedures.

Upon the successful transfer and application of camera lucida strategies, clinically normal and pathological pregnancies will be analyzed to identify 3D properties that may be impossible to find in 2D sections. This microscopic approach may also allow validating the conventional histological allocation of villous sections to positions in the tree. This is because modern 3D variants of the camera lucida technique generate digital 3D models of trees while allowing the same tree to be analyzed again using a conventional technique and

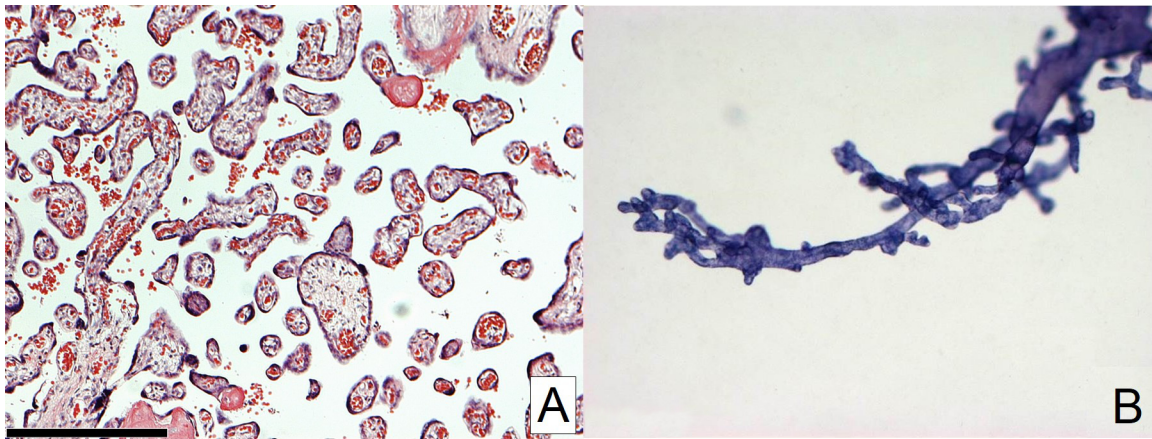


Figure 1.7 The microscopic villous tree of human placentas. (A) Histological section of a villous tree stained with hematoxylin/eosin. The stromal architecture inside the sectioned villi is visible. The cross-sections of branches belong to an unknown number of villous trees. (B) Whole-mount section of an isolated villous tree stained with hematoxylin. A single villous tree is visible. The 3D positions of nodes (branching points) and the branching topology are evident. The scale bar of (A) are equivalent for (B) and represent $250\ \mu\text{m}$ (modified from [123]).

then by histology.

1.6 The lack of animal models of the functional microscopic anatomy of the human placenta

Research in prenatal programming has principally relied on material from human placentas [74, 124] and only occasionally uses other mammal species, mainly focusing on aspects such as epigenetic mechanisms [125]. To investigate placental function and morphology, studies using animals as model organism must be performed cautiously [126, 127] because of the unusually large species divergences in implantation and placentation, even between otherwise closely related mammal species [128].

Placentation is a late consequence of implantation. Some species exhibit a superficial implantation, which results in epitheliochorial placentas (i.e., the trophoblast (chorion) and uterine epithelium stay intact and become opposed to each other), whereas other species have variable degrees of deep implantation [128]. In deep implantation, the implanting blastocyst and its outer layer, the trophoblast, destroy the uterine epithelium and invade into the underlying connective tissue to the endothelial layer or (e.g., in humans) even

through the maternal endothelium [128]:

- epitheliochorial: the placental trophoblast is standing in contact with the epithelium of the uterine glands, examples are pig (*Sus*) and horse (*Equus*).
- synepitheliochorial: the placental trophoblast is standing in contact with the maternal connective tissue, examples are ewe (*Ovis*) and cow (*Bos*).
- endotheliochorial: the placental trophoblast is standing in contact with the endothelium of maternal vessel, examples are cat (*Felis*), dog (*Canidae*), and bat (*Microchiroptera*).
- hemochorial: the placental trophoblast is standing direct in contact with maternal blood, examples are mouse (*Mus*), rabbit (*Leporidae*), man (*Homo*), apes (*Catarrhini*), and monkeys (*Platyrrhini*).

These differences lead to variations in the feto-maternal exchange depending on the type of placental barrier [128]. Thus, the diffusion distance between the mother and fetus vary between epitheliochorial, synepitheliochorial, endotheliochorial, and hemochorial placentation. As a result, many animal species that could theoretically be used to model the conditions of pregnancy have completely different placental barriers.

Furthermore, even between species having hemochorial placentas, substantial differences in structure exist. Although some primates and humans have a villous placenta with a principally two-layered trophoblast, some new world monkeys (e.g., *Callithrix jacchus*) have a non-villous, folded or tubal placenta. Rodents have a labyrinthine placenta (no villous tree at all) and a three-layered trophoblast with two syncytial layers. Overall, apes have the greatest similarity to humans in their microscopic placental structure, but the complex differentiation of different villous types, which is essential for human pregnancies, is missing [128].

The combination of all these aspects leads to one important question: Why is the incidence of IUGR and/or PE in genetically unmodified mice and rats zero [76,77,85]? However, some studies have addressed general phenomena (e.g., the epigenetic mechanisms of prenatal programming and nutritional effects) in placental research that can be studied with model organisms [129–132].

Because of the uniqueness of human placentation and its clinical complications, it is necessary to use human placentas to study these phenomena and diseases. In practice, human

placentas become available at birth, and their examination is readily possible. This is the approach used in the present study.

2 Aim of this thesis

The objectives of this thesis were as follows:

1. Validate a collection of clinically normal human placentas by comparison with macroscopic data available in the literature and demonstrate that the placental shape can be analyzed independent of the placental size (Publication I).
2. Demonstrate the feasibility of quantitative 3D microscopic and topological analysis of the villous trees of term human placentas and correlate the microscopic data obtained with the macroscopic data of human placentas (Publication II).
3. Validate the conventional 2D histological analysis of villous types against 3D microscopically determined topological branching patterns and determine the observer independence and sensitivity of 2D histological analysis (Publication III).
4. Demonstrate that quantitative 3D microscopic and topological analysis of human placental villous trees reveals previously undiscovered features of placentas from patients with IUGR (Publication IV).

3 Abstracts of publications

3.1 Publication I

Birth weight correlates with size but not shape of the normal human placenta

Abstract

Introduction: Studies on developmental programming rely on various measures of size and form of the human placenta. Size and form are not independent of each other and covariation patterns were not determined systematically.

Methods: Twenty-two morphologic parameters were determined on 418 placentas from uncomplicated singleton pregnancies. We determined (i) placenta weight and birth weight, (ii) form parameters such as diameters, thickness, roundness, and eccentricity of cord insertion, and (iii) shape variability by geometric morphometry. Geometric morphometry analyzes shape variability independent of size. We define the technical terms form and shape according to the language of geometric morphometry.

Results: Placenta weight correlated with birth weight. The form parameters correlated variably with placenta weight and shape. Shape variability did not correlate with birth weight and placenta weight.

Discussion and conclusions: The correlation of placenta weight with birth weight stays a cornerstone of prenatal programming. Shape analysis shows that form parameters are hybrids of size and shape. Shape variability can be interpreted as an outcome of adaptation of a placenta to maternal factors and the associated uterine habitat. Correlation analysis of the whole data array provides a rigorous statistical frame to interpret published data and plan new studies.

Reference

Haeussner E , Schmitz C, Edler von Koch F, Frank HG. - Birth weight correlates with size but not shape of the normal human placenta. Placenta. 2013 July 34(7):574-82

URL Link

<http://www.sciencedirect.com/science/article/pii/S0143400413002075>



Birth weight correlates with size but not shape of the normal human placenta



E. Haeussner^{a,1}, C. Schmitz^a, F. von Koch^{b,2}, H.-G. Frank^{a,*,2,3}

^a Department of Anatomy II, Ludwig-Maximilians-University, Anatomische Anstalt, Pettenkoferstrasse 11, 80336 Munich, Germany

^b Clinic for Obstetrics and Gynecology Dritter Orden, Menzinger Str. 44, 80638 Munich, Germany

ARTICLE INFO

Article history:
Accepted 17 April 2013

Keywords:
Placenta anatomy and histology
Placenta diagnosis
Placenta growth and development
Placenta shape and size
Prenatal exposure delayed effects
Geometric morphometric analysis

ABSTRACT

Introduction: Studies on developmental programming rely on various measures of size and form of the human placenta. Size and form are not independent of each other and covariation patterns were not determined systematically.

Methods: Twenty-two morphologic parameters were determined on 418 placentas from uncomplicated singleton pregnancies. We determined (i) placenta weight and birth weight, (ii) *form* parameters such as diameters, thickness, roundness, and eccentricity of cord insertion, and (iii) *shape* variability by geometric morphometry. Geometric morphometry analyzes *shape* variability independent of size. We define the technical terms *form* and *shape* according to the language of geometric morphometry.

Results: Placenta weight correlated with birth weight. The *form* parameters correlated variably with placenta weight and *shape*. *Shape* variability did not correlate with birth weight and placenta weight.

Discussion and conclusions: The correlation of placenta weight with birth weight stays a cornerstone of prenatal programming. *Shape* analysis shows that *form* parameters are hybrids of size and *shape*. *Shape* variability can be interpreted as an outcome of adaptation of a placenta to maternal factors and the associated uterine habitat. Correlation analysis of the whole data array provides a rigorous statistical frame to interpret published data and plan new studies.

© 2013 Elsevier Ltd. All rights reserved.

1. Introduction

Postnatal health risks associated with severe obstetric syndromes were known long before the Barker Hypothesis on prenatal origins of postnatal health was formulated (see e.g. Refs. [1,2]). Research on developmental programming has to explain programming phenomena in the offspring of uncomplicated pregnancies (i) without relevant clinical or histological placental pathology, and (ii) with birth weight and placenta weight within the normal range of distribution [3].

Constitutive to the concept of human developmental programming was that postnatal health outcomes correlate with gross morphologic parameters of the placenta at birth. Meanwhile, it is known that numerous gross morphologic parameters of the placenta correlate with specific postnatal outcomes (for reviews see e.g. Refs. [4,5] and in particular Table 1 in Ref. [5]). The subsets of gross morphologic parameters of the placenta at birth used in different studies vary. Systematic data on covariation patterns of the numerous placental parameters with each other are missing or

incomplete. Moreover, new gross morphologic parameters of the placenta [6,7] and new mathematic derivations of existing gross morphologic parameters of the placenta [6,8,9] have been introduced. Comparability of studies on developmental programming is complicated by this situation.

In principle, gross morphologic parameters of the placenta can be scalar measures such as determination of placenta weight or vectorial measures such as rectangular diameters and eccentricity of cord insertion. A vectorial measure is understood here as (i) being determined by or derived from conventional euclidean measurements (distances, areas, etc.) and (ii) describing an aspect of the form/symmetry of the placental disc. Certainly, correlations of vectorial measures with postnatal health outcomes were shown [4,26]. However, vectorial measures are not independent of size (weight) of the placenta.

In contrast to conventional vectorial measures like e.g. breadth, length, or thickness of a placenta, *shape* variability defined by geometric morphometry is by algorithm independent of size irrespective of the object under examination. The tools of geometric morphometry were implemented to analyze evolution of *shape* across species or during adaptation to ecological niches independent from size of the respective species/organisms (see e.g. Refs. [10,11]). In the present study, we determine placental *shape* by geometric morphometry.

* Corresponding author. Tel.: +49 89218072662.

E-mail address: hans-georg.frank@med.uni-muenchen.de (H.-G. Frank).

¹ Results are part of the doctoral thesis of EH.

² Both authors contributed equally as senior authors.

³ In memoriam, with great respect and with many thanks: Peter Kaufmann.

Table 1
Summary of descriptive data analysis stratified by gender (male, female) and delivery mode (vaginal, section). Data are mean values \pm standard deviation. For description of parameters in column titles see Sections 2.2–2.3.2 and Table 3.

Part a	n	GA [weeks]	BW [g]	PW [g]	PW/BW	BETA (β)	FPR corrected	RULER_L [cm]	RULER_S [cm]	RULFACE [cm ²]	THICK [cm]	DELAY [min]
All	418	39.56 \pm 1.16	3428.63 \pm 440.17	512.93 \pm 102.12	0.15 \pm 0.02	0.76 \pm 0.02	0.90 \pm 0.14	20.09 \pm 2.51	17.20 \pm 2.08	273.10 \pm 55.86	1.71 \pm 0.34	486.31 \pm 375.36
Male	223	39.48 \pm 1.27	3462.90 \pm 464.23	515.47 \pm 108.85	0.15 \pm 0.03	0.76 \pm 0.02	0.90 \pm 0.15	20.15 \pm 2.56	17.31 \pm 2.09	275.44 \pm 55.87	1.72 \pm 0.33	486.51 \pm 379.80
Female	195	39.66 \pm 1.02	3390.89 \pm 409.72	509.84 \pm 94.30	0.15 \pm 0.02	0.77 \pm 0.02	0.89 \pm 0.14	20.03 \pm 2.46	17.09 \pm 2.07	270.45 \pm 56.03	1.70 \pm 0.36	487.76 \pm 371.45
Vaginal	226	39.93 \pm 1.20 (***)	3477.94 \pm 452.00 (**)	496.41 \pm 90.51 (**)	0.14 \pm 0.02 (***)	0.76 \pm 0.02 (***)	0.93 \pm 0.13 (***)	19.81 \pm 2.38 (*)	17.13 \pm 1.84	268.37 \pm 53.88 (**)	1.70 \pm 0.37	551.96 \pm 394.15 (**)
Section	192	39.13 \pm 0.94 (***)	3371.58 \pm 420.48 (**)	532.29 \pm 111.70 (**)	0.16 \pm 0.03 (***)	0.77 \pm 0.02 (***)	0.86 \pm 0.15 (***)	20.43 \pm 2.63 (*)	17.29 \pm 2.34	278.71 \pm 57.90 (**)	1.72 \pm 0.32	410.34 \pm 337.29 (**)
Part b	n	AoP [cm ²]	RoP factor	CoA_UC [cm]	UC_CON_L [cm]	UC_CON_S [cm]	CON_PC1 factor	CON_PC2 factor	UC_PC1 factor	UC_PC2 factor	UC_PC1 factor	UC_PC2 factor
All	418	300.55 \pm 56.25	0.81 \pm 0.08	3.52 \pm 2.09	14.09 \pm 2.30	5.59 \pm 2.06	0.000195 \pm 0.54851	−0.000014 \pm 0.46747	−0.002655 \pm 0.372092	0.000664 \pm 0.272851	−0.001457 \pm 0.370565	0.011392 \pm 0.267845
Male	223	300.64 \pm 54.09	0.81 \pm 0.08	3.49 \pm 2.13	14.07 \pm 2.33	5.62 \pm 2.08	0.003644 \pm 0.054098	−0.002000 \pm 0.044464	−0.001457 \pm 0.370565	0.011392 \pm 0.267845	−0.001457 \pm 0.370565	0.011392 \pm 0.267845
Female	195	300.44 \pm 58.76	0.81 \pm 0.08	3.55 \pm 2.05	14.11 \pm 2.27	5.55 \pm 2.04	−0.003748 \pm 0.055576	0.002258 \pm 0.49246	−0.004024 \pm 0.374780	−0.011605 \pm 0.278649	−0.004024 \pm 0.374780	−0.011605 \pm 0.278649
Vaginal	226	294.03 \pm 52.13 (*)	0.81 \pm 0.08	3.40 \pm 2.05	13.88 \pm 2.26	5.66 \pm 2.05	0.003524 \pm 0.052853	−0.002180 \pm 0.041628	−0.002590 \pm 0.362432	−0.008105 \pm 0.286607	−0.002590 \pm 0.362432	−0.008105 \pm 0.286607
Section	192	308.22 \pm 59.97 (*)	0.80 \pm 0.08	3.66 \pm 2.14	14.33 \pm 2.33	5.50 \pm 2.07	−0.003722 \pm 0.57003	0.002537 \pm 0.052131	−0.002730 \pm 0.384104	0.010986 \pm 0.256073	−0.002730 \pm 0.384104	0.010986 \pm 0.256073

Significance levels are indicated by asterisks ($p < 0.001$ (**); $p < 0.01$ (*); $p < 0.05$ (°)). Part a. General parameters and gross morphological parameters obtained directly from the placenta. Part b. Gross morphological parameters as determined from digitized photographs of placentas.

To discriminate clearly, we use the language of geometric morphometry [10] throughout and connect the term *shape* specifically with parameters generated by geometric morphometry, while the term *form* is used with conventional vectorial parameters. We hypothesized that *shape* of the human placenta is determined by other mechanisms than size. More specifically we hypothesized that size primarily reflects the endogenous nutritional trophotropism of the feto-placental unit, while *shape* variability primarily reflects flexible morphologic adaptation of placentas to their individual intrauterine habitat.

This study is addressing the issues above. We determined 22 parameters of placentas from uncomplicated singleton pregnancies and report about correlation analysis with birth weight and covariation patterns of scalar measures, *form* parameters, and *shape* parameters.

2. Materials and methods

2.1. Study design

The study used a cohort of 418 placentas from clinically normal pregnancies that were collected between May 2011 and August 2012. Absence of clinically relevant pathology was assessed by the obstetricians based on the course of pregnancy and delivery. A key factor for inclusion was that histopathological examination of the placenta was not considered necessary by the obstetrician. Placentas were collected after Informed Consent of parents was obtained. Placentas were excluded if: no Informed Consent of mother/parents could be obtained, language skills of mother/parents were not good enough to understand the informations about the study, or psychiatric problems or any other condition caused doubts on the mother/parents ability to decide independently. Table 2 in the supplementary materials summarizes the data of this study according to actual editorial recommendations [12]. This project was approved by the ethics committee of the Ludwig-Maximilians-University (LMU) Munich, Germany, under the number 084–11.

2.2. Parameters derived from the placenta

Immediately after delivery in the hospital (Clinic for Obstetrics and Gynecology Dritter Orden, Munich, Germany), the placentas were labeled and transferred individually into tight, thin, and flexible plastic sacs and cooled in a refrigerator at 4°–8 °C in the direct vicinity of the delivery rooms. Only anonymized data on hospital patient code, child gender (GENDER), gestational age (GA), delivery mode (DELMOD), birth weight (BW), and time of birth were provided with the packages. Once daily the placentas were transferred under constant cooling to the laboratory of the Department of Anatomy at the LMU (Munich, Germany) for gross examination and histologic processing. Time of arrival at the Department of Anatomy and time of birth were used to calculate the delay of processing (DELAY). Placentas were weighed prior to sampling, fixation, and tissue processing. Placenta weight (PW) was measured as the weight of the unfixed placenta without the umbilical cord. *Chorion frondosum* (placental disc) and *Chorion laeve* (membranes) were not separated. The ratio of PW to BW (BW; PW_BW_Ratio) was calculated from PW and BW. The allometric scaling parameters (see Ref. [8]) BETA and fetal-placental ratio (FPR_corr) were calculated from PW and BW according to [8]. Placental thickness (THICK) was determined by diagnostic ultrasound (Convex Scanner HS 3000, Honda Electronics, Tokyo, Japan) after positioning in a flat tray with the chorionic side facing up. The ultrasound head was placed gently and without pressure on the chorionic surface near the umbilical cord. The longest diameter across the umbilical cord (RULER_L) and the diameter perpendicular to the longest diameter across the umbilical cord (RULER_S) were measured with a ruler. RULER_L and RULER_S were used to calculate the surface area of the placenta (RULFACE; equations see Table 3). A systematic random sampling procedure was implemented by placing the tray with the placenta under a projector (SceneLights Technologie, Mini-LED LB 936, PEARL, Buggingen, Germany). A pre-defined dot pattern was randomly projected onto the chorionic side of the placenta (see Fig. 1b). Sampling started with the first dot lying fully inside the placental disc. Six sampling points were evenly spaced from each other by a regular interval of dots and labeled with colored pins. The tray was photographed (Canon Digital Camera Power Shot G12, Canon, Krefeld, Germany) with a ruler as a photographic scale (see Fig. 1c). From each of the six sampling sites, probes with an edge length (chorionic side) of about 0.5–1 cm were taken such that the whole depth of the placental disc was included. All probes were then fixed in phosphate buffered formalin (4.5%) for at least 24 h. All samples were processed routinely and embedded in paraffin. Sections were stained with hematoxylin/eosin (HE).

2.3. Parameters derived from placental photographs

2.3.1. Calculations of form parameters

Additional macroscopic parameters (see Fig. 1d,e) were analyzed with the Stereo Investigator (SI) Software (Workstation version (10.31; for 64-bit); MBF Bioscience,

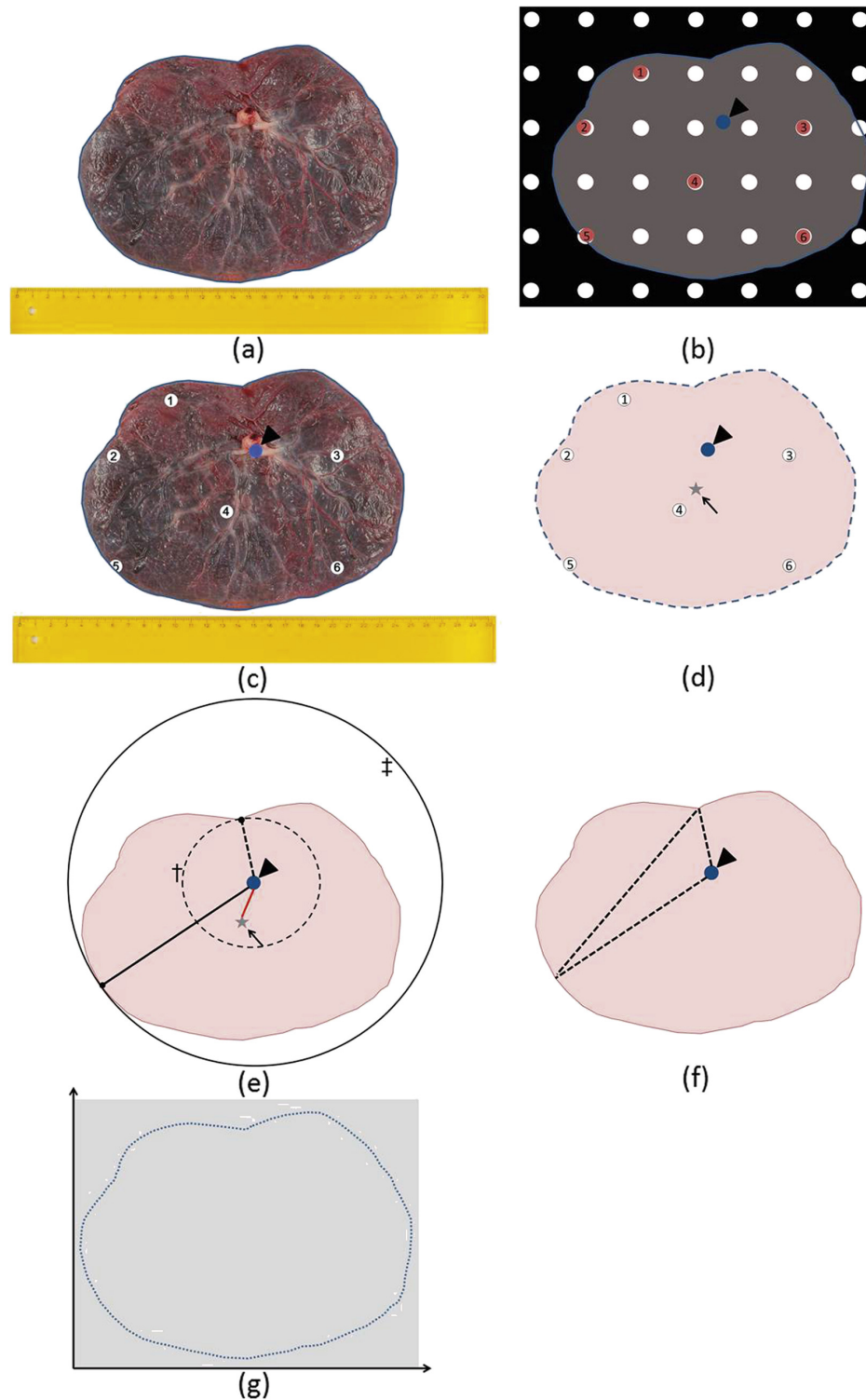


Fig. 1. (a–c) Illustrations of the labeling and sampling procedures. (a) A placenta without markers before the sampling procedure. (b) A schematic drawing of the placenta with the black and white dot pattern for systematic random sampling being projected on top. The Pins 1–6 are the sampling sites (in Figure (b) in red, in Figures (c,d) in white). The blue pin (arrowhead) marks the cord insertion. (c) A placenta from the chorionic side after the labeling procedure and before sampling of tissue. Digital images as shown in (c) were used for further processing. The ruler was used to record diameters and to calibrate measurements on the digitized photograph. (d–g) Processing of digital images. For description of parameters, see sections 2.2–2.3.2. (d,e) Determination of area of the placental surface (AoP), center of an area (CoA, grey asterisk and arrow) and distances (CoA_UC, red line in e;

Williston, VT, USA). The photographs were calibrated with the internal measuring system of the SI software using the ruler included. Along the outer rim of the placental disc, at the transition from *chorion frondosum* to *chorion laeve*, a contour was traced. Additional digital markers were set for each sampling site 1–6 and the umbilical cord insertion point (see in Fig. 1d). The parameters area of the placenta (AoP), roundness of the placental disc (RoP), center of the area of the placental disc (CoA), longest distance between umbilical cord insertion point (UC) and contour (CON) of the placental disc (UC_CON_L), and shortest distance between umbilical cord insertion point and contour of the placental disc (UC_CON_S) were calculated by SI (see Fig. 1d,e). The distance between CoA and UC was calculated (CoA_UC). UC_CON_L and UC_CON_S were determined using the nearest neighbor algorithm of SI [13]. Graphical illustrations of these procedures are given in Fig. 1; equations are shown as supplementary material in Table 3.

2.3.2. Calculation of shape parameters by geometric morphometry

For analysis of shape [11,14] with Morphologika² (Morphologika) [15], text files with sets of landmark or semilandmark coordinates were prepared. These input files were generated using two sources of coordinates:

1. With SI as source, we used the coordinates of UC, UC_CON_L and UC_CON_S connected as wireframe in Morphologika (see Fig. 1f).
2. We calibrated the photographs of each placenta with the software tpsDig2 [16], then encircled the placentas with a contour. The closed contour was resampled such that 100 sliding semilandmarks [17,18] were generated over the entire length of the contour (see Fig. 1g).

In Morphologika we used, “Generalized Procrustes Analysis” (GPA) and, “Principal Component Analysis” (PCA) with the calculation option, “Full Tangent Space Projection”. The resulting Principal Components (PC) describe variability of shape such that the PC with highest variability of shape gets the lowest number ([19]; thus, PC1: highest variability; PC2: 2nd highest variability). GPA superimposed points in a room for calculation of a best fit with PCA. The Principal Components UC_PC1 and UC_PC2 were obtained from analysis of the wireframes comprising shortest and longest distances from the cord insertion to the contour (see 1. above). The Principal Components CON_PC1 and CON_PC2 were obtained from analysis of the contour of the placentas (see 2. above).

2.4. Statistical analysis

Descriptive statistics and correlation analyses were performed in SPSS Statistics (Version 20, IBM, Ehningen, Germany). For all parameters, mean and standard deviation were calculated. Data correlations were analyzed using multiple nonparametric bivariate correlation (Kendall-Tau-b) analysis with Bonferroni correction for multiple post-hoc comparisons. Bonferroni correction adjusts the significance threshold (p) to the number of comparisons (n) as follows: $p = 0.05/n$ with $p > 0.00238$. Non-normal distribution of data was assumed, based on recent reports on probability distributions of placental morphometric data [20]. Linear regression analyses were performed with GraphPad Prism (Version 5.04, GraphPad Software, San Diego, CA, USA).

3. Results

No signs of inflammation, disturbed trophoblast differentiation, excessive fibrinoid formation, or irregular maturation of the villous tree showed up during qualitative histological examination of HE-sections. Combined with the clinical assessment of a normal course of pregnancy and delivery, the cohort investigated in the present study may be considered a set of reference data free of severe pathology. Analysis of gross morphologic parameters demonstrated that, even in this collection of normal placentas, variability is substantial (Table 1). Furthermore, most of the parameters analyzed did not show statistically significant gender-dependent differences. The delivery mode correlated significantly with GA, BW, PW, as well as with the BW-including parameters PW_BW_Ratio, BETA, and FPRcorr. GA and BW were younger/lower in the section group, while PW and the PW_BW_Ratio, BETA and FPRcorr were higher (Table 1).

PW is a scalar measure of placental size. In the present study, the correlation of PW with BW was shown by correlation (Kendall-Tau-b) analysis with Bonferroni correction (Fig. 2). Linear regression analysis of PW as a function of BW revealed a slope of 0.1367 PW(g)/BW(g) that was significantly different from zero (see Fig. 3a). The PW_BW_Ratio is a direct estimation of the relation between PW and BW (Fig. 3b). As a group, the allometric scaling factors BETA and FPRcorr and PW_BW_Ratio are all scalar estimates of the crucial relation between PW and BW, showed very similar correlation patterns with other parameters (Fig. 3c,d), and correlated very closely with each other. PW_BW_Ratio, BETA, and FPRcorr are summarized as BW-including parameters.

The shape parameters (PC) behaved very different from PW, BW, and the BW-including parameters (see Fig. 4). CON_PC1, CON_PC2, UC_PC1, and UC_PC2 did not correlate with either BW (see Fig. 3l,m,o,p), PW (see Fig. 4m,q), or any of the BW-including parameters. Principal Component Analysis of the best fit of CON_PC1 and CON_PC2 showed that the preferred shape of the normal human placenta is roundish, though not circular (see Fig. 5a,c). This is also shown by vectorial analysis of roundness (RoP, an average of 0.81 (expected value for perfect roundness is 1.0)). The Principal Components UC_PC1 and UC_PC2 describe shape of the cord insertion in relation to the contour of the placenta. They do not converge to a common shape (see Fig. 5b). Instead, shape of cord insertion was highly variable (see Fig. 5b). DELAY correlated significantly with CON_PC1 and UC_PC1, but not with any other parameter.

Vectorial form parameters were RULER_L, RULER_S, RULFACE, THICK, AoP, CoA_UC, UC_CON_S, UC_CON_L, and RoP. As a group, the form parameters were characterized by significant correlations with both scalar parameters and shape parameters; there are also a number of correlations between various parameters of this group (see Fig. 2). By this correlation pattern, the form parameters position themselves in between scalar parameters (e.g. PW, BW and BW-including parameters) and shape parameters (e.g. CON_PC1). Among the form parameters, two subgroups of parameters can be identified by their somewhat more pronounced covariability pattern with scalar parameters and shape parameters: (i) RULER_L, RULER_S, RULFACE, THICK, and AoP show significant correlations with PW, BW, and the BW-including parameters. RULER_L, RULER_S, and RULFACE also correlated with either CON_PC1 or CON_PC2. (ii) CoA_UC, UC_CON_S, UC_CON_L, and RoP correlate significantly with shape parameters, especially with CON_PC1, UC_PC1, and UC_PC2. Their covariability with PW, BW, and BW-including parameters is less intense than for RULER_L, RULER_S, RULFACE, THICK, and AoP.

4. Discussion

The present study shows, for the first time, that shape and size of the placenta have different functional meanings and can be determined independently. Specifically, gross morphologic parameters of the placenta at birth can conceptually be related to either placenta size (placenta weight), size-independent description of placental shape (shape parameters), or hybrids of these two independent poles (form parameters). The qualitative change and the potential associated with this new view can best be illustrated by a recent example. In a statement like “The breadth of the placenta

UC_CON_S, straight dotted line in e; UC_CON_L, straight black line in e). Nearest Neighbor-based measuring routine for determination of UC_CON_S and UC_CON_L: The values are determined by intersections of a continuously growing circle around cord insertion as center with the contour of the placental disc. The distance of the first intersection (small circle (single cross) with dotted line) to umbilical cord insertion is UC_CON_S. The distance of the last intersection (large circle (double cross) with straight line) to umbilical cord insertion is UC_CON_L. (f) The triangle formed by umbilical cord insertion, UC_CON_S, and UC_CON_L is the wireframe, which was analyzed by Procrustes Analysis and subsequent Principal Component Analysis in Morphologika² (Principal Components UC_PC1 and UC_PC2). (g) The contour of the placental disc as outlined in the program tpsDig2. 100 sliding semilandmarks were placed equidistantly along this contour (symbolized by dotted line) and their coordinates used in Morphologika² (Principal Components CON_PC1 and CON_PC2).

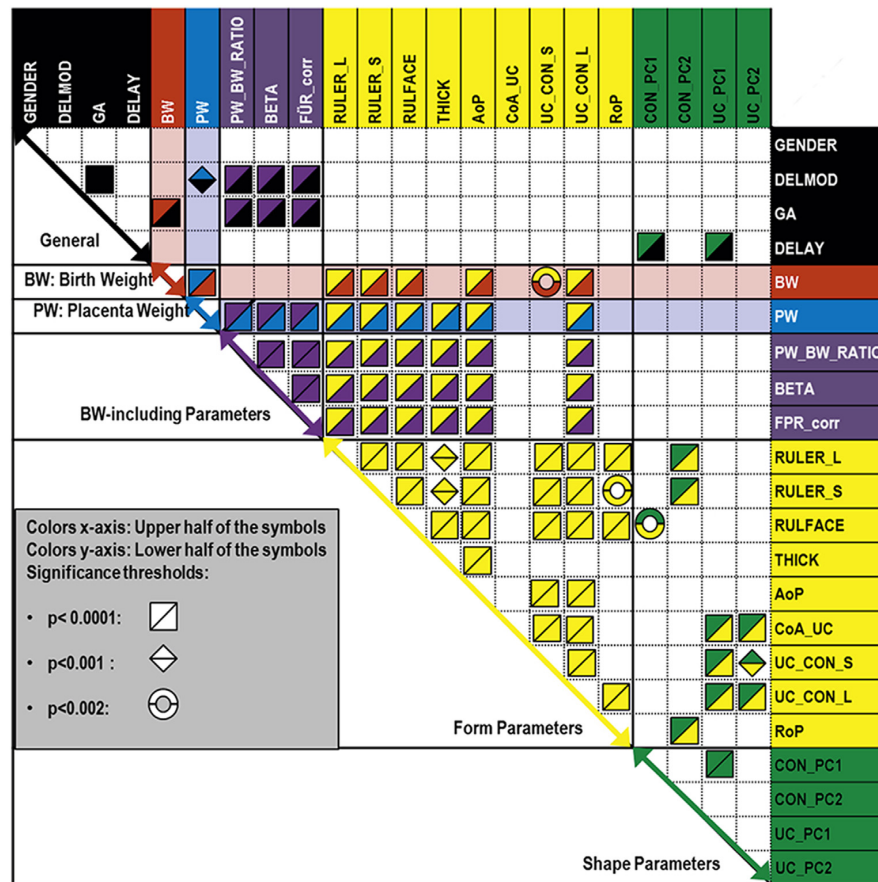


Fig. 2. Graph of the results of Bonferroni-corrected nonparametric bivariate multiple correlation analysis. The analysis results are shown in a two-dimensional array with each square corresponding to one comparison in one direction. Empty boxes belong to comparisons that did not reach the level of statistical significance (see section 2.4). The parameter groups are color-coded on y-axis and x-axis in general parameters (black), birth weight (BW; red), placenta weight (PW; blue), BW-including parameters (magenta), *form* parameters (yellow), and *shape* parameters (green). Row and column of BW and PW are marked by a slightly red (BW) or blue (PW) background. Upper half of the symbols reflect the color code of the x-axis, lower half of the symbols reflects the color code on the y-axis. The symbol type represents significance levels (see grey box inside the figure). For description of parameters, see Sections 2.2–2.3.2 and Table 3. Table 4 in the supplementary materials shows the numerical data.

should be interpreted as a combination of two different measurements: placental size and irregularity of the placental surface.” (quoted from the Abstract of [21]), the term “irregularity of the placental surface” can now be interpreted quantitatively as *shape* variability.

Mean values and variability of BW and PW reported in the present study are in line with recent European reference compilations of birth weight and placenta weight of unfixed placentas without trimming of membranes [22]. The BW-including parameters PW_BW_Ratio, BETA, and FPRcorr are calculated derivatives of PW and BW [8]. We were not able to identify any potentially meaningful difference between PW_BW_Ratio, BETA, and FPRcorr (see Fig. 3b–d). BW-including parameters are exchangeable. We recommend the continued usage of PW_BW_Ratio since many historical data (see e.g. Ref. [23]) report the ratio of placenta weight to birth weight (PW_BW_Ratio in the present study). PW_BW_Ratio (see Fig. 3b) guarantees broadest comparability of data.

In the present study, size-independent analysis of *shape* variability provided by geometric morphometry [10,24,25] was transferred to research on human placentas. *Shape* analysis provides the complementary second viewpoint on gross morphologic

parameters of the placenta at birth; it complements the view provided by *shape* independent analysis of placenta size (weight) on the many *form* parameters being hybrids of size and *shape* properties.

None of the *shape* parameters (CON_PC1, CON_PC2, UC_PC1, and UC_PC2) correlated with birth weight or placenta weight (see Fig. 2). Absence of correlation with placenta weight confirmed their independence from placental size (see Fig. 4m,q). Absence of correlation with birth weight shows that *shape* alone (at the gross anatomy level) will not predict birth weight (see Fig. 3l,m,o,p). *Shape* parameters are thus qualitatively different from placental size measured by PW and also from BW and the BW-including parameters. Their role for developmental programming is not yet analyzed, but it can be expected that their spectrum of correlations with postnatal health outcomes will also be quantitatively and qualitatively different from that of PW and BW.

We show that the *shape* of the placental disc converges toward a roundish, but not precisely circular, common *shape* (CON_PC1 and CON_PC2, see Fig. 5a,c). Roundness determination by the *form* parameter RoP confirmed that the average placenta is round, but not circular (see also [26,27]). Asymmetry of the placental disc in connection with cord insertion (UC_PC1 and UC_PC2, see Fig. 5b,d)

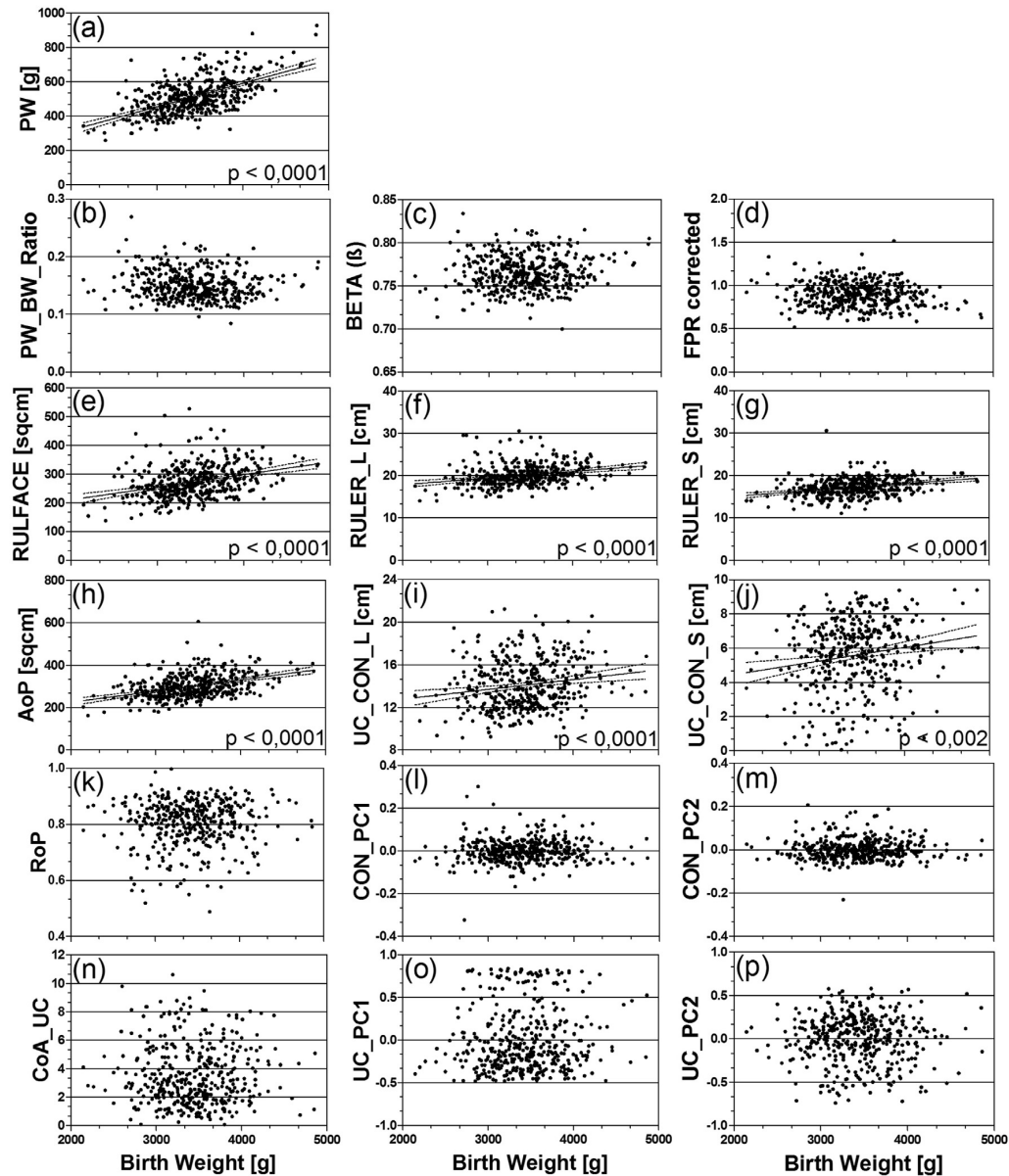


Fig. 3. (a–p) The graph illustrates correlation/non-correlation of various parameters with birth weight. x-axis in all subfigures a–p shows birth weight in gramm (g). If the respective parameter on the y-axis correlated statistically significantly with birth weight, the p-value of the correlation analysis is given above the x-axis and a linear regression analysis was performed. The resulting straight line and the 95% confidence intervals are shown. For description of parameters, see sections 2.2–2.3.2. (a) Placenta weight (PW). (b–d) BW-including parameters PW_BW_Ratio (b), BETA (c), and FPRcorr (d). (e–j, k, n) Form parameters RULFACE (e), RULER_L (f), RULER_S (g), AoP (h), UC_CON_L (i), UC_CON_S (j), RoP (k), and CoA_UC (n). (l, m, o, p) Shape parameters CON_PC1 (l), CON_PC2 (m), UC_PC1 (o), and UC_PC2 (p).

revealed that there is no clear convergence to a common *shape* pattern of cord insertion or asymmetry of the placental disc in relation to cord insertion (see Fig. 5).

Placenta weight is a reliable predictor of postnatal health; studies with very large case numbers clearly show this [28,29]. Placenta weight can be a stronger predictor of postnatal health than placental form [30]. PW, BW, and PW_BW_Ratio are reliable estimates of placental efficiency. None of them correlates significantly with any of the *shape* parameters CON_PC1, CON_PC2, UC_PC1, and UC_PC2. *Shape* variability is not firmly linked with PW, BW, or PW_BW_Ratio of normal human placentas. High variability and

missing convergence to a common *shape* of the two *shape* parameters measuring eccentricity of cord insertion (UC_PC1 and UC_PC2) makes it unlikely that there is significant evolutionary pressure toward a specific *shape* of cord insertion (see Figs. 4 and 5; for interpretation of *shape* variability in evolutionary context see e.g. Refs. [31,32]). Our data do not support the conclusion [6] that eccentric cord insertion necessarily compromises efficiency of the normal human placenta.

Rather, the placenta would best serve reproductive success if it can adapt flexibly to the difficult and – for each conceptus anew – unpredictable situation in utero. *Shape* adaptation could be an

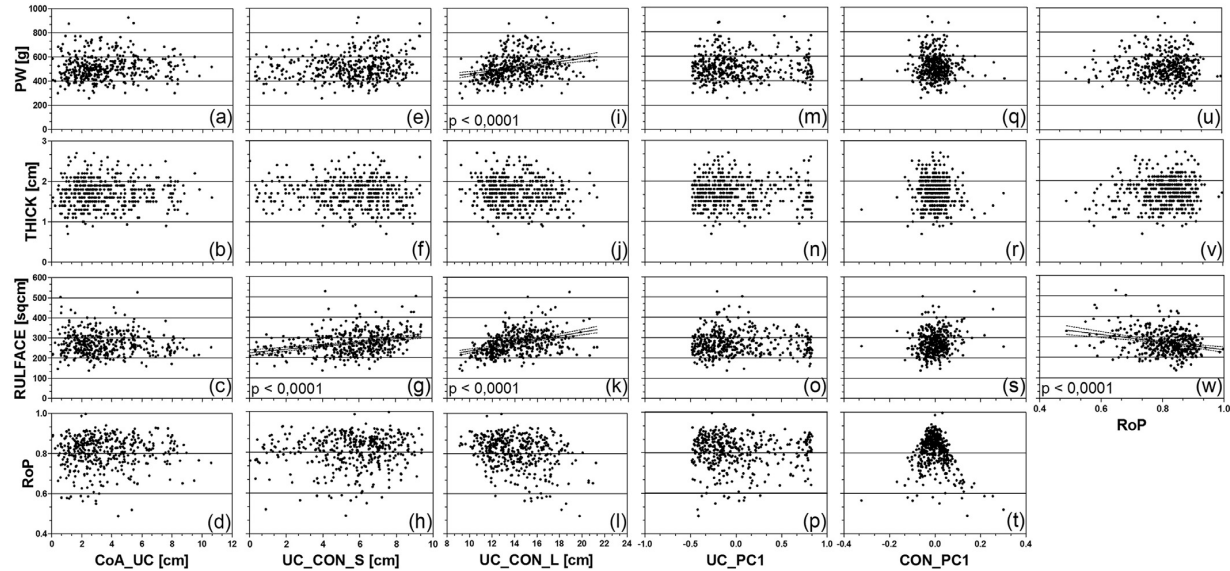


Fig. 4. (a–w) Matrix of scatter plots with on the x-axes parameters estimating eccentricity of cord insertion, namely the *form* parameters CoA_UC (a–d), UC_CON_S (e–h), UC_CON_L (i–l), and the *shape* parameter UC_PC1 (m–p). In addition the *shape* parameter CON_PC1 (q–t) and the *form* parameter RoP (u–w) are shown, both describing the outer contour of the placental disc. On the y-axes placenta weight (a,e,i,m,q,u) as measure of placental size and the *form* parameters THICK (b,f,j,n,r,v), RULFACE (c,g,k,o,s,w), and RoP (d,h,l,p,t) are shown. If the parameters shown in one of the plots (a–w) correlated statistically significantly with each other, the p-value of the correlation analysis is given above the x-axis and a linear regression analysis was performed. The resulting straight line and the 95% confidence intervals are shown. For description of parameters, see sections 2.2–2.3.2.

important component of the flexible placental response to the uterine habitat. Uterine habitat is summarizing here the various maternal and uterine influences (mechanical and gross anatomical uterine factors, body size of the mother, parity, site of placentation, general nutritive factors, cellular and molecular factors, maturity

and function of the endometrium, immunological factors, maternal metabolic and endocrine factors, etc.) which the implanting conceptus and the developing placenta encounter.

This view is supported by a recent study, comparable in sample size to the present study, focusing on the influence of maternal body

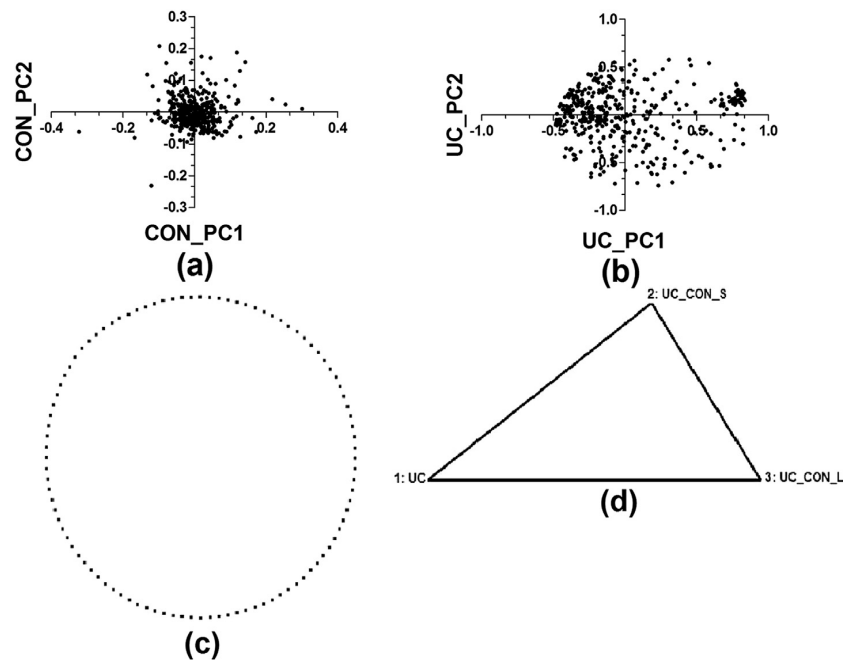


Fig. 5. (a,b) Scatter graphs of *shape* parameters. For description of parameters, see sections 2.2–2.3.2. CON_PC1 is shown with CON_PC2 (a) and UC_PC1 is shown with UC_PC2 (b). The scatter graphs illustrate *shape* variability in the sample of placentas as deviation from best fits shown in (c,d). For CON_PC1 and CON_PC2, there is a convergence to a round common *shape* shown as best fit in (c). There is no convergence of *shape* variability for UC_PC1 and UC_PC2 (b). (c,d) Graphical representation of best fit analysis for CON_PC1 and CON_PC2 (c) and UC_PC1 and UC_PC2 (d).

parameters on placental parameters [33]. The ratio of placenta weight to birth weight (PW_BW_Ratio in the present study) did not correlate with any parameter of maternal body size [33]. Instead, there were several statistically significant correlations of *form* parameters (length–breadth difference of the placenta and ratio of length and breadth to birth weight) with maternal size parameters [33]. Similarly, associations of postnatal risk of coronary heart disease with maternal body parameters and placental *form* parameters (difference of length to breadth and surface area) but not with placenta weight were reported in large study populations (e.g. in Refs. [34], quote from page 2298 bottom to 2299): “... the trend in coronary heart disease with an oval placental surface was confined to men with short mothers. The interaction between the effects of ovality and mothers height was statistically significant (P for interaction = 0.03)”. The concept provided in the present study would support the complementary interpretation that the primary risk association could have been with *shape* indirectly recognized by the *form* parameter “ovality” combined with lack of correlation with placenta weight.

Since the *form* parameters in these [33,34] and certainly also other studies transmit some *shape* information (see below), we hypothesize that *shape* variability is (i) an important and biologically necessary option by which the placenta adapts to maternal/uterine environmental conditions, and (ii) that *shape* variability provides important contributions to conceptional understanding of prenatal programming. Functionally adequate size (as measured by placenta weight) and efficiency (as measured by PW_BW_Ratio) of the normal human placenta occur with considerably variable *shape*.

A feature of our data is the statistically significant correlation of the *shape* parameters CON_PC1 and UC_PC1 with the technical parameter DELAY. There is no correlation with PW, and we can exclude that blood loss during storage and transport caused the progressive *shape* change (emptied packages with blood inside were weighed, too; data not shown). We hypothesize that the ring of smooth muscle surrounding the placental disc [35] and crossing into the chorionic plate contributes to progressive postnatal *shape* change without corresponding weight change.

It is well known ([36] and also by Barker et al. [37], discussion remarks on page 14 therein) that cord insertion is determined during the 1st trimester of pregnancy. Size enlargement of the placenta occurs predominantly beyond the 20th week of gestation and reflects adaptation to nutritional requirements. *Shape* analysis of cord insertion thus takes a long view back in pregnancy [6], while analysis of size has a more limited backwards perspective.

The large group of *form* parameters (RULER_L, RULER_S, RULFACE, THICK, AoP, CoA_UC, UC_CON_S, UC_CON_L, and RoP) showed various degrees of covariability with PW, BW, BW-including parameters, and *shape* parameters. Extent of contribution of specific size and *shape* properties represented in each of these parameters is certainly different, but unknown (see Fig. 2). In some of them, the association with size seems to be more prominent; in others there is a more obvious association with *shape*. Certainly, *form* parameters correlate with postnatal health outcomes [4]. So far, it remains unclear as to which extent such correlations could be a consequence of their covariability with size, their covariability with *shape*, or to a specifically meaningful contribution of *shape* and size information with regard to the postnatal health outcome being examined.

In summary, the present study transfers analysis of *shape* variability by geometric morphometry to quantitative placental gross anatomy. This generates a systematic quantitative framework of gross analysis of the human placenta. The view on utero–placental interactions as a kind of ecological adaptation process – in analogy to biological ecology, for which geometric morphometry was developed – sheds new light on normal placental development via interpretation of *shape* variability. In combination with placental *shape*

analysis as novel concept, the broad statistical array analysis of macroscopic morphologic parameters of a substantial number of normal human placentas provides a rational basis for future studies on developmental programming and for interpretation of published data.

Acknowledgments

The authors acknowledge the skilful technical assistance and diligent work of the whole team of technicians of the Department of Anatomy, namely B. Aschauer, A. Baltruschat, U. Fazekas, S. Kerling, C. Köhler, B. Mosler and S. Tost. We would also like to express our thanks to the obstetricians, midwives, and nurses of the hospital, Dritter Orden, who enabled the clinical work of this study with great care and engagement. For proofreading and helpful discussions on preparation of the manuscript, we would like to thank N. Angstman, A. Asikoglu, N. Csaszar, M. Kiessling, S. Milz, and M. Pfaff.

Appendix A. Supplementary data

Supplementary data related to this article can be found at <http://dx.doi.org/10.1016/j.placenta.2013.04.011>.

References

- [1] Steiner ES, Sanders EM, Phillips EC, Maddock CR. Very low birth weight children at school age: comparison of neonatal management methods. *Br Med J* 1980;281(6250):1237–40.
- [2] Stewart A, Turcan D, Rawlings G, Hart S, Gregory S. Outcome for infants at high risk of major handicap. *Ciba Found Symp* 1978;59:151–71.
- [3] Schmitz C, Frank HG. Discrete placental dysfunction: the overlooked player in prenatal roots of neuropsychiatric diseases? *Neuroembryology* 2002;1(4):169–75.
- [4] Burton GJ, Barker DJP, Moffett A, Thornburg K, editors. The placenta and human developmental programming. Cambridge: Cambridge University Press; 2011.
- [5] Godfrey KM. The role of the placenta in fetal programming—a review. *Placenta* 2002;23:20–7.
- [6] Yampolsky M, Salafia CM, Shlakhter O, Haas D, Eucker B, Thorp J. Centrality of the umbilical cord insertion in a human placenta influences the placental efficiency. *Placenta* 2009;30(12):1058–64.
- [7] Kikuchi A, Unno N, Shiba M, Sunagawa S, Ogiso Y, Kozuma S, et al. Multifractal description of the maternal surface of the placenta. *Gynecol Obstet Invest* 2008;66(2):127–33.
- [8] Salafia CM, Misra DP, Yampolsky M, Charles AK, Miller RK. Allometric metabolic scaling and fetal and placental weight. *Placenta* 2009;30(4):355–60.
- [9] Salafia CM, Yampolsky M. Metabolic scaling law for fetus and placenta. *Placenta* 2009;30(5):468–71.
- [10] Zelditch ML, Swiderski DL, Sheets HD, Fink WL. Geometric morphometrics for biologists. 1st ed. Academic Press; 2004.
- [11] Bookstein FL. Morphometric tools for landmark data: geometry and biology. Cambridge University Press; 1997.
- [12] Nelson DM, Burton GJ. A technical note to improve the reporting of studies of the human placenta. *Placenta* 2011;32(2):195–6.
- [13] Schmitz C, Grolms N, Hof PR, Boehringer R, Glaser J, Korr H. Altered spatial arrangement of layer V pyramidal cells in the mouse brain following prenatal low-dose X-irradiation. A stereological study using a novel three-dimensional analysis method to estimate the nearest neighbor distance distributions of cells in thick sections. *Cereb Cortex* 2002;12(9):954–60.
- [14] Bookstein FL. The measurement of biological shape and shape change: lecture notes in biomathematics. Berlin: Springer-Verlag; 1978.
- [15] O’Higgins P, Jones N. Morphologika2: tools for statistical shape analysis. Hull: Hull York Medical School. Available from: <https://sites.google.com/site/hymsfme/home>; 2006.
- [16] Rohlf FJ. tpsDig2: SB morphometrics. New York: Stony Brook University. Available from: <http://life.bio.sunysb.edu/morph/index.html>; 2010.
- [17] Weber GW, Bookstein FL. Virtual anthropology: a guide to a new interdisciplinary field. 1st ed. Springer; 2010.
- [18] Bookstein FL. Landmark methods for forms without landmarks: morphometrics of group differences in outline shape. *Med Image Anal* 1997;1(3):225–43.
- [19] Dryden IL, Mardia KV. Statistical shape analysis. London: John Wiley and Sons; 1998.
- [20] Gill JS, Woods MP, Salafia CM, Vvedensky DD. Probability distributions for measures of placental shape and morphology 2011. arXiv:1109.2057[q-bio.QM].
- [21] Yampolsky M, Salafia CM, Misra DP, Shlakhter O, Gill JS. Is the placental disk really an ellipse? *Placenta* 2013;34:391–3.

- [22] Burkhardt T, Schaffer L, Schneider C, Zimmermann R, Kurmanavicius J. Reference values for the weight of freshly delivered term placentas and for placental weight-birth weight ratios. *Eur J Obstet Gynecol Reprod Biol* 2006;128(1–2):248–52.
- [23] Boyd JD, Hamilton WJ. *The human placenta*. Cambridge: Heffer; 1970.
- [24] Neubauer S. Endocranial shape changes during growth in chimpanzees and humans: a morphometric analysis of unique and shared aspects. *J Hum Evol* 2010;59:555–66.
- [25] Neubauer S, Gunz P, Hublin JJ. The pattern of endocranial ontogenetic shape changes in humans. *J Anat* 2009;215:240–55.
- [26] Barker DJP, Osmond C, Thornburg KL, Kajantie E, Eriksson JG. The lifespan of men and the shape of their placental surface at birth. *Placenta* 2011;32(10):783–7.
- [27] Yampolsky M, Salafia CM, Shlakter O, Haas D, Eucker B, Thorp J. Modeling the variability of shapes of a human placenta. *Placenta* 2008;29(9):790–7.
- [28] Risnes KR, Romundstad PR, Nilsen TL, Eskild A, Vatten LJ. Placental weight relative to birth weight and long-term cardiovascular mortality: findings from a cohort of 31,307 men and women. *Am J Epidemiol* 2009;170(2):622–31.
- [29] Hemachandra AH, Klebanoff MA, Duggan AK, Hardy JB, Furth SL. The association between intrauterine growth restriction in the full-term infant and high blood pressure at age 7 years: results from the collaborative perinatal project. *Int J Epidemiol* 2006;35(4):871–7.
- [30] Khalife N, Glover V, Hartikainen AL, Taanila A, Ebeling H, Jarvelin MR, et al. Placental size is associated with mental health in children and adolescents. *PLoS One* 2012;7(7):e40534.
- [31] Mitteroecker P, Gunz P, Neubauer S, Müller G. How to explore morphological integration in human evolution and development? *Evol Biol* 2012;39(4):536–53.
- [32] Singh N, Harvati K, Hublin JJ, Klingenberg CP. Morphological evolution through integration: a quantitative study of cranial integration in Homo, Pan, Gorilla and Pongo. *J Hum Evol* 2012;62(1):155–64.
- [33] Winder NR, Krishnaveni GV, Veena SR, Hill JC, Karat CLS, Thornburg KL, et al. Mother's lifetime nutrition and the size, shape and efficiency of the placenta. *Placenta* 2011;32(11):806–10.
- [34] Eriksson JG, Kajantie E, Thornburg KL, Osmond C, Barker DJP. Mother's body size and placental size predict coronary heart disease in men. *Eur Heart J* 2011;32(18):2297–303.
- [35] Nanaev AK, Kosanke G, Kemp B, Frank HG, Huppertz B, Kaufmann P. The human placenta is encircled by a ring of smooth muscle cells. *Int J Dev Biol* 2010;54(2–3):525–30. *Placenta* 2000;21(1):122–125.
- [36] Salafia CM, Yampolsky M, Shlakter A, Mandel DH, Schwartz N. Variety in placental shape: when does it originate? *Placenta* 2012;33(3):164–70.
- [37] Barker DJP, Eriksson JG, Alwasel SH, Fall CHD, Roseboom TJ, Osmond C. The maternal and placental origins of chronic disease. In: Burton GJ, Barker DJP, Moffett A, Thornburg K, editors. *The placenta and human developmental programming*. Cambridge: Cambridge University Press; 2011. p. 5–16.

Supplementary Materials

Parameter	Clinical characteristics of pregnancies for placentas studied	
Gestational Age (weeks)	Average = 39,56	SD = $\pm 1,16$
Delivery mode	Vaginal n = 226	Section n = 192
Birth weight (g)	Average = 3428,63	SD = $\pm 440,17$
Placental weight (g)	Average = 512,93	SD = $\pm 102,12$
Baby's sex	Male n = 223	Female n = 195
Delivery to processing (min)	Average = 486,31	SD = $\pm 375,36$

Table 2: The table was assembled according to [12]; categories without data in the present study were omitted. . „=” refers to the term „equal”, „min” refers to minutes, and „n” refers to number. Gestational age was available in weeks and days. Days were calculated to give a decimal fraction of a seven day week.

Full Name / Description	Acronym	Value / Equations
Child gender	GENDER	Male or Female
Gestational age	GA	Weeks, days as decimal value
Delivery mode	DELMOD	Caesarean section or vaginal delivery
Birth weight	BW	Birth weight in g
Interval between birth and start of tissue processing	DELAY	Time in min
Weight of the placental disc and membranes without umbilical cord	PW	Placenta weight in g
Thickness of the placental disc, determined by ultrasound	THICK	Thickness in cm
Longest diameter across the umbilical cord	RULER_L	Length in cm
Diameter rectangular to RULER_L across the umbilical cord	RULER_S	Length in cm
Placental surface as calculated from RULER_L and RULER_S	RULFACE	$RULFACE = \frac{RULER_L}{2} \times \frac{RULER_S}{2} \times \pi$ [37]
Ratio of PW to BW	PW_BW_Ratio	$PW_BW_Ratio = \frac{PW}{BW}$ [23]
Allometric scaling estimated by scaling factor β	BETA	$\beta = \frac{\log PW}{\log BW}$ [6]
Allometric scaling estimated by fetal-placental ratio	FPRcorr	$FPRcorr = \frac{PW^{0.75}}{BW}$ [6]
Area encircled by the contour of the placental disc determined in SI. The latter area was considered a non-self interacting closed polygon defined by n vertices $(X_0, Y_0), (X_1, Y_1), \dots, (X_{n-1}, Y_{n-1})$. For determination of the area see equation.	AoP	$AoP = \frac{1}{2} (X_0 Y_n - X_n Y_0) + \sum_{i=1}^{n-1} (X_{i+1} Y_i - X_i Y_{i+1}) $
Roundness of the contour of the placental disc as determined in SI (see equation; Max Diameter is the longest distance found in SI between two points of the contour)	RoP	$RoP = \frac{4\pi AoP}{\pi * Max Diameter^2}$
Center of the area encircled by the placental disc as determined in SI. CoA was determined in SI for the area enclosed by the contour of the placental disc; the latter area was considered a non-self interacting closed polygon defined by n vertices $(X_0, Y_0), (X_1, Y_1), \dots, (X_{n-1}, Y_{n-1})$. CoA is the point with coordinates C_X and C_Y (see equations), A is the area for which CoA was determined.	CoA	$C_X = \frac{1}{6A} \sum_{i=0}^{n-1} (X_i + X_{i+1}) (X_i Y_{i+1} - X_{i+1} Y_i)$ $C_Y = \frac{1}{6A} \sum_{i=0}^{n-1} (Y_i + Y_{i+1}) (X_i Y_{i+1} - X_{i+1} Y_i)$ $A = \frac{1}{2} \sum_{i=0}^{n-1} (X_i Y_{i+1} - X_{i+1} Y_i)$
Distance between CoA and umbilical cord insertion	CoA_UC	Length in cm
Shortest distance between umbilical cord insertion point and the contour of the placental disc. UC_CON_S was determined using the SI-procedure „Nearest Neighbor“ (see also [13])	UC_CON_S	Length in cm; calculated in SI: $d = \sqrt{(X_0 - X_1)^2 + (Y_0 - Y_1)^2 + (Z_0 - Z_1)^2}$ [13]
Longest distance between umbilical cord insertion an the contour of the placental disc. UC_CON_L was determined using the SI-procedure „Nearest Neighbor“ (see also [13])	UC_CON_L	Length in cm; calculated in SI: $d = \sqrt{(X_0 - X_1)^2 + (Y_0 - Y_1)^2 + (Z_0 - Z_1)^2}$ [13]
Results of General Procrustes Analysis (GPA) and Principal Component Analysis (PCA) are Principal Components (PC). They describe statistically independent modes of variation of the contour of the placental disc. The Principal Components with number one is the one with highest variability, number two is the Component with 2nd highest variability.	CON_PC1 CON_PC2	Factor without dimension
Results of General Procrustes Analysis (GPA) and Principal Component Analysis (PCA) are Principal Components (PC). They describe statistically independent modes of variation of the wireframe formed by the umbilical cord insertion and the intersection of UC_CON_L and UC_CON_S with the contour of the placental disc. The PC with number one is the one with highest variability, number two is the Component with 2nd highest variability.	UC_PC1 UC_PC2	Factor without dimension

Table 3: Description of the parameters determined in the present study; including abbreviations and equations

Table 4	Kendall-Tau-b	GENDER	DELMOD	GA	BW	PW	PW_BW_Ratio	BETA (β)	FPR _{corr}	RULER _L	RULER _S	RULFACE	THICK	DELAY	AoP	CoA _{UC}	UC_CON _S	UC_CON _L	RoP	CON_PC1	CON_PC2	UC_PC1
GENDER	Corr. Coeff.	1,000	-,015	,045	-,071	-,012	,037	,026	-,025	-,025	-,031	-,046	-,009	,007	-,011	,024	-,015	,011	-,023	-,052	,037	-,003
	Sig. (2-side)		,758	,268	,076	,766	,353	,512	,540	,541	,458	,250	,834	,869	,791	,546	,717	,777	,571	,193	,352	,936
DELMOD	Corr. Coeff.	-,015	1,000	-,356	-,117	,138	,240	,222	-,220	,105	,024	,076	,031	-,120	,093	,052	-,034	,080	-,063	-,041	,036	-,016
	Sig. (2-side)	,758		,0001	,004	,001	,0001	,0001	,0001	,011	,561	,057	,454	,003	,020	,197	,395	,046	,115	,310	,365	,693
GA	Corr. Coeff.	,045	-,356	1,000	,293	-,012	-,246	-,186	,183	-,007	,051	,013	-,053	,062	,027	-,025	,040	-,017	,052	,025	-,054	,061
	Sig.(2-side)	,268	,0001		,0001	,728	,0001	,0001	,0001	,837	,139	,692	,131	,063	,424	,457	,228	,620	,118	,456	,110	,068
BW	Corr. Coeff.	-,071	-,117	,293	1,000	,383	-,064	,057	-,065	,241	,237	,256	,095	-,010	,291	,002	,103	,125	,004	,046	,011	,044
	Sig.(2-side)	,076	,004	,0001		,0001	,052	,083	,048	,0001	,0001	,0001	,005	,767	,0001	,941	,002	,0001	,895	,157	,743	,175
PW	Corr. Coeff.	-,012	,138	-,012	,383	1,000	,555	,676	-,684	,320	,309	,340	,303	-,049	,394	,079	,067	,224	-,009	-,003	,014	,009
	Sig.(2-side)	,766	,001	,728	,0001		,0001	,0001	,0001	,0001	,0001	,0001	,0001	,134	,0001	,015	,040	,0001	,778	,939	,678	,773
PW_BW_Ratio	Corr. Coeff.	,037	,240	-,246	-,064	,555	1,000	,879	-,872	,193	,168	,200	,293	-,059	,228	,097	-,007	,169	-,027	-,043	,024	-,016
	Sig. (2-side)	,353	,0001	,0001	,052	,0001		,0001	,0001	,0001	,0001	,0001	,0001	,071	,0001	,003	,838	,0001	,418	,187	,467	,633
BETA (β)	Corr. Coeff.	,026	,222	-,186	,057	,676	,879	1,000	-,991	,242	,218	,252	,312	-,062	,288	,097	,016	,193	-,024	-,036	,019	-,006
	Sig. (2-side)	,512	,0001	,0001	,083	,0001	,0001		,0001	,0001	,0001	,0001	,0001	,060	,0001	,003	,627	,0001	,456	,271	,555	,846
FPR _{corr}	Corr. Coeff.	-,025	-,220	,183	-,065	-,684	-,872	-,991	1,000	-,244	-,221	-,254	-,314	,062	-,291	-,096	-,017	-,194	,023	,035	-,018	,006
	Sig.(2-side)	,540	,0001	,0001	,048	,0001	,0001	,0001		,0001	,0001	,0001	,0001	,060	,0001	,003	,595	,0001	,479	,289	,574	,848
RULER _L	Corr. Coeff.	-,025	,105	-,007	,241	,320	,193	,242	-,244	1,000	,370	,685	-,113	-,026	,578	-,030	,166	,304	-,376	,092	,210	,076
	Sig.(2-side)	,541	,011	,837	,0001	,0001	,0001	,0001	,0001		,0001	,0001	,001	,448	,0001	,370	,0001	,0001	,0001	,006	,0001	,025

Table 4	Kendall-Tau-b	GENDER	DELMOD	GA	BW	PW	PW_BW_Ratio	BETA (β)	FPR _{corr}	RULER_L	RULER_S	RULFACE	THICK	DELAY	AoP	CoA_UC	UC_CON_S	UC_CON_L	RoP	CON_PC1	CON_PC2	UC_PC1
RULER_S	Corr. Coeff.	-.031	.024	.051	.237	.309	.168	.218	-.221	.370	1.000	.707	-.118	-.027	.559	-.001	.233	.206	.104	.060	-.124	.004
	Sig.(2-side)	.458	.561	.139	.0001	.0001	.0001	.0001	.0001	.0001		.0001	.001	.427	.0001	.967	.0001	.0001	.002	.078	.0001	.914
RULFACE	Corr. Coeff.	-.046	.076	.013	.256	.340	.200	.252	-.254	.685	.707	1.000	-.135	-.020	.672	-.016	.224	.286	-.138	.100	.046	.035
	Sig.(2-side)	.250	.057	.692	.0001	.0001	.0001	.0001	.0001	.0001	.0001		.0001	.538	.0001	.630	.0001	.0001	.0001	.002	.160	.292
THICK	Corr. Coeff.	-.009	.031	-.053	.095	.303	.293	.312	-.314	-.113	-.118	-.135	1.000	.018	-.145	.043	-.070	-.073	.047	-.063	.022	-.022
	Sig.(2-side)	.834	.454	.131	.005	.0001	.0001	.0001	.0001	.001	.001	.0001		.587	.0001	.201	.040	.031	.164	.064	.522	.522
DELAY	Corr. Coeff.	.007	-.120	.062	-.010	-.049	-.059	-.062	.062	-.026	-.027	-.020	.018	1.000	-.009	.054	-.067	.026	-.017	.190	.006	-.178
	Sig.(2-side)	.869	.003	.063	.767	.134	.071	.060	.060	.448	.427	.538	.587		.790	.096	.041	.437	.608	.0001	.862	.0001
AoP	Corr. Coeff.	-.011	.093	.027	.291	.394	.228	.288	-.291	.578	.559	.672	-.145	-.009	1.000	-.017	.242	.319	-.090	.090	.021	.039
	Sig.(2-side)	.791	.020	.424	.0001	.0001	.0001	.0001	.0001	.0001	.0001	.0001	.0001	.790		.611	.0001	.0001	.006	.006	.522	.238
CoA_UC	Corr. Coeff.	.024	.052	-.025	.002	.079	.097	.097	-.096	-.030	-.001	-.016	.043	.054	-.017	1.000	-.623	.593	.023	.027	-.013	-.178
	Sig.(2-side)	.546	.197	.457	.941	.015	.003	.003	.003	.370	.967	.630	.201	.096	.611		.0001	.0001	.489	.415	.683	.0001
UC_CON_S	Corr. Coeff.	-.015	-.034	.040	.103	.067	-.007	.016	-.017	.166	.233	.224	-.070	-.067	.242	-.623	1.000	-.333	.044	-.002	-.030	.177
	Sig.(2-side)	.717	.395	.228	.002	.040	.838	.627	.595	.0001	.0001	.0001	.040	.041	.0001	.0001		.0001	.177	.955	.364	.0001
UC_CON_L	Corr. Coeff.	.011	.080	-.017	.125	.224	.169	.193	-.194	.304	.206	.286	-.073	.026	.319	.593	-.333	1.000	-.164	.094	.079	-.117
	Sig.(2-side)	.777	.046	.620	.0001	.0001	.0001	.0001	.0001	.0001	.0001	.0001	.031	.437	.0001	.0001	.0001		.0001	.004	.016	.0001
RoP	Corr. Coeff.	-.023	-.063	.052	.004	-.009	-.027	-.024	.023	-.376	.104	-.138	.047	-.017	-.090	.023	.044	-.164	1.000	-.092	-.365	-.046
	Sig.(2-side)	.571	.115	.118	.895	.778	.418	.456	.479	.0001	.002	.0001	.164	.608	.006	.489	.177	.0001		.005	.0001	.160

Table 4	Kendall-Tau-b	GENDER	DELMOD	GA	BW	PW	PW_BW_Ratio	BETA (β)	FPR _{corr}	RULER _L	RULER _S	RULFACE	THICK	DELAY	AoP	CoA _{UC}	UC_CON _S	UC_CON _L	RoP	CON_PC1	CON_PC2	UC_PC1
CON_PC1	Corr. Coeff.	-,052	-,041	,025	,046	-,003	-,043	-,036	,035	,092	,060	,100	-,063	,190	,090	,027	-,002	,094	-,092	1,000	-,071	-,174
	Sig.(2-side)	,193	,310	,456	,157	,939	,187	,271	,289	,006	,078	,002	,064	,0001	,006	,415	,955	,004	,005		,031	,0001
CON_PC2	Corr. Coeff.	,037	,036	-,054	,011	,014	,024	,019	-,018	,210	-,124	,046	,022	,006	,021	-,013	-,030	,079	-,365	-,071	1,000	,016
	Sig.(2-side)	,352	,365	,110	,743	,678	,467	,555	,574	,0001	,0001	,160	,522	,862	,522	,683	,364	,016	,0001	,031		,628
UC_PC1	Corr. Coeff.	-,003	-,016	,061	,044	,009	-,016	-,006	,006	,076	,004	,035	-,022	-,178	,039	-,178	,177	-,117	-,046	-,174	,016	1,000
	Sig.(2-side)	,936	,693	,068	,175	,773	,633	,846	,848	,025	,914	,292	,522	,0001	,238	,0001	,0001	,0001	,160	,0001	,628	
UC_PC2	Corr. Coeff.	-,020	,025	-,018	-,014	-,005	-,009	-,009	,009	-,018	,023	,003	-,013	-,090	-,039	-,114	,114	-,123	,068	-,090	,012	,003
	Sig.(2-side)	,611	,528	,595	,680	,872	,784	,779	,779	,590	,488	,934	,705	,006	,231	,0001	,001	,0001	,039	,006	,711	,934

Table 4: Table of the results of Bonferroni-corrected nonparametric bivariate multiple correlation analysis (Kendall-Tau b; done in IBM SPSS Statistics Version 20). The table shows correlation analysis of each parameter with each other in both directions. For description of parameters, see sections 2.2-2.3.2 and table 3. For each comparison, the correlation coefficient (Corr. Coeff.) and the two-sided sigma (Sig. 2-side) are given. N is 418 throughout. Significance levels after Bonferroni correction are $p < 0,0001$, $p < 0,001$ and $p < 0,002$. Bonferroni correction set the significance level to $p > 0,00238$. This threshold is derived from $p = \frac{0,05}{n \text{ comparisons}}$ with $n \text{ comparisons} = 22$.

3.2 Publication II

Novel 3D microscopic analysis of human placental villous trees reveals unexpected significance of branching angles

Abstract

The villous trees of human placentas delineate the fetomaternal border and are complex three-dimensional (3D) structures. Thus far, they have primarily been analyzed as thin, two-dimensional (2D) histological sections. However, 2D sections cannot provide access to key aspects such as branching nodes and branch order. Using samples taken from 50 normal human placentas at birth, in the present study we show that analysis procedures for 3D reconstruction of neuronal dendritic trees can also be used for analyzing trees of human placentas. Nodes and their branches (e.g., branching hierarchy, branching angles, diameters, and lengths of branches) can be efficiently measured in whole-mount preparations of isolated villous trees using high-end light microscopy. Such data differ qualitatively from the data obtainable from histological sections and go substantially beyond the morphological horizon of such histological data. Unexpectedly, branching angles of terminal branches of villous trees varied inversely with the fetoplacental weight ratio, a widely used clinical parameter. Since branching angles have never before been determined in the human placenta, this result requires further detailed studies in order to fully understand its impact.

Reference

Haeussner E , Buehlmeier A, Schmitz C, Edler von Koch F, Frank HG. - Novel 3D microscopic analysis of human placental villous trees reveals unexpected significance of branching angles. Scientific Reports. 2014 August 4:6192

URL Link

<http://www.nature.com/srep/2014/140826/srep06192/full/srep06192.html>



OPEN

SUBJECT AREAS:
INTRAUTERINE GROWTH
CELLULAR NEUROSCIENCE

Received
16 April 2014

Accepted
8 August 2014

Published
26 August 2014

Correspondence and
requests for materials
should be addressed to
H.-G.F. (hans-georg.
frank@med.uni-
muenchen.de)

* These authors
contributed equally to
this work.

Novel 3D Microscopic Analysis of Human Placental Villous Trees Reveals Unexpected Significance of Branching Angles

Eva Haeussner¹, Antonia Buehlmeier¹, Christoph Schmitz¹, Franz Edler von Koch^{2*} & Hans-Georg Frank^{1*}

¹Ludwig-Maximilians-University, Anatomische Anstalt, Pettenkoferstrasse 11, 80336 Munich, Germany, ²Clinic for Obstetrics and Gynaecology Dritter Orden, Menzinger Str. 44, 80638 Munich, Germany.

The villous trees of human placentas delineate the fetomaternal border and are complex three-dimensional (3D) structures. Thus far, they have primarily been analyzed as thin, two-dimensional (2D) histological sections. However, 2D sections cannot provide access to key aspects such as branching nodes and branch order. Using samples taken from 50 normal human placentas at birth, in the present study we show that analysis procedures for 3D reconstruction of neuronal dendritic trees can also be used for analyzing trees of human placentas. Nodes and their branches (e.g., branching hierarchy, branching angles, diameters, and lengths of branches) can be efficiently measured in whole-mount preparations of isolated villous trees using high-end light microscopy. Such data differ qualitatively from the data obtainable from histological sections and go substantially beyond the morphological horizon of such histological data. Unexpectedly, branching angles of terminal branches of villous trees varied inversely with the fetoplacental weight ratio, a widely used clinical parameter. Since branching angles have never before been determined in the human placenta, this result requires further detailed studies in order to fully understand its impact.

The villous tree is the core part of the functionally relevant microarchitecture of the human placenta^{1–4}. The surface of the villous tree is covered by the villous trophoblast, a syncytialized epithelium in direct apical contact with maternal blood that controls fetomaternal exchange.

Tree-like structures are generally characterized by nodes, which are cornerstones of a complex three-dimensional (3D) pattern of branches⁵. Due to the 3D nature of their branching structure, advanced morphological analysis of trees requires 3D analysis. The correlation of function with 3D structure of trees has been convincingly demonstrated in the field of neuroscience. The digital variants of camera lucida techniques have become the gold standard of computer-assisted quantitative morphological and functional 3D reconstruction of neuronal dendritic trees^{6–9}. Completely new research fields were e.g. opened by the recent finding of the group of TC Südhof that neuroligin-3 mutations in autism are associated with altered 3D dendritic trees and thus altered neuronal connectivity¹⁰. Conceptual understanding of neuronal diversity and connectivity was revolutionized by this type of 3D analysis of dendritic trees¹¹. Cortical neurons in the brain are classified by the 3D structure of their dendritic trees^{12,13}. Moreover, such 3D morphological and multiple reconstruction of cortical neuronal axons and dendritic trees are an important tool to reconstruct the connectome of whole cortical columns, one of the most vivid fields of current neuroscience¹⁴. Similarly, such 3D analysis of the structure of placental villous trees should provide an important link between the mechanisms of villous branching^{4,15} and the capability of the placenta to adapt to varying functional requirements during pregnancy.

The quantitative histological analysis of the villous trees of human placentas has usually been based on thin two-dimensional (2D) histological sections that must be statistically representative 2D samples of the 3D space under examination, allowing mathematically founded statements on elements of the 3D space by the analysis of thin 2D histological sections^{16,17}. However, all analyses of thin 2D histological sections of the human placenta suffer from the fact that nodes and, thus, the branching structure itself are excluded from the analysis. Nodes are not visible on thin 2D histological sections; there is not even a histological nomenclature for nodes. This is exemplified in Figure 1 by a comparison of the histology of a thin 2D histological section with the 3D aspect of an isolated villous tree of a human placenta.

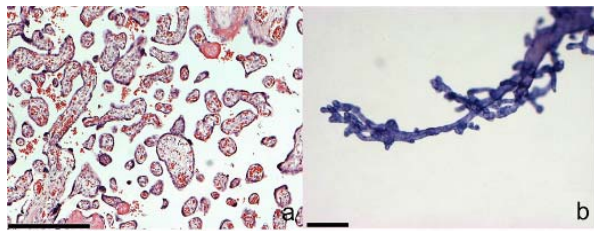


Figure 1 | Comparison of the histology of villous trees of the human placenta and their 3D aspects. (a,b) Comparison of the microscopic aspects of a thin (4–6 μm) histological section of a human placenta after staining with hematoxylin/eosin (a) with the microscopic aspects of a whole-mount isolated villous tree after staining with hematoxylin (b). The scale bars in a and b are 250 μm . (a) Various cross- and longitudinal sections of villi can be recognized. The stromal architecture inside the sectioned villi is visible. The cross-sections of branches belong to an unknown number of villous trees. (b) A single villous tree is visible, and branches are not sectioned. The hierarchical positions of nodes (branching points) and the branching topology can be recognized.

This disadvantage has not been changed by other morphological approaches, particularly by scanning electron microscopy or confocal microscopy. Scanning electron microscopy delivers a 3D impression. Because this impression is not easily quantified in x,y and z, scanning electron microscopy was primarily used to illustrate qualitative aspects of the villous tree. The latter was frequently combined with histology¹⁸ or with transmission electron microscopy^{4,19}. Confocal microscopy can replace physical sectioning by optical sectioning; although software extensions allow post-microscopic 3D reconstruction²⁰, confocal microscopy is primarily a technology that uses extremely thin, optical 2D histological sections. Three-dimensional reconstructions of capillary networks inside of only the last branch of the villous tree (terminal villi) of the human placenta were evaluated by confocal microscopy^{21–23}. Nevertheless, the efficient 3D analysis of villous trees of human placentas across two or more generations of entire branches remains a challenge.

We have hypothesized that the computer-assisted modern camera lucida strategies known from neuroscience can be adapted to the analysis of isolated villous trees of human placentas. Furthermore, we have hypothesized that this adapted camera lucida approach will deliver quantitative 3D data of qualitatively novel information regarding the villous tree of the human placenta. To verify these hypotheses, we isolated villous trees from 50 normal human placentas by careful and diligent dissection under a dissecting microscope. Tissue samples were analyzed with a software, NeuroLucida (MBF Bioscience, Williston, VT, USA), which was originally developed for the analysis of dendritic trees of neurons^{7–9} using settings adapted to the requirements of villous branching. In parallel, thin 2D histological sections (2D sections) of systematically and randomly sampled tissue blocks of a comparable collection of 50 normal human placentas were used to determine volume densities and absolute volumes of placental tissue components using stereology software, Stereo Investigator (MBF Bioscience).

We found that the villous tree of the human placenta can be analyzed with the NeuroLucida approach, that novel and, thus far, unreachable variables can be extracted, and that some of these novel data correlate with the fetoplacental weight ratio, which is a widely used clinical parameter.

Results

Three-dimensional analysis. The whole-mount preparations of villous trees of human placentas prepared for the present study could easily be viewed under a microscope in three dimensions (Fig. 2), and 3D camera lucida datasets could be established in

parallel (Fig. 3); details of these procedures are outlined in the methods section. The 3D data obtained in the present study can be viewed and analyzed in various formats (Fig. 4). To distinguish the novel 3D approach of the present study from histological nomenclature, the parts of villous trees originating at the branching points (nodes) were called branches (b), not villi. Branches were classified by their distance to the nearest terminal end (terminal distance ordering of branches (bT)). The distance to the nearest terminal end was measured in nodes. Thus bT0 designates a branch in terminal position, bT1 a branch one node apart from the nearest terminal end, and, generally, bTX designates a branch X nodes apart from the nearest terminal end (Fig. 4).

We found none of the analyzed branches more than three nodes apart from the nearest terminal end. Accordingly, all analyzed branches were bT0, bT1, bT2 or bT3. The branching of the villous trees was primarily dichotomous. Trichotomous nodes rarely occurred (we recorded 11 trichotomous nodes of 454 analyzed nodes). The villous trees under investigation could be fully reconstructed in 3D (Supplementary Movies S1–4).

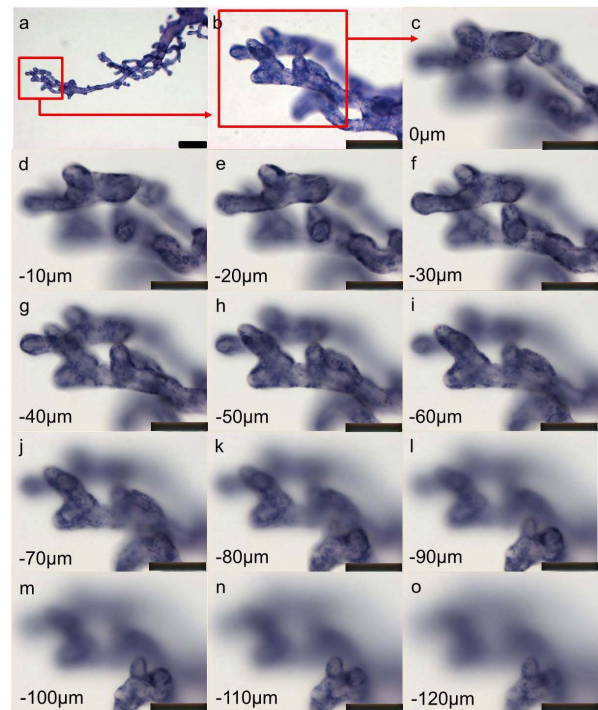


Figure 2 | Whole-mount preparations of villous trees of the human placenta preserve the three-dimensional (3D) character. (a–o) Example of the 3D character (depth) of a whole-mount preparation of an isolated villous tree of a human placenta that was stained with hematoxylin. The example starts with an overview at low magnification ((a), 5 \times objective; scale bar = 250 μm) and shows a screenshot of a single microscopic field of view at working magnification ((b), 20 \times objective; scale bar = 25 μm). The red box in a and b highlights the approximative area of the field of view, which is shown in (c–o) (scale bar = 25 μm). The analysis used live microscopic images at working magnification, whereas the calibrated x, y, z-stage of the used microscope recorded the positions of the focus planes in x, y, and z. (c–o) show an exemplary shift of the focus plane in the z-direction; screenshots were taken from the continuous stream every 10 μm (from 0 μm (c) to 120 μm (o)). Levels of z are given relative to the highest focus plane ((c); 0 μm) in the lower left corner of (c–o).

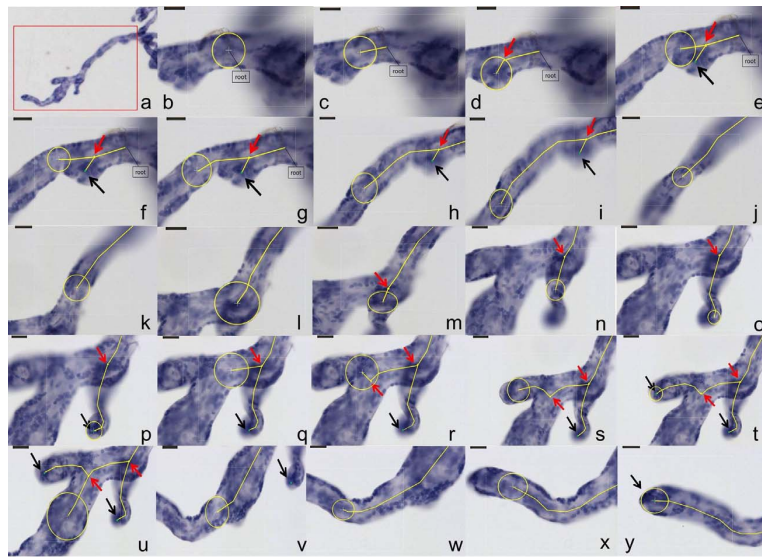


Figure 3 | Computer-assisted viewing generates a quantitative digital three-dimensional (3D) replica of villous trees of the human placenta.

(a–y) Example illustrating the procedure by which the NeuroLucida software assisted in generating a digital and quantitative 3D replica of a whole-mount preparation of an isolated villous tree of a human placenta. The entire instrument and software setup was calibrated such that the software recorded 3D-coordinates of all positions and mouse functions. Measurement and 3D-reconstruction were simultaneous processes. (a) shows an overview at low magnification ($2\times$ objective). The red box in (a) delineates the region of interest. The region of interest is larger than a single microscopic field-of-view at working magnification ($20\times$ objective). (b–y) Screenshots taken at working magnification ($20\times$ objective; scale bar = $25\ \mu\text{m}$ on the top of each tile) while the tracing of the villous tree in the region of interest was in progress. The coordinates of the centerpoint of the yellow circle and the diameter of this circle were recorded while the villous tree was traced in x, y, and z. The work flow started with the most proximal point of the region of interest (root point of the model, (b)). The yellow circle shown could be adjusted to the diameter of the villus in focus using the mouse wheel function. Its moving center defined the center line (yellow line) of each branch. Branching points (nodes; shown as yellow dots with associated red arrows) could be placed by clicking functions. Similarly, terminal ends were defined using the mouse wheel function and are shown as green dots with associated black arrows.

There were statistically significantly ($p < 0.001$) more branches in positions bT0 and bT1 than in position bT2 (Fig. 5A). The dichotomous branching pattern of the villous tree was also indicated by a statistically significant ($p < 0.05$) linear correlation between the numbers of bT0 and bT1 branches of the villous trees (Fig. 5B). The mean ratio of all numbers of bT0 and bT1 branches across all peripheral villous trees analyzed in the present study was 1.30 (Fig. 5B; see also branching scheme in Fig. 4). In contrast, the ratio of the number of bT1 and bT2 branches varied over a wide range (Fig. 5C). The dichotomous branching pattern did not change across the positional transition from bT1 to bT2.

The bT2 branches had a statistically significantly ($p < 0.05$) larger mean diameter than the bT0 branches (Fig. 6A). The distributions of the mean diameters of the bT0, bT1, and bT2 branches broadly overlapped. The mean diameters of the bT0 and bT1 branches correlated statistically significantly ($p < 0.05$; Fig. 6B); the same was found for the mean diameters of the bT1 and bT2 branches ($p < 0.05$; Fig. 6C).

The mean length of the bT0 branches was statistically significantly smaller than the mean length of the bT1 and bT2 branches ($p < 0.01$; Supplementary Figure S1). The distributions of mean lengths of the bT0, bT1, and bT2 branches broadly overlapped. The length of individual bT0 branches plotted against the angle at which they branch off their respective bT1 branch (planar branching angle of branch bT0) showed a broad distribution of planar branching angles, whereas extremely long branches only occurred at planar branching angles below 60° (see Supplementary Figure S1). The 3D datasets of the present study were used as input for a branching analysis, which consisted of a modified Sholl-analysis (for details see methods section and Supplementary Figure S2). This analysis delivered mathematical estimates of branching characteristics, specifically the Sholl-

coefficient k and the branching parameter $\log a$ (Supplementary Figure S2; Supplementary Table S1).

Means and standard deviations of all 3D parameters are provided in Supplementary Table S1.

Clinical data, tissue processing and histology. Clinical data of the two placenta collections used in the present study were not statistically significantly different from each other (Supplementary Table S2). The histopathological evaluation of HE sections of the placentas analyzed in the present study showed no histopathological deviations. No signs of autolytic change or tissue decomposition were detected. The processing time leading up to availability of raw data for an individual sample was estimated for quantitative analysis on thin 2D histological sections (76.1 h) and NeuroLucida-assisted 3D analysis (19.8 h), see Supplementary Table S3. The volume estimates of various tissue components are provided in Supplementary Table S4. The mean volume of the villous tree was determined to be $197.03\ \text{ml}$ ($\pm 48.62\ \text{ml}$ standard deviation).

Nonparametric multiple comparison analysis. Nonparametric multiple comparison analysis of the clinical parameters placenta weight (PW), birth weight (BW), fetoplacental weight ratio (PW/BW), and the 3D parameters of the villous tree showed a statistically significant negative correlation ($p < 0.05$) of PW/BW with the mean planar branching angle of the bT0 branches (Fig. 7A). Accordingly, with increasing PW/BW, the mean planar branching angle of the bT0 branches decreased.

The volume densities of the villous tree and intervillous space determined by design-based stereology from thin 2D histological sections did not correlate with PW, BW, or PW/BW (Fig. 7B,C). The absolute volumes of the villous tree and intervillous space calculated from the respective volume densities (using placental weight

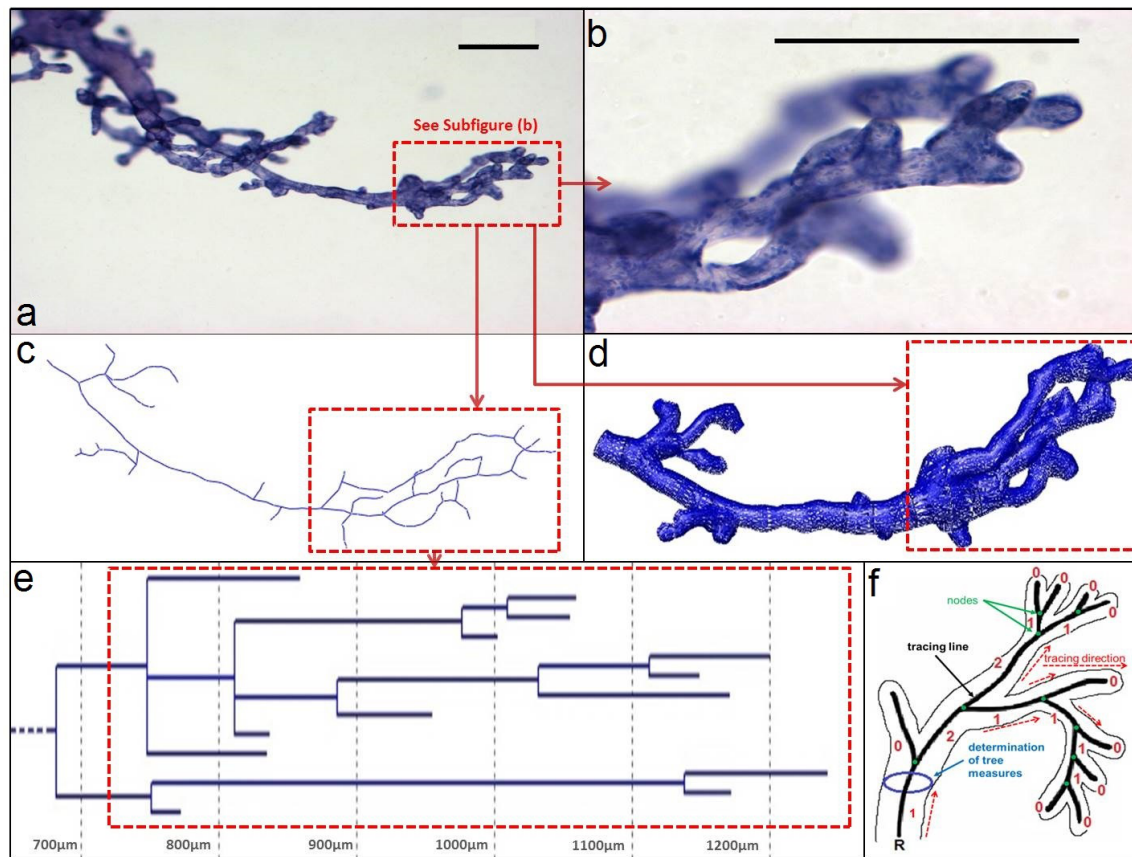


Figure 4 | The 3D data can be viewed and analyzed in various formats. (a–e) Example illustrating different graphing options of a three-dimensional data set obtained with Neurolucida software (MBF Bioscience) assisted reconstruction of a whole-mount preparation of a villous tree of a human placenta. (a) Overview of a hematoxylin-stained peripheral villous tree as viewed at low magnification (5× objective; scale bar = 250 μm). (b) Detailed view of a subtree within a single microscopic field of view at the magnification used for tracing the villous tree with Neurolucida software (20× objective; scale bar = 250 μm). The part of the visual field containing the subtree shown in (b) is labeled by rectangular red boxes in (a) and (c–e). (c–e) Various options to visualize the 3D data sets obtained by Neurolucida software. The center lines of traced branches are shown in the skeletonized view (c); 3D reconstructions of the traced branches based on diameters are shown in (d). The dendrogram view in (e) shows the total segmental length and hierarchical relations of branches. (f) Sketch of the working process in the Neurolucida software showing the tracing direction (from root to terminal ends) and the classification of branches by the terminal distance (from terminal ends to root, in numbers), the labeling of nodes/branching points and the determination of tree measures. (f) Was modified from the Neurolucida Explorer software with permission from MBF Bioscience.

and the average density of placental tissue, for details see methods section) correlated statistically significantly with PW, BW, and PW/BW (data not shown). However, it should be noted that these correlations of the absolute volumes with PW, BW, and PW/BW are due to usage of PW as a factor in the calculation of the volume density raw data; PW, BW, and PW/BW correlate with each other²⁴ and thus also with the absolute volumes.

Discussion

The present study used a novel, quantitative 3D approach to analyze the peripheral parts of villous trees of normal human placentas. In the present study, we show that the 3D analysis of the peripheral human placental villous tree is less laborious than the established analysis strategies (Supplementary Table S3) due to efficient tissue processing and rapid data acquisition. This is enabled by the fact that the Neurolucida-supported 3D analysis is not dependent on any type of pre-existing 3D reconstruction (e.g. from confocal microscopy image stacks or from other sectioning/reconstruction tools), but rather generates its own 3D image during the measurement; the measurement is thus not an extra step. This principle of simultan-

eous measurement and 3D imaging is thus an elegant and convenient feature of the Neurolucida approach. If the adaptations and precautions of the present study are considered, almost any high quality research microscope equipped for neuronal dendrite tracing will be able to deliver valuable 3D data regarding the villous tree of human placenta. There is no specific requirement for scanning electron microscopy^{18,25}, confocal microscopy, or other sophisticated sectioning/3D reconstruction approaches^{20,26} in order to obtain such data. This analysis is analogous to the current state of neuroscience, where the majority of the neuronal dendritic and axonal 3D analyses are based on bright-field microscopy^{7–9} due to its broad compatibility with basic histological staining methods.

The 3D analysis in the present study is specifically designed for the analysis of tree structures in 3D. A core feature of this method is the ability to view trees while the trees are simultaneously being reconstructed as a digital replica²⁷. Many details that are invisible on thin 2D histological sections can be analyzed by 3D methods²⁸. Such details include, but are not limited to nodes, branching angles, diameters, and lengths of branches in relation to the branching hierarchy/topology. Possible limitations of this method stem from the

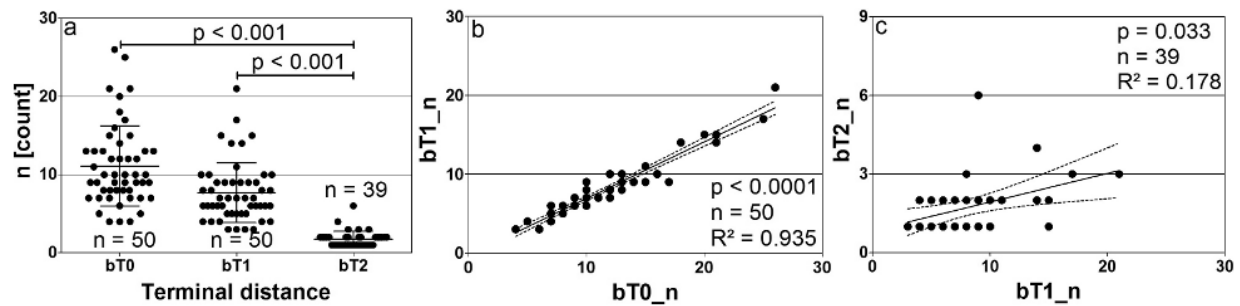


Figure 5 | Branch numbers reveal construction rules of the peripheral villous tree of the human placenta. (a–c) Number of branches. Each dot represents the number of branches of a single isolated villous tree fragment. (a) Number of branches (n[count]) stratified by the terminal distance to which the branches belong (bT0, bT1, and bT2). The mean, standard deviation, and number of samples are shown. The number of branches in positions bT1 and bT2 was found to be statistically significantly lower than the number of branches in position bT0. The values of p and the number (n) of villous trees evaluated are given inside the graph. (b,c) Correlation of the number of branches in two neighboring terminal distance positions. The regression lines (straight line) are shown together with their 95% confidence interval (dashed lines). The p-value, expressing the statistically significant deviation of the slope from zero, R^2 a measure of the goodness of fit, and the number of villous trees evaluated (n) are given inside the graphs. (b) Number of bT1 (bT1_n) branches as a function of the number of bT0 (bT1_0) branches. (c) Number of bT2 (bT2_n) branches as a function of the number of bT1 (bT21_n) branches.

maximally feasible focus distance of the objective or the villi being too crowded or too thick to be viewed in full depth under a bright-field microscope. With the tracing of villous trees, quantitative microscopic tracing operates at the upper end of the feasible scale. Therefore, the present study focused on the most peripheral part (1–2 mm) of the villous tree of the human placenta. Nevertheless, to the best of our knowledge, no other light microscopic method is able to follow villous trees of the human placenta over an analysis interval of 2 mm with comparable ease and efficiency. Moreover, the focus of this 3D analysis on the most peripheral branches of the villous tree is not necessarily compromising its biological relevance. The peripheral branches of the villous tree arise during the second half of pregnancy^{2,4,19,29–31}. Important clinical syndromes, such as preeclampsia and intrauterine growth retardation, also develop during the second half of pregnancy^{4,32}.

The analysis of thin 2D sections/images primarily delivers quantitative data regarding the corresponding 3D space (see, e.g., Supplementary Table S4); thus, the analysis of thin 2D histological sections is highly dependent on the sampling procedures. Using sectioning, the analysis of thin 2D histological sections avoids the potential limitations of optical intransparency or tissue thickness.

Aspects other than the volume densities determined in the present study (e.g., star volumes, surface areas, etc.) can also be analyzed on thin 2D histological sections^{33,34}. However, structural details that are invisible in thin 2D histological sections cannot be analyzed in such sections. Notably, nodes, branches, branching angles, and branching hierarchy/topology are invisible in thin 2D histological sections (see Fig. 1).

Thus, it is obvious that 3D analysis and the analysis of thin 2D histological sections supplement each other (see also Supplementary Tables S1 and S4). The conventional analysis of thin 2D histological sections can make statistically valid estimates of placental properties. However, such analysis neither produces nor takes into account data describing the 3D branching structure of the villous tree. Three-dimensional analysis performs absolute measurements of nodes, branches, and their relations with each other and associated parameters, all of which cannot be done by analysis of thin 2D histological sections.

We found that branches in positions bT0 and bT1 occurred at a fixed rate in relation to each other (see Fig. 5B). This finding is self-interpreted because of the general dichotomous branching pattern of the villous tree. However, although the dichotomous branching pat-

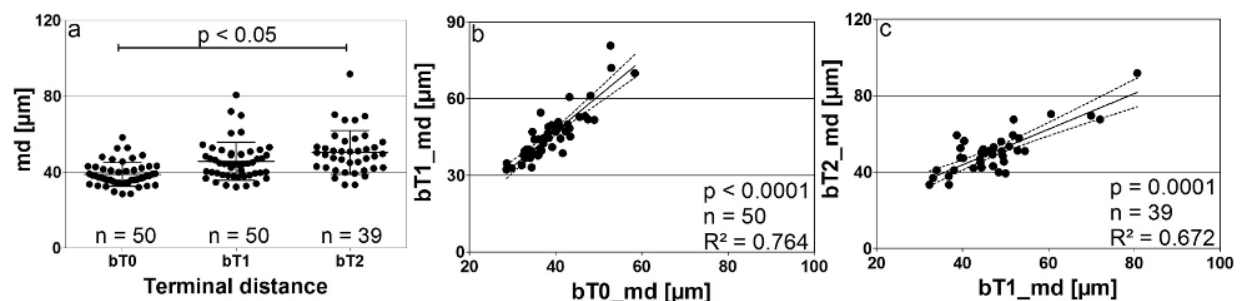


Figure 6 | Diameter distributions of branches of the human placenta. (a–c) Each dot represents the mean diameter of branches of a single isolated villous tree fragment. (a) Mean diameters of branches (md [μm]), separated into various branch terminal distance (bT0, bT1, and bT2). The mean, standard deviation, and individual mean diameters (dots) are shown. The mean diameters of branches in position bT2 statistically significantly differ from the mean diameters of branches in position bT0. The p-values and number of villous trees evaluated (n) are given in the graph. (b,c) Correlation of mean diameters of branches in two neighboring hierarchical positions. The regression line (solid line) is shown with a 95% confidence interval (dashed lines). The value of p describing statistically significant deviation of the slope from zero, R^2 as a measure of the goodness of fit, and the number villous trees evaluated (n) are given in the graphs. (b) The mean diameters of bT1 (bT1_md) branches as a function of the mean diameters of bT0 (bT0_md) branches. (c) The mean diameters of bT2 (bT2_md) branches as a function of the mean diameters of bT1 (bT1_md) branches.

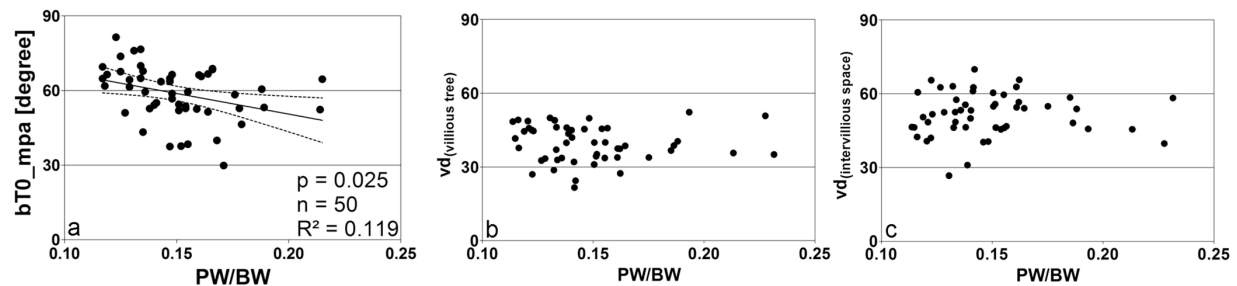


Figure 7 | The mean planar branching angle of terminal branches in the human placenta correlates with the fetoplacental weight ratio. Scatter plots of results of the 3D analysis (a) and analysis of thin 2D histological sections (b,c) against the fetoplacental weight ratio (PW/BW ratio, dimensionless factor). (a) The mean planar branching angles ($n = 50$) of the bT0 branches (bT0_mpa). The p-value inside the graph was calculated using the multiple nonparametric correlation analysis (Spearman-rho, corrected for multiple comparison according to Benjamini and Hochberg, 1995⁴¹). Linear correlation analysis (straight line) was calculated with 95% confidence intervals (dashed lines); R^2 is a measure for the goodness of linear fit. (b,c) Scatter plots of volume density of the villous tree (y-axis; $vd_{\text{villous tree}}$; (b)) and volume density of the intervillous space (y-axis; $vd_{\text{intervillous space}}$; (c)) as a function of the PW/BW ratio. Volume densities did not correlate with the PW/BW ratio in the multiple nonparametric correlation analysis.

tern remains constant, the numbers of branches in positions bT1 to bT2 considerably varied (see Fig. 5C). Taken together, this result would be consistent with the interpretation that branches bT0, bT1, and the nodes connecting these branches form a repetitively occurring 3D building unit of the peripheral villous tree, and that these 3D building units are attached to branches in bT2 at a highly variable rate.

Sholl analysis is an important tool for the classification of neurons and their connectivity in the brain³⁵. The strength of this analysis lies in the mathematical recognition of general branching patterns. The present study showed that Sholl analysis can be adapted to the villous tree of the human placenta. Whether Sholl analysis will be able to discriminate between branching patterns of normal placentas and those patterns of complicated pregnancies is beyond the scope of the present study.

For the first time, the present study determined the diameters, lengths, and linked parameters, such as surface area and volume, of branches of the peripheral 2 mm of the villous tree, without interference from sectioning artifacts, in many villous trees. Diameters and, to a certain extent, lengths and numbers are principally recognizable as cross-sections of villi in thin 2D histological sections and could potentially be used to reversely identify the terminal/non-terminal position of a sectioned branch. The present study showed statistically significant differences in diameters and lengths from bT0 over bT1 to bT2 (see Figs. 5–7). However, the reverse diagnosis of the terminal or non-terminal position of a given branch by one of these parameters is not feasible due to broad overlap in parameter distributions. Although this is the case, the 3D data of the present study did not suffer from the additional scatter of diameter distributions, which would be caused by the histological sectioning of branches in various angles. Thus, it is not feasible to determine positions of sectioned branches of the most peripheral 2 mm of the villous tree (bT0, bT1, and bT2) on thin 2D histological sections using, e.g., their diameters. This finding is in full agreement with early morphological descriptions of villi in the peripheral part of the villous tree of the human placenta²⁹.

The diameters of branches in each of the positions bT0, bT1, and bT2 showed a linear correlation across these positions in the same villous tree, i.e., thicker branches in position bT2 produced on average thicker branches in positions bT1, and bT1 branches produced on average thicker branches in positions bT0 (see Fig. 6B,C). These diameter relations across branches of the same tree are possibly a tree-specific feature individually characterizing each villous tree.

Branching angles and nodes are structures that are invisible on thin 2D histological sections. These structures “disappear” by the reduction of the 3D tree structure to 2D sections (see Fig. 1) and

have never been determined by any known 2D or 3D method of placental analysis. Branching angles and nodes could possibly reflect the different mechanisms of branching that are associated with the villous tree, namely villous sprouting via mesenchymal villi for stem villus branching and angiogenesis-related branching of terminal villi from intermediate villi⁴. Angiogenesis-related branching of terminal villi from intermediate villi is seen as an especially important mechanism of placental functional adaptation¹⁵.

Unexpectedly, in the present study, the branching angles of branches bT0 correlated with the fetoplacental weight ratio PW/BW (Fig. 7A). In contrast, no parameter obtained by the conventional analysis of thin 2D histological sections correlated with the PW/BW ratio (Fig. 7B,C). The PW/BW ratio is a widely used clinical parameter^{1,4,36}. It is outside the scope of the present study to explore possible functional relations between branching angles of terminal branches (bT0) of the villous tree and the PW/BW ratio. However, the plotting of branching angles of terminal branches against the length of terminal branches showed that the branching angles scattered over a wide range and extremely long terminal branches occurred at angles below 60° (Supplementary Figure S1). These properties indicated that the terminal branches are much more heterogeneous in structure than previously expected based on the description of terminal villi from histology of thin 2D histological sections^{2,4,29}. A detailed exploration of the structural heterogeneity of terminal branches will likely enable further conceptual understanding of the correlation between the PW/BW ratio and terminal branching angles.

In summary, the present study successfully adapted camera lucida-based analysis strategies to the peripheral part of the villous trees of normal human placentas. Nodes and node-related branching structures (branching hierarchy, angles, diameters, and lengths) can now be efficiently measured in 3D. Such primary 3D data can be further processed into secondary parameters by, e.g., Sholl analysis. Branching angles are typical 3D parameters and are correlated with the fetoplacental weight ratio PW/BW, a widely used clinical parameter. The latter encourages the exploration of possible alterations of the 3D structure of villous trees of human placentas from obstetrically complicated pregnancies, particularly preeclampsia and intrauterine growth retardation.

Methods

Study design. The present study used 100 human placentas split into two samples of 50 placentas from clinically normal pregnancies. Both cohorts of placentas were collected at the Department of Obstetrics and Gynecology of the hospital “Dritter Orden”, Munich, Germany. The normal course of each pregnancy was assessed by obstetricians based on clinical information regarding the pregnancy and delivery. Placentas were collected after informed consent of mothers/parents was obtained.



Placentas were excluded when: no informed consent of the mothers/parents could be obtained, the language skills of the mothers/parents limited the understanding of information concerning the study, or psychiatric problems or any other condition caused doubts regarding the mothers/parents ability to independently decide. All work was conducted according to relevant guidelines and regulations. This study was approved by the ethics committee of the Ludwig-Maximilians-University (Munich, Germany) under the number 084-11. All data were anonymized. The thickness of the placenta was determined by ultrasound. The placenta weight (PW) was measured prior to tissue sampling and processing without the umbilical cord but with membranes²⁴. The birth weight (BW) was determined immediately after birth, and the fetoplacental weight ratio (PW/BW) was calculated¹ (Supplementary Table S2).

The cohort of placentas used for the quantitative analysis of thin 2D histological sections was collected between April 2011 and September 2011. The cohort of placentas used for the preparation of single villous trees and subsequent Neurolucida-assisted 3D-analysis was collected between February 2012 and April 2013.

Common procedures for both placenta collections. All placentas were cooled at 4°C immediately after birth and processed within 5.26 h (Median; Max = 23.41 h, Min = 2.31 h; samples for thin 2D histological sections) or 3.28 h (Median; Max = 8.20 h, Min = 1.35 h; samples for 3D analysis) at the Department of Anatomy II of Ludwig-Maximilians-University (Munich, Germany). Six sampling sites were chosen systematically and randomly from each placenta²⁴, and tissue blocks containing the entire thickness of the placenta were collected, fixed and embedded in paraffin as previously described²⁴.

Sections of all specimens were stained with hematoxylin/eosin (HE). All HE sections were qualitatively evaluated in order to confirm the absence of signs of tissue damage/autolysis, inflammation and/or disturbed differentiation of trophoblast.

Two-dimensional thin histological sections. From the six blocks of paraffin-embedded tissue of each placenta, the number 5 was chosen by the roll of a dice. From each placenta, sections of the fifth tissue block were used for the volume estimations on thin 2D histological sections (see Supplementary Table S3).

Whole-mount preparations of villous trees. For the preparation of single, isolated peripheral parts of villous trees (henceforth called “peripheral villous trees”), an additional sample (edge length of 2–3 cm) was collected within a distance of 5 cm from the umbilical cord insertion and transferred to physiological saline at 4°C. The preparation of peripheral villous trees began within one hour after sampling and was performed under a binocular microscope (M400, Wild Heerbrugg, Heerbrugg, Switzerland) with additional light (KL 1500 electronic, Schott/Zeiss, Jena, Germany). Free bushes of peripheral villi were identified, removed using small scissors, and fixed in 4.5% formaldehyde (Roti-Histofix, Carl Roth, Karlsruhe, Germany) in small glass jars overnight. The probes were rinsed 3 × 10 minutes with tap water, bleached in 3% H₂O₂ for 20 minutes, and washed 3 × 5 minutes in distilled water. Mayer’s hematoxylin was applied for 7 minutes at room temperature with gentle agitation, and then the probes were washed in distilled water (acidified by acetic acid to a pH of 2.4) for 3 minutes. Bluing was achieved in tap water for 5 minutes and the probes were then transferred back to distilled water. Following a graded series of ethanol (50%, 70%, 80%, 96% and 100%; 5 min each), the probes were transferred to a mixture of ethanol/xylene (1:1, 5 min) and then to fresh and pure xylene 2 × 5 min. From xylene, the probes were infiltrated with xylene/DPX (1:1, 4 h, DPX: Mountant for histology, Sigma Aldrich nr. 06522, Munich, Germany), and mounted in DPX on a concave slide with enough room to allow the unfolding of the villous tree and such that the 3D structure of the peripheral villous trees remained intact. These preparations have a true 3D character and are free from oppressing contact with the concave slide or cover glass (see Fig. 2).

Analysis of thin 2D histological sections. Volume estimates were performed according to the Cavalieri principle^{37,38} on single thin (4–6 µm) histological sections using a computerized stereology workstation, which consisted of a modified light microscope (Axioskop; Zeiss, Jena, Germany) with motorized specimen stage for automatic sampling (MBF Bioscience) and stage controller (Type MAC 6000; Ludl Electronics, Hawthorne, NY, USA), focus encoder (Type MT 1271; Heidenhain, Traunreut, Germany), CCD color video camera (1600H × 1200V pixels; MBF Bioscience, Williston, VT, USA) and stereology software (Stereo Investigator version 10; MBF Bioscience). This approach delivers volume densities as raw data, which were allocated to the villous tree (stratified by the villous stroma, vessel lumen, endothelium, and syncytiotrophoblast), to the intervillous space and to the fibrinoid. Then, absolute volumes were calculated by multiplying volume densities with the placental volume (placental volume is defined by the placental weight (PW) divided by the density of placental tissue (1.03 g/ml)).

Computer-assisted 3D analysis. Peripheral villous trees were previewed at low magnification (2× microscope objective; Fig. 3A). Tracing with Neurolucida (version 10.54; MBF Bioscience) was performed using a 20× objective (Fig. 3B–Y) with the working direction from the proximal toward the terminal end of the peripheral villous tree (Fig. 3B–Y). Tree ordering for measurements was set to “Terminal Distance Ordering” (Figs. 3B–Y and 2) because the terminal end was the biologically defined end of the isolated peripheral villous trees. Terminal Distance Ordering classifies branches according to their distance in nodes from the terminal end of the villous tree. While viewing the tree, nodes and branches were individually labeled and circumferences of the villi were continuously recorded by mouse wheel functions

(Fig. 3B–Y). The measuring system generated a digital 3D replica of the peripheral villous tree under investigation in parallel to the process of tracing. These data were analyzed with Neurolucida Explorer software (MBF Bioscience) using the option “branching structure analysis”. The outcomes can be visualized in various ways in Neurolucida or Neurolucida Explorer software (Fig. 4, Supplementary Movies S1–4).

We used two microscope systems: (i) an Axioskop (Zeiss, Goettingen, Germany) with a motorized XYZ specimen stage (Maerzhäuser, Wetzlar, Germany), an LEP MAC6000 XYZ 3-axis stage controller (Ludl), a focus encoder (Type MT 1271; Heidenhain), and a color digital camera (3/4” CCD chip 1.92 MP, 1600H × 1200V pixel, MBF Bioscience; and (ii) a BX50 (Olympus, Tokyo, Japan) with motorized XYZ specimen stage (MBF Bioscience), an LEP MAC6000 XYZ 3-axis stage controller (Ludl), focus encoder (Type MT 1271; Heidenhain) and color digital camera (1/2” CCD chip, 1392 × 1040 pixels, MBF Bioscience).

The parts of villi connecting two nodes or connecting a terminal end with a node were named branches (b). Branches were further classified by their distance to the nearest terminal end (bT, with the T indicating classification by terminal distance). The distance was measured by the number of nodes to the nearest terminal end. Thus, “bT0” encodes a branch in the terminal position, “bT1” encodes a branch one node apart from the nearest terminal position, and in general, “bTX” encodes a branch X nodes apart from the nearest terminal end (Fig. 2F). We collected the numbers of nodes and branches on each level of “Terminal Distance Ordering” and data regarding the planar branching angle, diameter, length, surface area, and volume of each individual branch. These data were aggregated by the terminal distances of branches for each villous tree as the mean planar branching angle (bTX_mpa), mean diameter (bTX_md), mean length (bTX_ml), mean surface area (bTX_ms) and mean volume (bTX_mv).

The planar branching angle of a given branch was defined as the change in the direction of the branch with respect to the previous branch. The direction of each branch was derived from its endpoints (a node or a terminal end). Of 50 peripheral villous trees, 11 did not show bT2 branches (n = 39 for bT2). Of the remaining 39 bT2 branches, the planar branching angle of bT2 branches could not be determined for six samples due to a missing previous branch (n = 33 for bT2_mpa).

Sholl analysis. Sholl analysis is a mathematical approach for the analysis of dendritic trees³⁹, and Sholl analysis routines are included in software tools designed for tracing dendritic trees, such as Neurolucida²⁷. The tracing direction and analysis direction are usually identical (from perikaryon (root) to terminal end) in the Sholl analysis of dendritic trees. For the placenta, this direction had to be changed because there is only one physiologically defined end of an isolated villous tree; the terminal end. Thus, villous trees were traced from the root (stem villus) to the terminal end, whereas Sholl analysis was manually performed in an opposite direction from terminal end toward the root (see Supplementary Figure S2).

The Sholl analysis of villous trees was performed on the dendrograms exported from Neurolucida Explorer software (see Supplementary Figure S2). The Sholl analysis included the villous trees between the first node (near the terminal end) and the last node (near the root) of the tree under investigation. A grid of measuring lines representing concentric circles was placed in 50 µm intervals from the terminal end to the root. All grid lines falling into the analysis interval between the first and last node were included. The first grid line falling into the analysis interval was set to 1 µm. This setting delivers a set of data linking the distance, in µm, and the number of intersecting branches (for details see Supplementary Figure S2). The distances were transformed to the area of the respective concentric circle, and the Sholl plot was performed as usual³⁹. The number of intersections with branches by area (N/area) was plotted on the y-axis (logarithmically) whereas distances were plotted on the x-axis (logarithmically). Then, the Sholl regression coefficient (k) was determined by linear regression as the slope of the straight line, together with the y-intercept at X = 0 (log a) in GraphPad Prism software (Version 5.04, GraphPad Software, San Diego, CA, USA), see Supplementary Figure S2.

Statistical analyses. For all investigated parameters (Supplementary Tables S1, S3, S4), the mean and standard deviation were calculated using SPSS software (Version 20, IBM, Armonk, NY, USA)⁴⁰. Because normal distribution could not be confirmed by Kolmogorov-Smirnov test (SPSS), further statistical analyses were based on non-parametric procedures. Multiple non-parametric bivariate correlation (Spearman-rho) analyses with post-hoc corrections for multiple comparisons according to Benjamini and Hochberg⁴¹ (p-value < 0.05) were performed in R⁴² using the package “psych”⁴³ for multiple comparisons and the function p.adjust for post hoc corrections. Linear regression analyses⁴⁰ and Kruskal-Wallis tests with Dunn’s multiple comparison adjustments were performed in GraphPad software.

1. Boyd, J. D. & Hamilton, W. J. *The human placenta*. (Heffer, Cambridge, 1970).
2. Kaufmann, P. Development and differentiation of the human placental villous tree. *Bibl. Anat.* **22**, 29–39 (1982).
3. Kingdom, J., Huppertz, B., Seaward, G. & Kaufmann, P. Development of the placental villous tree and its consequences for fetal growth. *Eur. J. Obstet. Gynecol. Reprod. Biol.* **92**, 35–43 (2000).
4. Benirschke, K., Burton, G. & Baergen, R. N. *Pathology of the human placenta*. (Springer, Berlin and London, 2012).
5. Barker, S. B., Cumming, G. & Horsfield, K. Quantitative morphometry of the branching structure of trees. *J. Theor. Biol.* **40**, 33–43 (1973).



6. Wollaston, W. H. Description of the Camera Lucida. *Philosophical Magazine* **27**, 343–347 (1807).
7. Halavi, M., Hamilton, K. A., Parekh, R. & Ascoli, G. A. Digital reconstructions of neuronal morphology: three decades of research trends. *Front. Neurosci.* **6**, 49–61 (2012).
8. Marx, M., Günter, R. H., Hucko, W., Radnikow, G. & Feldmeyer, D. Improved biocytin labeling and neuronal 3D reconstruction. *Nat. Protoc.* **7**, 394–407 (2012).
9. Aguiar, P., Sousa, M. & Szucs, P. Versatile morphometric analysis and visualization of the three-dimensional structure of neurons. *Neuroinformatics* **11**, 393–403 (2013).
10. Földy, C., Malenka, R. C. & Südhof, T. C. Autism-associated neuroligin-3 mutations commonly disrupt tonic endocannabinoid signaling. *Neuron* **78**, 498–509 (2013).
11. Eisenstein, M. Neural circuits: Putting neurons on the map. *Nature* **461**, 1149–1152 (2009).
12. Helmstaedt, M., Sakmann, B. & Feldmeyer, D. The relation between dendritic geometry, electrical excitability, and axonal projections of L2/3 interneurons in rat barrel cortex. *Cereb. Cortex* **19**, 938–950 (2009).
13. Oberlaender, M. *et al.* Three-dimensional axon morphologies of individual layer 5 neurons indicate cell type-specific intracortical pathways for whisker motion and touch. *Proc. Natl. Acad. Sci. USA* **108**, 4188–4193 (2011).
14. Oberlaender, M. *et al.* Cell type-specific three-dimensional structure of thalamocortical circuits in a column of rat vibrissa cortex. *Cereb. Cortex* **22**, 2375–2391 (2012).
15. Kaufmann, P., Mayhew, T. M. & Charnock-Jones, D. S. Aspects of human fetoplacental vasculogenesis and angiogenesis. II. Changes during normal pregnancy. *Placenta* **25**, 114–126 (2004).
16. Howard, C. V. & Reed, M. G. *Unbiased stereology: Three-dimensional measurement in microscopy*. (BIOS Scientific Publ., Oxford, 1998).
17. Mayhew, T. M. Stereology and the placenta: where's the point? – a review. *Placenta* **27**, S17–25 (2006).
18. Castellucci, M., Scheper, M., Scheffen, I., Celona, A. & Kaufmann, P. The development of the human placental villous tree. *Anat. Embryol. (Berl)* **181**, 117–128 (1990).
19. Habashi, S., Burton, G. J. & Steven, D. H. Morphological study of the fetal vasculature of the human term placenta: scanning electron microscopy of corrosion casts. *Placenta* **4**, 41–56 (1983).
20. Karen, P., Jirkovska, M., Tomori, Z., Demjenova, E., Janacek, J. & Kubinova, L. Three-dimensional computer reconstruction of large tissue volumes based on composing series of high-resolution confocal images by GlueMRC and LinkMRC software. *Microsc. Res. Tech.* **62**, 415–422 (2003).
21. Jirkovska, M. *et al.* Topological properties and spatial organization of villous capillaries in normal and diabetic placentas. *J. Vasc. Res.* **39**, 268–278 (2002).
22. Jirkovska, M., Janacek, J., Kalab, J. & Kubinova, L. Three-dimensional arrangement of the capillary bed and its relationship to microrheology in the terminal villi of normal term placenta. *Placenta* **29**, 892–897 (2008).
23. Jirkovska, M. *et al.* The branching pattern of villous capillaries and structural changes of placental terminal villi in type 1 diabetes mellitus. *Placenta* **33**, 343–351 (2012).
24. Haeussner, E., Schmitz, C., Koch, F. V. & Frank, H. G. Birth weight correlates with size but not shape of the normal human placenta. *Placenta* **34**, 574–582 (2013).
25. Burton, G. J. The fine structure of the human placental villus as revealed by scanning electron microscopy. *Scanning Microsc.* **1**, 1811–1828 (1987).
26. Kubinová, L. *et al.* Confocal stereology and image analysis: methods for estimating geometrical characteristics of cells and tissues from three-dimensional confocal images. *Physiol. Res.* **53 Suppl 1**, S47–55 (2004).
27. Glaser, J. & Glaser, E. Neuron imaging with neurolucida — A PC-based system for image combining microscopy. *Comput. Med. Imag. Grap.* **14**, 307–317 (1990).
28. van Oppenraaij, R. H. F. *et al.* Vasculogenesis and angiogenesis in the first trimester human placenta: An innovative 3D study using an immersive virtual reality system. *Placenta* **30**, 220–222 (2009).
29. Kaufmann, P., Sen, D. K. & Schweikhart, G. Classification of human placental villi. I. Histology. *Cell Tissue Res.* **200**, 409–423 (1979).
30. Sen, D. K., Kaufmann, P. & Schweikhart, G. Classification of human placental villi. II. Morphometry. *Cell Tissue Res.* **200**, 425–434 (1979).
31. Mayhew, T. M. Fetoplacental angiogenesis during gestation is biphasic, longitudinal and occurs by proliferation and remodelling of vascular endothelial cells. *Placenta* **23**, 742–750 (2002).
32. Rath, W. *Geburtshilfe und Perinatalogie*. (Thieme, Stuttgart, 2010).
33. Karimu, A. L. & Burton, G. J. Star volume estimates of the intervillous clefts in the human placenta: How changes in umbilical arterial pressure might influence the maternal placental circulation. *J. Dev. Physiol.* **19**, 137–142 (1993).
34. Mayhew, T. M. & Sisley, I. Quantitative studies on the villi, trophoblast and intervillous pores of placentae from women with well-controlled diabetes mellitus. *Placenta* **19**, 371–377 (1998).
35. Radley, J. J. *et al.* Chronic behavioral stress induces apical dendritic reorganization in pyramidal neurons of the medial prefrontal cortex. *Neuroscience* **125**, 1–6 (2004).
36. Cetin, I. & Taricco, E. [Clinical causes and aspects of placental insufficiency] *The Placenta and Human Developmental Programming* [Burton, G., Barker, D., Moffett, A. & Thornburg, K. (eds.)] [114–125] (Cambridge University Press, Cambridge, 2011).
37. Gundersen, H. J. & Jensen, E. B. The efficiency of systematic sampling in stereology and its prediction. *J. Microsc.* **147**, 229–263 (1987).
38. Schmitz, C. & Hof, P. R. Design-based stereology in neuroscience. *Neuroscience* **130**, 813–831 (2005).
39. Sholl, D. A. Dendritic organization in the neurons of the visual and motor cortices of the cat. *J. Anat.* **87**, 387–406 (1953).
40. Bronstein, I. N. & Semendjajew, K. A. *Taschenbuch der Mathematik* (Deutsch, Thun, 2001).
41. Benjamini, Y. & Hochberg, Y. Controlling the false discovery rate: a practical and powerful approach to multiple testing. *J. R. Stat. Soc. Series B* **57**, 289–300 (1995).
42. R Core Team. R: A Language and Environment for Statistical Computing. Vienna and Austria: R Foundation for Statistical Computing. URL: <http://www.R-project.org/> (Date of access: 12/04/2014) (2013).
43. Revelle, W. psych: Procedures for Psychological, Psychometric, and Personality Research. Evanston and Illinois: Northwestern University. URL: <http://CRAN.R-project.org/package=psych> (Date of access: 12/04/2014) (2013).

Acknowledgments

The authors acknowledge the skillful technical assistance and diligent work of the entire team of technicians of the Department of Anatomy II at LMU Munich, namely B. Aschauer, A. Baltruschat, U. Fazekas, S. Kerling, C. Stanglmair, B. Mosler and S. Tost. We would also like to express our thanks to the obstetricians, midwives, and nurses of the Dritter Orden hospital (Munich, Germany) who enabled the clinical work of this study with great care and engagement. Benedikt Kropp assisted with R graphics code. P. Angstman assisted in video compression. For proofreading and helpful discussions regarding the preparation of the manuscript, we would like to thank N. Angstman, N. Csaszar, S. Milz and K. Sternecker. Three-dimensional analysis is part of the doctoral thesis of E.H. The analysis of thin 2D histological sections is part of the doctoral thesis of A.B.

Author contributions

E.H. performed the 3D analysis. A.B. performed analysis on thin 2D histological sections. F.v.K., C.S. and H.G.F. designed the study. F.v.K. was responsible for obstetrical tasks. E.H. and H.G.F. prepared figures and tables. H.G.F., C.S., F.v.K. and E.H. wrote the manuscript.

Additional information

Supplementary information accompanies this paper at <http://www.nature.com/scientificreports>

Competing financial interests: The authors declare no competing financial interests.

How to cite this article: Haeussner, E., Buehlmeier, A., Schmitz, C., von Koch, F.E. & Frank, H.-G. Novel 3D Microscopic Analysis of Human Placental Villous Trees Reveals Unexpected Significance of Branching Angles. *Sci. Rep.* **4**, 6192; DOI:10.1038/srep06192 (2014).

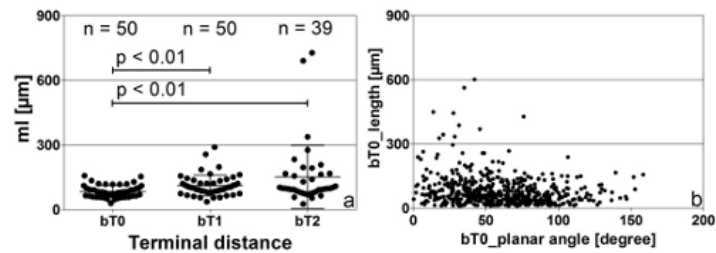


This work is licensed under a Creative Commons Attribution-NonCommercial-ShareAlike 4.0 International License. The images or other third party material in this article are included in the article's Creative Commons license, unless indicated otherwise in the credit line; if the material is not included under the Creative Commons license, users will need to obtain permission from the license holder in order to reproduce the material. To view a copy of this license, visit <http://creativecommons.org/licenses/by-nc-sa/4.0/>

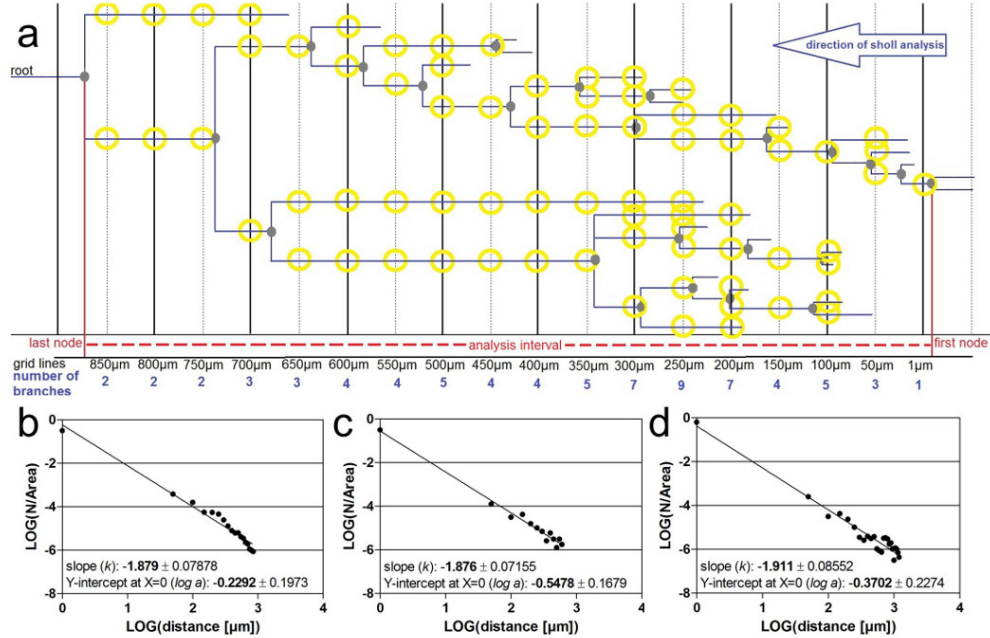
Novel 3D Microscopic Analysis of Human Placental Villous Trees Reveals Unexpected Significance of Branching Angles

Eva Haeussner, Antonia Buehlmeyer, Christoph Schmitz,
Franz Edler von Koch, and Hans-Georg Frank

Supplementary Figures



Supplementary Figure S1: Very long terminal branches of the villous tree of the human placenta have a small planar branching angle. (a) Each dot represents the mean length of branches of a single isolated villous tree. The mean, standard deviation and mean lengths (dots) of bT0 branches (bT0_ml), bT1 branches (bT1_ml), and bT2 branches (bT2_ml) are shown. The mean length of the bT0 branches was statistically significantly different from the mean length of the bT1 and bT2 branches. (b) Mean length of the bt0 branches as a function of their planar angle..



Supplementary Figure S2: Sholl analysis of 3D data extracted from the villous trees of human placentas. (a) Illustration of the process of data extraction and subsequent Sholl analysis.

The data extraction was based on the nodes (grey points) and branches (lines) of the dendrogram view with its x-scale in μm . The direction of analysis was defined from terminal end to the root and confined to the interval (analysis interval; red dashed line) between the first node (red solid line on the right; most distal branching point) and the last node (red solid line on the left; node most proximal to the root). Measuring lines were placed every $50\mu\text{m}$ and perpendicular to the branches (vertical black lines; $100\mu\text{m}$ intervals straight lines, $50\mu\text{m}$ dotted lines). The grid of measuring lines started at the terminal end of the villous tree. The first of the measuring lines falling into the analysis interval was placed at $1\mu\text{m}$, and the following lines were arranged in $50\mu\text{m}$ intervals. At each measuring line the number of intersections (yellow circles) with branches of the dendrogram was determined (blue numbers at the very bottom). The position of each measuring line in the analysis interval in μm and the number of branches at the respective measuring line were the raw data used for the Sholl-analysis. (b-d) Log/Log plots of three exemplary Sholl analyses. N/area is on the y-axis and formed by the number of intersections (N) and by the area, which is defined by the distance of the respective grid line in μm taken to the square and multiplied with π ($\frac{N}{\text{area}} = \frac{N}{\text{distance}^2 \cdot \pi}$). The distance of the grid line in μm is on the x-axis. The straight lines in (b to d) were defined by linear regression, with their slope being the Sholl regression coefficient k with its y intersection being $\log a$.

Supplementary Tables

Supplementary Table S1: Descriptive statistics of parameters of the villous tree of the human placenta obtained by 3D analysis.

Parameter	n	mean	SD
bT0_mpa [degree]	50	58.78	10.907
bT1_mpa [degree]	50	44.17	13.317
bT2_mpa [degree]	33	32.11	17.185
bT0_md [μm]	50	38.91	6.273
bT1_md [μm]	50	45.80	9.943
bT2_md [μm]	39	50.56	11.513
bT0_n	50	11.10	5.140
bT1_n	50	7.70	3.824
bT2_n	39	1.74	1.019
bT0_ml [μm]	50	84.36	27.716
bT1_ml [μm]	50	110.79	48.119
bT2_ml [μm]	39	150.96	146.023
bT0_ms [μm^2]	50	9988.39	4062.634
bT1_ms [μm^2]	50	15961.31	8105.258
bT2_ms [μm^2]	39	24688.72	28400.659
bT0_mv [μm^3]	50	97887.70	58713.082
bT1_mv [μm^3]	50	194404.61	143229.858
bT2_mv [μm^3]	39	335151.75	474652.064
sholl K-value	50	2.00	0.243
sholl Log a	50	0.104	0.156

Parameters are number (n), mean, and standard deviations (SD) of Neurolucida-derived parameters determined in the present study. Normal human placentas (n=50, one isolated peripheral villous tree per placenta) were investigated. Positions were encoded by (i) bT0: branch (b) in terminal position (T0), (ii) bT1: branch one node apart from the nearest terminal, and (iii) bT2: branch two nodes apart from the nearest terminal. Other parameters were expressed by the position code combined with: _mpa, mean planar branching angle; _md, mean diameter; _n, number; _ml, mean length; _ms, mean surface area; _mv, mean volume. Parameters determined by Sholl analysis were labelled with *sholl*. In 11 analyzed peripheral villous trees, bT2 positions were not found (reducing n to 39 for bT2_md and bT2_ml). In another 6 investigated peripheral villous trees, the branching angle of bT2 could not be determined because no previous segment was present (reducing n to 33 for bT2_mpa).

Supplementary Table S2: Clinical data of the two placenta collections used in the present study.

Parameter	3D Analysis			Histology		
	n	mean	SD	n	mean	SD
delivery mode	50			50		
—vaginal	21			26		
—sectio	29			24		
gestational week	50	39.34	1.08	50	39.65	1.20
birth weight [g]	50	3463	589	50	3412	426
placenta weight [g]	50	523	121	50	503	94
PW/BW ratio	50	0.150	0.023	50	0.149	0.028
thickness [cm]	50	1.73	0.35	50	1.59	0.43

3D Analysis: Cohort of placentas analyzed by Neurolucida-assisted 3D analysis. Histology: Cohort of placentas analyzed by thin 2D histological sections. The number (n) of placentas, mean and standard deviation of each parameter are given. The t-test with paired variables show no statistically significant differences between the two collections were observed.

Supplementary Table S3: Estimation of total processing time in hours [h] per sample and per step.

Process Steps	Processing Time in [h]	
	3D Analysis	Histology
Sampling of Tissue	0.3	0.3
Fixation	12	24
Bleaching/Rinsing	1	—
Dehydration/Embedding	—	48
Cutting/Deparaffination	—	2
Staining/Mounting	6	0.3
Computer-Assisted Analysis	0.5	1.5
Σ Processing Time/Sample	19.8	76.1

Three-dimensional analysis with Neurolucida software (3D Analysis) was compared to the analysis of thin 2D histological sections using Stereo Investigator software (Histology). Hematoxylin staining (3D Analysis) or hematoxylin/eosin staining (HE, Histology) were used. The estimated total processing time in hours is given as Σ Processing Time/Sample. The absence of a certain step from one of the work flows is indicated (—).

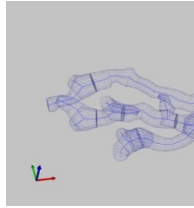
Supplementary Table S4: Descriptive statistics of parameters obtained from thin 2D histological sections of villous trees of human placentas.

Structure	n	mean Vol. [ml]	SD	mean Vol.Fr.	SD
Villous Tree	50	197.03	48.62	39.41	7.41
— <i>Villous Stroma</i>	50	102.50	34.18	20.59	6.03
— <i>Vessel Lumen</i>	50	52.59	23.09	10.37	3.77
— <i>Endothelium</i>	50	15.51	8.62	3.18	1.65
— <i>Syncytiotrophoblast</i>	50	26.43	9.73	5.26	1.60
Fibrinoid	50	43.01	28.40	8.66	5.18
Intervillous Space	50	263.97	69.08	51.65	8.85

Parameters were number (n), mean absolute volume (mean Vol.) with standard deviation (SD), dimensionless mean volume fraction (mean Vol.Fr.) with SD. The data were stratified by structural components (villous tree, fibrinoid, intervillous space); substructures (villous stroma, vessel lumen, endothelium, syncytiotrophoblast) are indented (—). For each normal human placenta one systematically and randomly sampled tissue block and one thin 2D histological section per tissue block were investigated.

Supplementary Movies

a) Still images for supplementary movies:



Still image 1: The still image shows a single frame of supplementary movie 1.



Still image 2: The still image shows a single frame of supplementary movie 2.



Still image 3: The still image shows a single frame of supplementary movie 3.



Still image 4: The still image shows a single frame of supplementary movie 4.

- b) Captions for supplementary movies 1-4; the movies are provided as separate files

Supplementary Movie S1: The movie shows the Neurolucida-based three-dimensional reconstruction of a villous tree of a human placenta. The reconstructed tree turns around its x-axis (red). In a first phase of the movie, the entire reconstructed peripheral villous tree is shown. The second phase of the movie enlarges the most peripheral part of the villous tree.

Supplementary Movie S2: The movie shows an example of the visualization of the three-dimensional (3D) data set obtained by the analysis of a single isolated peripheral villous tree of a human placenta using Neurolucida software. The single isolated peripheral villous tree is shown in a blue skeletonized view and turns clockwise to provide insight into the 3D nature of the data.

Supplementary Movie S3: The movie shows an example of the visualization of the three-dimensional (3D) data set obtained by the analysis of a single isolated peripheral villous tree of a human placenta using Neurolucida software. The single isolated peripheral villous tree is shown in a blue skeletonized view and turns clockwise to provide insight into the three-dimensional nature of the data.

Supplementary Movie S4: The movie shows an example of the visualization of the three-dimensional data set obtained by the analysis of a single isolated peripheral villous tree of a human placenta using Neurolucida software. The single isolated peripheral villous tree is shown in a blue skeletonized view and turns clockwise to provide insight into the three-dimensional nature of the data.

3.3 Publication III

Does 2D-histologic identification of villous types of human placentas at birth enable sensitive and reliable interpretation of 3D structure?

Abstract

Introduction: The villous tree of human placentas is a complex three-dimensional (3D) structure which enables fetomaternal exchange. Current concepts of microscopic analyses are based on the analysis of two-dimensional (2D) histologic sections. For this approach, the assessment of the stromal core of sectioned villi is of key importance. The classification of stromal properties of sectioned villi allows allocation of villous sections to villous types which are named by their expected position in villous trees (terminal, intermediate, and stem villi).

Method: The present study takes these current concepts of placental histology as hypothesis and validates them against predetermined 3D positions of branches of villous trees. The 3D positions were determined prior to histologic sectioning using a recently introduced 3D-microscopic approach. Individual histologic sections of villi were classified by their stromal structures and inter rater variability of these histologic assessments were determined.

Results/discussion: Inter rater variability was high and indicates substantial observer influence on the outcome of histologic assessments. Cross-match of villous types with the predetermined positions of villous branches of villous trees revealed substantial mismatch between the outcome of stromal classification and 3D-position of the sectioned villi in the placental villous trees.

Reference

Haeussner E , Aschauer B, Burton GJ, Huppertz B, Edler von Koch F, Müller-Starck J, Salafia C, Schmitz C, Frank HG. - Does 2D-histologic identification of villous types of human placentas at birth enable sensitive and reliable interpretation of 3D structure? Placenta. 2015 December 36(12):1425-32

URL Link

<http://www.sciencedirect.com/science/article/pii/S0143400415300631>



Does 2D-Histologic identification of villous types of human placentas at birth enable sensitive and reliable interpretation of 3D structure?



Eva Haeussner^{a,1}, Beate Aschauer^a, Graham J. Burton^b, Berthold Huppertz^c,
Franz Edler von Koch^{d,2}, Jens Müller-Starck^a, Carolyn Salafia^{e,f}, Christoph Schmitz^a,
Hans-Georg Frank^{a,*}

^a Ludwig-Maximilians-University, Department of Anatomy II, Munich, Germany

^b University of Cambridge, Department of Physiology, Development and Neuroscience, Cambridge, UK

^c Medical University of Graz, Institute of Cell Biology, Histology and Embryology, Graz, Austria

^d Clinic for Obstetrics and Gynecology, Dritter Orden, Munich, Germany

^e Placental Analytics LLC, Larchmont, USA

^f New York Methodist Hospital, Department of Obstetrics and Gynecology and Pediatrics, NY, USA

ARTICLE INFO

Article history:

Received 31 July 2015

Received in revised form

28 September 2015

Accepted 5 October 2015

Keywords:

Placenta

Villous tree

Anatomy

3D structure

Classification

Branching pattern

ABSTRACT

Introduction: The villous tree of human placentas is a complex three-dimensional (3D) structure which enables fetomaternal exchange. Current concepts of microscopic analyses are based on the analysis of two-dimensional (2D) histologic sections. For this approach, the assessment of the stromal core of sectioned villi is of key importance. The classification of stromal properties of sectioned villi allows allocation of villous sections to villous types which are named by their expected position in villous trees (terminal, intermediate, and stem villi).

Method: The present study takes these current concepts of placental histology as hypothesis and validates them against predetermined 3D positions of branches of villous trees. The 3D positions were determined prior to histologic sectioning using a recently introduced 3D-microscopic approach. Individual histologic sections of villi were classified by their stromal structures and inter rater variability of these histologic assessments were determined.

Results/discussion: Inter rater variability was high and indicates substantial observer influence on the outcome of histologic assessments. Cross-match of villous types with the predetermined positions of villous branches of villous trees revealed substantial mismatch between the outcome of stromal classification and 3D-position of the sectioned villi in the placental villous trees.

© 2015 The Authors. Published by Elsevier Ltd. This is an open access article under the CC BY-NC-ND license (<http://creativecommons.org/licenses/by-nc-nd/4.0/>).

1. Introduction

The villous tree of the human placenta is of key importance for pre- and postnatal health [1]. The concepts that are believed to underpin development of the placental villous tree influence planning, design and conduct of both basic and clinically applied research projects [1–7].

Infarction, infection, inflammation and malignant or pre-malignant disturbances of placental tissues are routinely

diagnosed by the pathologist, as in many other organs. However, pathological assessment of the villous tree is especially challenging due to rapid developmental changes. Mismatches between the developmental stage of the villous tree and gestational age and/or deviations from the normal developmental pathways of the villous tree have functional impact [1].

The present study focuses on the formal quality of histologic interpretation of the structure of the villous tree. How reliable and reproducible are such procedures, which rely on identification of various parts of the villous tree histologically? To what degree is this interpretation process observer dependent?

The current concepts of histological identification of (sub-) structures of the villous tree of the human placenta evolved towards the end of the last century. They are mainly based on the comparison of routine wax-embedded or semi-thin histologic

* Corresponding author. Department of Anatomy II, Pettenkoferstr. 11, 80336 Munich, Germany.

E-mail address: hans-georg.frank@med.uni-muenchen.de (H.-G. Frank).

¹ Results are part of the doctoral thesis of EH.

² Both authors contributed equally as senior authors.

sections with scanning electron microscopic pictures of comparable, but not identical, regions of the villous tree [8–11]. These concepts make use of the villous vasculature and stromal elements which become visible by histologic sectioning. The trophoblast, by contrast, is largely neglected. The present study will thus use the term “stromal classification” for the current histologic nomenclature. Using stromal classification, villous types were defined and the maturation of the stroma was used to identify developmental relationships (e.g. immature intermediate villi representing precursors of stem villi) between the villous types. Stromal classification is also the basis for access to three-dimensional ordering of branches of the villous tree. This was originally established by two subsequent steps [8–11]:

- 1) The villous types of the stromal classification were matched to scanning electron microscopic pictures that allowed a 3D view of the villous tree. Matching was qualitative and necessarily indirect since histologic sectioning and scanning electron microscopy are incompatible methods.
- 2) The villous types were allocated to specific positions of the villous tree as outlined by their names (e.g. terminal, intermediate, or stem villi). Stem villi represent the supporting framework of the villous tree and are characterized by a dense fibrous stroma. After several generations of branching they give rise to intermediate villi, from which the majority of terminal villi, the principal functional units for exchange, arise. The stromal core undergoes a progressive transformation along this pathway, with a reduction in fibrous tissue and a transition from arteries, to arterioles and finally to capillary plexuses.

Currently the linkage of stromal classification (two-dimensional (2D)) with positional nomenclature (three-dimensional (3D)) is a key strategy by which 2D-histologic analysis of the villous tree gains insight into villous 3D structure and developmental status.

In the present study, we take the above mentioned linkage strategies as hypotheses (a–c):

- a) Examiners skilled in microscopic anatomy are able to allocate cross-sectional profiles of peripheral villi to the histologic types of terminal villus, intermediate villus, or small stem villus with little or no inter-observer variability.
- b) The majority of terminal ends of branches of the villous tree of the term human placenta will be classified as being of the histological type “terminal villus”.
- c) Intermediate and small peripheral stem villi rarely occur in a terminal position of the villous tree.

To test these hypotheses, we used a recently introduced 3D microscopic approach by which we were able to determine 3D positions of branches of isolated peripheral villous trees [12] without sectioning.

None of the hypotheses (a–c) could be confirmed. The impact of these findings on comparability, reproducibility, and sensitivity of histologic examinations of the developmental status of villous trees of the human placentas at birth is discussed.

2. Materials and methods

2.1. Pre-existing 3D data

The present study used five isolated placental villous trees, selected randomly from an existing collection of 50 preparations of isolated placental villous trees. Details on these villous trees were published elsewhere and are included herein by Ref. [12] and Table S1. All villous trees have been analyzed in 3D using high-end

brightfield microscopy and quantitative analysis using the software, Neurolucida (MBF Bioscience, Williston, VT, USA). The available datasets contained nodes and the hierarchical position of each branch of the villous trees classified by its distance to the terminal end (bT0 = branch at the terminal (bT) end, bT1 = branch being one node away from the nearest terminal end, and bT2 = branch being two nodes away from the nearest terminal end), as well as measures associated with these branches (lengths, diameters, branching angles, surfaces and volumes), and a full 3D visualization (3D-Lucida, Figs. 1, 2) of the outer contour of the investigated villous trees.

2.2. Embedding, serial sectioning and staining

The initial 3D analysis was performed on intact villous trees without standard histological sectioning [12]. Firstly, the cover slips of the five selected preparations were removed by placing the slides into pure xylene until the cover slip spontaneously fell off the concave slide. From here on, they were processed in small glass jars using a routine embedding protocol [13]. Briefly, the isolated villous trees were incubated in pure xylene (two times 90 min), then transferred to ethanol (100%, first time 90min, then 48 h, then 5 h) and from ethanol passed into pure propylene oxide (three times 30 min.). Araldite mixture (44.63 g) was prepared from Araldite CY-212 (22.75 g, Serva Electrophoresis, Heidelberg, Germany), dodecenylsuccinic anhydride (DDSA, 21 g; Serva), and 2,4,6-Tris(dimethylaminomethyl)phenol (0.875 g, Serva). The preparations were infiltrated by araldite mixture/propylene oxide (1/1 V/V) overnight, transferred into araldite mixture for 6.5 h and finally placed in embedding moulds filled with araldite mixture. The araldite mixture was polymerized at 60 °C for 48 h.

Slides for mounting of serial sections were prepared by immersion in ethanol/ammonia (90 ml ethanol plus 10 ml ammonia) overnight, carefully washed and stored in bidistilled water until use. Blocks containing the isolated villous trees were oriented and trimmed to enable the formation of ribbons of serial sections [13]. Motorized sectioning at 1 µm/section was performed such that ribbons of sections containing 30–90 sections per object slide (3–10 object slides per villous tree) could be collected on the prepared glass slides, oriented and dried at 60 °C. The slides were stored at 70 °C until staining. For staining, slides were warmed to 60 °C and stained with 1% toluidine blue for 45s, washed with distilled water (3 times 5 min), dried on a drying plate at 60 °C and mounted under a cover slip with DPX mountant. Tables containing the sequence and orientation of all sections on the slides were prepared and allowed allocation of serial numbers to the several hundred sections of each of the isolated villous trees.

2.3. 2D virtual slides and 3D reconstruction

Each slide was transformed into a 2D digital (virtual) slide with a fully automated scanning microscope based on a M2 AxioImager (Zeiss, Goettingen, Germany) microscope equipped with a two-axis computer controlled stepping motor system (4" × 3" XY), automated slide loader for 1" × 3" glass slides with proScan III stage (Prior Scientific, Jena, Germany) and color digital camera (2/3 CCD chip 1.4 MP, 1388 × 1049 pixel), and focus encoder. The whole system was controlled by the software, Stereo Investigator (MBF Bioscience). Each slide was scanned in the region of interest which was defined to contain all ribbons of sections using a 10× objective. The viewing fields of the region of interest were stitched together by the software to deliver a single 2D virtual slide corresponding to its respective physical slide. In addition, a calibration slide with scale (µm) was scanned to enable later calibration of 3D reconstruction. The 2D virtual slides obtained were viewed in Biolumica

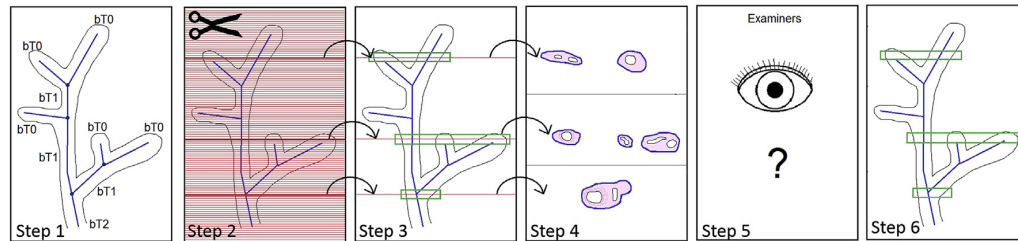


Fig. 1. Illustration of the steps (Step 1 – Step 5) during validation and quality analysis of histologic analysis of villous trees. Step 1 shows the 3D villous reconstruction in Neurolucida (3D-Lucida) with its positional ordering (bT0–bT2) and nodes (dark blue dots). 3D-Lucida data of the present study are shown in Fig. 2 (A–E; tiles with white background). Step 2 symbolizes the histotechnical process by which the villous trees were embedded in resin and serially sectioned at 1 μ m intervals. Step 3 demonstrates the reconstruction of the trees from the serial section stacks. Section numbers and positions in the tree become firmly linked (3D-Recon). 3D-Recon data of the present study are shown in Fig. 2 (A–E; tiles with gray background). Step 4 exemplifies how the 3D reconstructions of Step 3 serve as index system by which individual sections of branches of the villous trees can be selected from the stacks and photographed at high magnification. Step 5 and Step 6 illustrate the analysis process by histologic examiners (Step 5) and the cross-referencing to the 3D positions (Step 6).

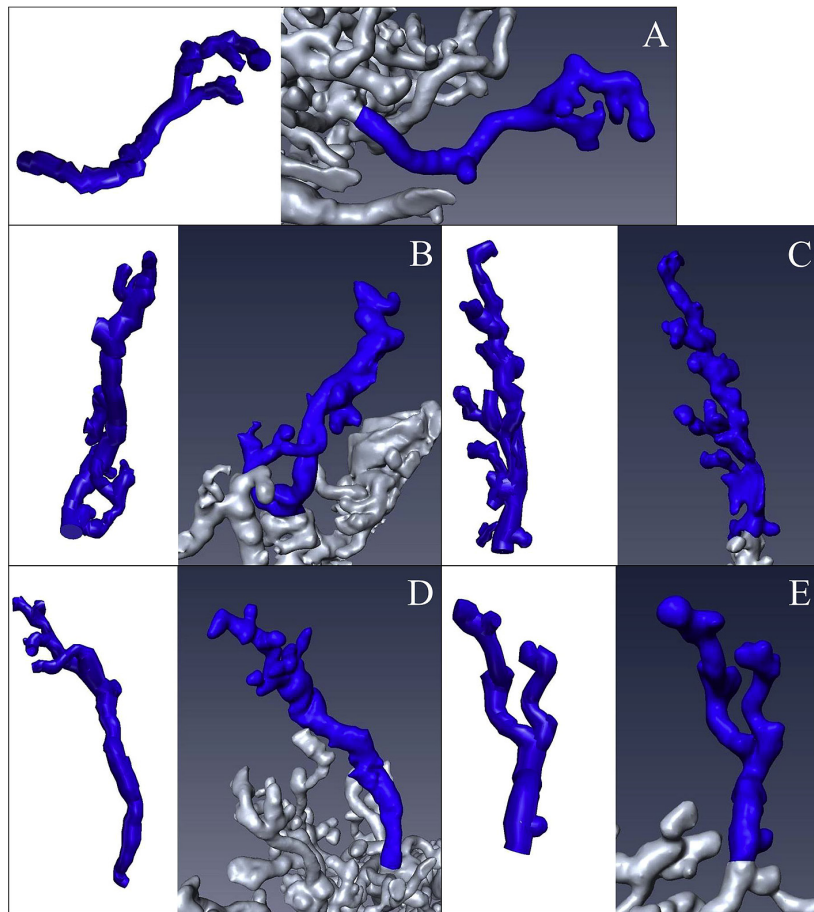


Fig. 2. (A–E) Direct comparisons of 3D-Lucida (left side of each tile, white background) with 3D-Recon; right side of the tile; gray background). A–E show each of the five villous trees of the present study.

viewer software (MBF Bioscience) and every 4th section was taken as a screenshot. These screenshots were confined to the outline of the desired section by loading each screenshot into Photoshop CS6 (Adobe, San Jose, CA, USA) software and manual outline and excision of the section area. The serial sections were then used for 3D reconstruction (3D-Recon, Figs. 1, 2) of the outer contour of the

isolated villous trees using the software, Amira (version 5.5.0; Visualization Sciences Group, FEI Company, Burlington, MA, USA). Only the outer contour of the villi was reconstructed. The surfaces were smoothed (option SmoothSurface, with 30 iterations). Every step was documented carefully to enable back-tracing of features in the 3D reconstruction down to the individual section number of the

isolated villous tree.

2.4. Histologic classification of sections

The branches of the villous trees were cross-matched between 3D-Lucida and 3D-Recon and corresponding branches were identified. The section numbers belonging to a cross-matched branch in 3D-Recon were traced back to the original ribbons of sections on the slides. The individual sections identified by this back-tracing procedure were then photographed at high resolution using an AxioPhot microscope (AxioPhot with AxioCam HRC, Zeiss, Goettingen, Germany) with a 100 \times objective under oil immersion (Fig. 3). These photographs were carefully chosen to be from internodal regions and as far away from the next node (branching point) of the villous tree as possible. A total of 165 microphotographs was taken for subsequent histologic examination. These 165 photographs belonged to a total of 95 branches which were identified by 3D-Lucida. Some of the 3D-Lucida branches were represented in this collection by different photographs taken at more than one level of a branch or by very similar, directly neighboring photographs. For those branches, one single photograph was selected randomly to become part of the diagnostic core collection. The diagnostic core collection (consisting of exactly 95 photographs with each photograph belonging to a single unique branch) was defined to give every branch the same weighting in the whole analysis; only those photographs belonging to the diagnostic core collection of 95 photographs were used for kappa-determination and for cross-tabulating of branches versus stromal classification. Besides the abovementioned core collection, an additional 70 photomicrographs were assessed by the examiners. These were either from longer branches of the villous trees (many in bT2) at different levels of the same branch (33 microphotographs), or were true duplicates of photomicrographs ($n = 37$). These were used to assess variability of repetitive classification of the same branch (or photograph) by the examiners.

An additional 25 photomicrographs of internodal regions of branches in all positions were taken and presented to the examiners to decide on the presence or absence of sinusoidal capillaries as an interpretation task with reduced complexity. Similarly, a collection of 42 photomicrographs of node regions was established; nodes were not classified by the six examiners.

The total collection of 165 photographs was classified histologically by assessment of the stromal core of the villi. This was achieved by six morphologists (EH, BA, GJB, BH, JMS, CaSa) in two rounds (team A: EH, BA, JMS and team B: GJB, BH, CaSa) using a formalized task description. Team A was built from morphologists who were not specific experts with long-standing experience in placental morphology. Team A reflects a typical constellation of morphologists as could be found at many research institutions. Team B consisted of experts with long-standing experience in placental microscopic anatomy and pathology. All examiners obtained a copy of the original description of histological classification of human placental villi [10] to harmonize their assessments. This publication was chosen because it used peripheral parts of villous trees (obtained by aspiration with biopsy needles, without high-caliber stem villi). Similarly to the present study, this study [10] thus excluded high-caliber stem villi and focused on the low-caliber small stem villi directly adjunct to the intermediate villi and terminal villi at the tips of the villous trees. Using this guideline, they individually and independently classified each photograph of a section into one of the three categories “terminal villus”, “intermediate villus”, or “stem villus” as e.g. depicted in Figs. S1, S2 and Table S2 of the reference publication [10]. Transitional categories were not allowed; only the absence of sufficient stromal tissue for assessment allowed allocation of the photograph to “nc”,

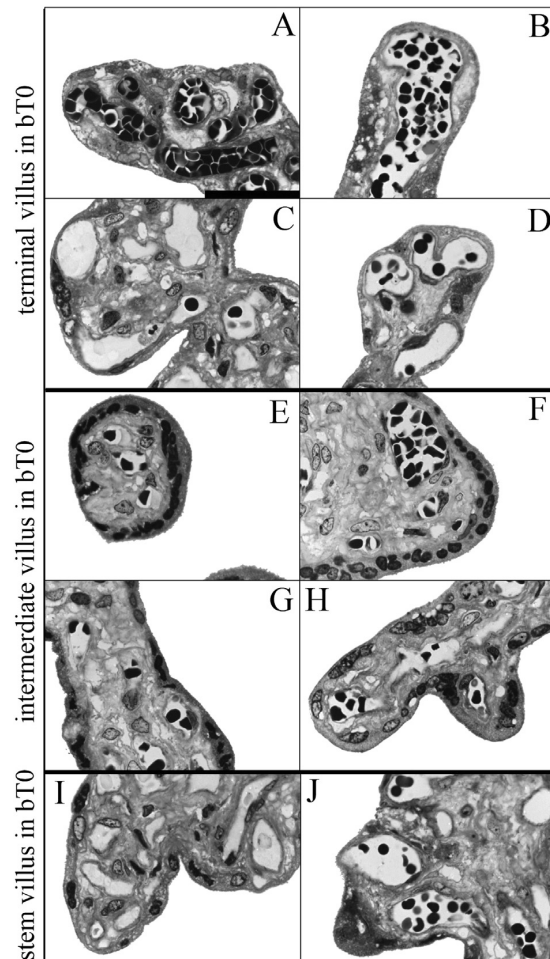


Fig. 3. (A–J) Samples of photomicrographs that were part of the core collection interpreted by the examiners in the present study. Note that the photomicrographs shown here all correspond to branches in bT0 (i.e. in terminal position as defined by 3D-Lucida). (A–D) Sections of branches in bT0, which were classified by teams A and B by at least majority decision to be terminal villi. (E–H) Sections of histologic villi corresponding to branches in bT0, which were classified by teams A and B by at least majority decision to be intermediate villi. (I–J) Sections of histologic villi corresponding to branches in bT0, which were classified by either team A or team B by majority decision as stem villi. The black bar in (A) corresponds to 25 μ m.

i.e. “not classifiable”. These classifications were collected and the inter-observer variability (Fleiss Kappa) was calculated in Excel [14,15] and rated on the scale provided by Landis and Koch [16]. Calculations of kappa were done for each team separately and across the assessments of all six examiners.

Each section was finally allocated to a villous category by a unanimous or majority vote deduced from the team-specific assessments (3 per team). Split votes (all three villous types identified by the three examiners of the team) were finally allocated to not classifiable (nc).

3. Results

Matching of branches identified in 3D-Lucida with corresponding branches of 3D-Recon was feasible (Fig. 1) and 3D-Recon could reasonably serve as a section-index system. Sections were

thus allocated to topological positions of their branches (bT0, bT1, or bT2).

Semi-thin histologic sections showed a technical quality which enabled assessment of the stromal core to determine the villous type of the sectioned branches (see Fig. 3, in Figs. S2–S4). The technical and morphological quality of the Araldit-embedded semi-thin sections reflected the formaldehyde-based fixation outcome and was at least comparable to the quality usually obtainable by formalin fixed and paraffin embedded samples (see Fig. S4).

Allocation of villous sections to villous types (terminal villi, intermediate villi, stem villi) by stromal classification was to a considerable degree observer dependent, as shown by the inter-observer variability measure (Fleiss-kappa, see Table 1A). This was observed despite the attempt to harmonize assessments by providing copies of the reference literature [10] as guidance to all examiners. According to the rating of kappa as a measure of inter-observer variability by Landis and Koch [16], the values of kappa for team A (0.294), team B (0.117), and overall (0.209) indicate substantial inter-observer variability. Landis and Koch classify scale values of 0 as “no agreement”, 0–0.20 as “slight agreement”, 0.21–0.40 as “fair agreement”, 0.41–0.60 as “moderate agreement”, 0.61–0.80 as “substantial agreement”, and 0.81–1 as “perfect agreement”. In this rating scheme, the inter-observer variability of the present study is at the edge of “slight agreement” to “fair agreement”. The determination of absence/presence of sinusoidal capillaries in villi was slightly less observer dependent (kappa values are close to 0.35, see Table 1B). None of the kappa values reached a level which can be classified as “moderate agreement”.

Since each group of examiners had three members, unanimous or majority decisions on the final allocation of a villous type to each section could be achieved (see Table 1) in most of the examined microphotographs. A numerical overview on classification of sections by terminal distance of the sectioned branch (3D-Lucida) or, by stromal classification, or the criterion of presence/absence of sinusoidal capillaries is given in Table 2A–E (extended version see Table S3). Matching of each section (stromal classification) with the corresponding branch (branch position) allowed cross-table analysis of stromal classification versus matched 3D positions (Table 3 (extended version see Table S4) and Fig. 3, Fig. S2). Especially at position bT0, but also in bT1 and bT2, there was unexpected and considerable mismatch between the position usually associated with 2D histological types (“terminal”, “intermediate”; see also Table 3 and Table S2) and the actual 3D position of the corresponding branch. Dendrograms of each villous

Table 1

The table summarizes the data on inter-rater variability. Kappa values of inter-rater variability calculated from the results of visual assessment of photomicrographs of various parts of the villous tree of human placentas by two teams of observers (Team A: morphologists, non-experts of the human placenta; Team B: morphologists, experts of the human placenta). The data were determined separately for each of the two teams of examiners (Team A, Team B) and for all examiners (All). Generally, the higher the kappa value, the higher the agreement between the examiners. (A) shows the data for the classification into the villous types (terminal villi, intermediate villi, stem villi), and (B) shows the data for classification with regard to presence or absence of sinusoidal capillaries.

Group of examiners	kappa
(A) Stromal classification: Villous types based on 2D-histology	
Team A	0.294
Team B	0.117
All	0.209
(B) Stromal classification: Absence/presence of sinusoidal capillaries	
Team A	0.357
Team B	0.351
All	0.357

Table 2

Results stratified by the individual villous trees 1–5 examined in the present study (A–E). The data show the numbers of sections falling into the same Terminal Distance category (A) or falling into the same histological category (B–E). (A) From each semi-thin histological section, the Terminal Distance of the respective branch measured in nodes to the nearest terminal end was known and is given as bT0 (terminal position), bT1 (being one node from the nearest terminal end), and bT2 (being two nodes apart from the nearest terminal end). (B, C) The stromal structures of each semi-thin histological section were histologically classified and allocated by majority decision within each team to the villous types terminal villus, intermediate villus, or stem villus. This was done in separate assessments by two teams of examiners. (B) shows the classifications of team A, (C) shows the classifications of team B. Sections which did not contain enough stroma to assign a histological classification or could not be allocated due to tripartite split votes were not classified (nc). (D, E) The stromal structures of each semi-thin histological section were histologically classified for presence or absence of sinusoids. This was done in separate assessments by two teams of examiners. (D) shows the classifications of team A, (E) shows the classifications of team B.

(A) Topological classification of sections by 3D-Lucida				
Villous tree	bT0	bT1	bT2	
1	7	4	1	
2	13	10	2	
3	9	6	1	
4	16	10	1	
5	8	6	1	
Σ1–5	53	36	6	
(B) Stromal classification of sections (2D Histology, Team A)				
Villous tree	Terminal villus	Intermediate villus	Stem villus	nc
1	1	11	0	0
2	7	4	13	1
3	4	8	0	4
4	14	7	4	2
5	10	3	1	1
Σ1–5	36	33	18	8
(C) Stromal classification of sections (2D Histology, Team B)				
Villous tree	Terminal villus	Intermediate villus	Stem villus	nc
1	1	11	0	0
2	14	9	2	0
3	10	6	0	0
4	17	10	0	0
5	15	0	0	0
Σ1–5	57	36	2	0
(D) Presence/absence of sinusoids (2D Histology, Team A)				
Villous tree	Non-sinusoidal villus	Sinusoidal villus		nc
1	8	1		0
2	1	3		0
3	4	2		0
4	1	2		0
5	0	3		0
Σ1–5	14	11		0
(E) Presence/absence of sinusoids (2D Histology, Team B)				
Villous tree	Non-sinusoidal villus	Sinusoidal villus		nc
1	7	2		0
2	1	3		0
3	4	2		0
4	0	3		0
5	0	3		0
Σ1–5	12	13		0

tree with all branches, the 95 microphotographs of the core collection and the 25 microphotographs used for assessment of sinusoidal capillaries are documented in the online Supplementary file (SFile 1). The online supplementary file simultaneously indicates for each of these microphotographs the position of the section in the dendrogram of the villous tree and the outcome of assessment by the examiners (SFile 1). The mismatch of the results could be observed in both teams and was

Table 3

(A–D) Cross-table of histologic classifications determined by team A and team B and topologic position given as Terminal Distance of the sectioned branch in the villous trees. The left column shows Terminal Distance of the respective branch measured in nodes to the nearest terminal end and is given as bT0 (terminal position), bT1 (being one node from the nearest terminal end), and bT2 (being two nodes apart from the nearest terminal end). (A, B) Allocation of a section to a respective histologic classification (terminal villus, intermediate villus, and stem villus) was achieved by majority decision within each team of examiners. (A) shows the results of team A. (B) shows the results of team B. The red fields mark combinations which do not occur with stromal classification (eg. stem villus at terminal position). (C, D) show classification by the presence/absence of sinusoidal capillaries (sinusoidal villus, non-sinusoidal villus) as determined by majority decision by each team of examiners (C) shows the results of team A. (D) shows the results of team B.

(A) Team A	terminal villus	intermediate villus	stem villus	All villous types Σ
bT0	30	13	5	48
bT1	5	18	11	34
bT2	1	2	2	5
Σ bT0-2	36	33	18	
(B) Team B	terminal villus	intermediate villus	stem villus	All villous types Σ
bT0	38	15	0	53
bT1	17	18	1	36
bT2	2	3	1	6
Σ bT0-2	57	36	2	
(C) Team A	non-sinusoidal villus	sinusoidal villus	All villous types Σ	
bT0	6	5	11	
bT1	5	5	10	
bT2	3	1	4	
Σ bT0-2	14	11		
(D) Team B	non-sinusoidal villus	sinusoidal villus	All villous types Σ	
bT0	4	7	11	
bT1	6	4	10	
bT2	2	2	4	
Σ bT0-2	12	13		

not dependent on the level of expertise of the examiners though the team-opinion of team B was somewhat closer to the actual 3D positions. The sections of branches in terminal position (bT0) belonged to all histological types of villi (Table 2 and Fig. 3). Only about 6 out of 10 of branches bT0 were classified as terminal villi by means of histological analysis (for details see Table 3). Also less than half of the villous cross-sections which were classified as intermediate villi actually were in terminal positions (bT0) (for details see Table 3). On the other hand, villi were histologically classified as terminal villi, but were not in a terminal position of the villous tree (Table 3 and Fig. 3, Fig. S4).

The classifications of the 70 photomicrographs outside the core collection are shown in Table 4. Besides villi, also nodes ($N = 42$) were localized in 3D-Lucida and 3D-Recon and sections of node regions were identified and photographed. Sections of nodes were not presented to the examiners since there is no concept for histologic classification of nodes. Typical histologic appearances of nodes are exemplified by a collection of photomicrographs in Fig. S3. Syncytial bridges, high amount of stroma and capillaries, and tangentially sectioned areas are visible. Without the 3D information being available in the present study, many of the structures shown in Fig. S3 would be histologically indistinguishable from villous cross sections and would thus potentially – and inappropriately – be treated as villous cross sections and allocated to villous types.

4. Discussion

The present study shows that the isolated peripheral villous trees contained branches which were two nodes apart from the nearest terminal end. A distance of two nodes provides topologic evidence that stem villi (adjunct to penultimate intermediate villi

and ultimate terminal villi) were present. The quantitative data of the present study closely correspond to the morphometric data determined for such stem villi [10,11]. High-caliber stem villi as described in sections of whole placental tissue (see, e.g. Ref. [17]) were not present in the samples of the present study.

4.1. 2D histologic classification – stromal classification – of villous sections is observer dependent

Though the examiners had guidelines and the same photographs, inter-observer variability only reached the level of a “fair agreement” and was below the values above 0.6 which would signal “substantial agreement” or “perfect agreement” [14–16]. While the stromal classification of villous types is a very complex histologic evaluation, the presence/absence of sinusoidal capillaries just picks one single histologic aspect of villous interpretation. Even this task revealed considerable inter-observer variability. Low kappa values could e.g. be due to issues with specimen preparation, lack of training slides, lack of data dictionary, and the assumption that internodal sectioning would be sufficient to ensure that we were not looking at a transitional zone between two villous types, etc. Since the values were low in both examiner groups at different levels of experience and the original description of villous types was provided to all examiners it is more likely that the target description itself is not uniform and precise enough.

The considerable degree of inter-observer variability will cause substantial scatter in any quantitative study being based on such stromal classification. Developmental identification using stromal classification of histologic sections will tend to have a bad signal to noise ratio. Only dramatic changes [18] due to extreme clinical circumstances will be reliably detectable.

Table 4

Summary of the assessment of photographs not belonging to the core collection. The photographs were assessed by all examiners which gives the total number of Assessments (Assessments (Total)). Some of the photographs were taken from one and the same branch at different levels (Photographs (same branch)), others were duplicate (Photographs (duplicate)). Terminal Distance of the respective branch was measured in nodes to the nearest terminal end and is given as bT0 (terminal position), bT1 (being one node from the nearest terminal end), and bT2 (being two nodes apart from the nearest terminal end). The times the respective photographs were allocated by the examiners to one of the villous types (Stromal classification) was counted and is given for terminal villi (TV), intermediate villi (IMV), and stem villi (SV).

Tree	Examiners	Photographs per tree	Photographs (same branch)	Photographs (duplicate)	Assessments (total)	Assessments (specific)	Terminal distance			Stromal classification		
							bT0	bT1	bT2	TV	IMV	SV
1	6	13	9	4	78	54			1	10	44	
						24		3	1	4	16	4
						42			2	4	12	26
2	6	18	7	11	108	66	1	9	1	10	39	17
						42			1	13	24	5
						36			1	12	20	4
3	6	13	7	6	78	30			1	5	19	6
						60		9	1	17	36	7
						30			1	10	18	2
4	6	15	5	10	90	36			5	18	16	2
						36						
						198			6	42	117	39
5	6	11	5	6	66	222	1	31	5	61	127	34
ALL	6	70	33	37	420							

4.2. 3D branch position and 2D structure are not as firmly linked as expected

An accepted and widely used principle in placental histology is that of stringent positional/structural linkage: Histologic villous nomenclature could be viewed as positional (terminal villus, intermediate villus, small stem villus); positions in the villous tree may reveal themselves by histologically recognizable (stromal) structures [9–11]. The concept has proven very attractive, because it transforms 2D histologic analysis into an indirect 3D analysis; archived morphological material is available in many laboratories and may serve as a resource for studies. The data obtained in the present study do not confirm the positional/histological linkage which is suggested by the positional nomenclature (Table 3). One of the main outcomes of the present study is that the real 3D structure (3D-Lucida) of the villous trees differed substantially from the virtual 3D structure of the same villous trees as deduced from stromal classification.

Moreover, the photographs presented to the examiners were taken from free branches as far away from the next node as feasible. As shown in Fig. S3, the appearance of nodes in 2D (without the 3D-informations used in the present study) cannot easily be differentiated from sectioned free internodal segments of a branch [18]. A histological section of a placenta will thus simultaneously show many villous sections stochastically combined with sections through nodes of numerous villous trees. However, it will neither disclose their real 3D position nor their nature of being a section between nodes or through a node [8,9,19–22]. In “real” situations scatter will thus even be higher than measured in the “experimental” situation of the present study. The magnitude of this problem is substantial. Table S3, in supplementary information, shows that branches in terminal or preterminal position (bT0, bT1) are roughly twice as long as their diameters. By a conservative statistical estimation, every third, but at least every fourth to fifth sectioned “villus” in 2D will then be a sectioned node. However, nodes were mentioned rarely in the literature of placental histology [10]. For nodes, there is no histologic classification at all; they are thus classified as if they would be free internodal branches, too. The present study shows for the first time that the occurrence of nodal sections in placental histology is qualitatively and quantitatively relevant.

The fact that nodes can complicate histological analysis was recognized earlier during discussions on the interpretation of syncytial nodes/bridges [19–23]. However, the issue of interpretation of syncytial nodes/bridges is possibly not more than a minor

example of the likely substantial impact which nodal structures have on the interpretation of placental histology [20].

4.3. Prospects of research

It is clear that there is no way to examine placental tissue by other means than histology – at least on a routine basis. It is also clear that the findings discussed above are disappointing.

The findings have implications for the quantitative assessment of the structure of the villous trees and the development of morphometrics [24]. Design-based stereological techniques have been applied to the placenta in order to determine, for example, patterns of placental growth or to estimate its exchange capacity [3,25]. Stereological analyses usually incorporate a hierarchical sampling procedure, during which the organ is broken down sequentially into its component parts [26]. The fineness of the sampling required depends on the research question being asked, but ultimately will be restricted by the ability to recognize reliably the objects in question. Thus, when assessing growth of the placenta across gestation, Jackson et al. [27] used the criteria of Kaufmann et al. [10] to identify the various villus subtypes. They found it impossible to distinguish between mature and immature villi using paraffin wax sections, and accepted that they may have also conflated some of the smaller stem villi and intermediate villi. Nonetheless, they showed that the volume of terminal villi increases exponentially after approximately 20 weeks, whereas those of the intermediate villi and stem villi increase linearly at slower rates throughout pregnancy. In other situations researchers have not tried to make such fine distinctions, and indeed it may not be necessary. For example, the rate of diffusional exchange across the placenta is determined by the Fick equation, and so is proportional to the surface area of the villous membrane and inversely proportional to its thickness. Estimating these two parameters enables a morphometric diffusing capacity for the placenta to be calculated [25], and comparisons to be made regarding functional capacity in different pathological states [3]. But what is the surface area that is physiologically important and should be estimated? Since stem villi contain few superficial capillaries they are unlikely to play a significant role in exchange, and should be considered part of the structural framework of the placenta. By contrast, intermediate and terminal villi are both well vascularized, and hence some studies have considered these together as the functional unit of the placenta for exchange [28,29]. This approach is supported by the findings presented here. Thus, in the light of our results researchers aiming to quantify placental structure must reappraise whether

they can reliably identify the villus subtypes using routine histological sections, and either adopt more advanced techniques to do so or qualify their conclusions accordingly.

Besides basic histology there are other techniques available to differentiate between the various villous types – even if this will also not allow a positional but rather a functional description of the villous tree. One of these techniques is looking at specific marker proteins by immunohistochemistry/immunofluorescence. Looking at markers within the villous stroma, the use of respective differentiation markers of mesenchymal cells has been established to identify the differentiation status of immature intermediate villi moving towards stem villi. Here the use of cytoskeletal markers has proved to be useful in assessing the differentiation of mesenchymal cells towards myofibroblasts in placental stem villi [30]. At the same time there does not seem to be a single marker available that discriminates a terminal from a mature intermediate villus. HLA-G and various types of keratins can be used as markers identifying trophoblast subtypes but cannot discriminate between villous types [31,32]. Also, proliferation and apoptosis markers have not been successful in differentiating between intermediate and terminal villi [33,34]. Finally, markers for endothelial cells and vessels were used in pathological cases [18] or were used to identify vascular arrangements in terminal villi, even using 3D reconstruction [35]. However, so far there are no markers available to easily differentiate the various villous types in the human placenta.

5. Conclusion

This study has shown that the current gold standard of defining villous types is far from being optimal. Its stromal assessment of villous cores does not help in assigning the positional localization of villi. It does, however, classify the villous tree on a more morphological/functional level. Hence, following this study the current standard is still valid but needs to be used with caution.

Acknowledgments

DFG, grant numbers INST 86/1495-1 FUGG, INST86/1452-1 LAGG.

The authors acknowledge the skillful technical assistance and diligent work of the entire team of technicians of the Department of Anatomy II at LMU Munich, namely A. Baltruschat, U. Fazekas, S. Kerling, C. Stanglmair, B. Mosler and S. Tost. We would also like to express our thanks to the obstetricians, midwives, and nurses of the Dritter Orden hospital (Munich, Germany) who enabled the clinical work of this study with great care and engagement. Results are part of the doctoral thesis of EH.

Authors, Institutions.

EH, BA, GJB, BH, JMS, and CaSa, performed the analysis. FvK, CSch and HGF designed the study. FvK was responsible for obstetrical tasks. EH and HGF prepared figures and tables. HGF, CSch, FvK and EH wrote the manuscript.

Appendix A. Supplementary data

Supplementary data related to this article can be found at <http://dx.doi.org/10.1016/j.placenta.2015.10.003>.

References

- [1] K. Benirschke, G.J. Burton, R.N. Baergen, *Pathology of the Human Placenta*, sixth ed., Springer, Berlin and London, 2012.
- [2] S.M. Almasry, M.A. Eldomiaty, A.K. Elfayomy, F.A. Habib, M.D. Safwat, Structural analysis of human placental stem and terminal villi from normal and idiopathic growth restricted pregnancies, *J. Mol. Histol.* 43 (2012) 263–271.
- [3] T.M. Mayhew, A stereological perspective on placental morphology in normal and complicated pregnancies, *J. Anat.* 215 (2009) 77–90.
- [4] H. Fox, N.J. Sebire, *Pathology of the Human Placenta*, Saunders Elsevier, Amsterdam, 2007.
- [5] J.C. Kingdom, P. Kaufmann, Oxygen and placental villous development: origins of fetal hypoxia, *Placenta* 18 (1997) 613–621.
- [6] J.C.P. Kingdom, L. Macara, C. Krebs, R. Leiser, P. Kaufmann, Pathological basis for abnormal umbilical artery doppler waveforms in pregnancies complicated by intrauterine growth restriction: A review, *Placenta Suppl.* 18 (1997) 291–309.
- [7] M. Vogel, *Atlas der morphologischen Plazentadiagnostik*, second ed., Springer, Berlin and Heidelberg, 1996.
- [8] B. Huppertz, G. Burton, J.C. Cross, J.C.P. Kingdom, Placental morphology: from molecule to mother – a dedication to Peter Kaufmann – a review, *Placenta Suppl.* 27 (2006) 3–8.
- [9] P. Kaufmann, M. Luckhardt, G. Schweikhart, S.J. Cantle, Cross-sectional features and three-dimensional structure of human placental villi, *Placenta* 8 (1987) 235–247.
- [10] P. Kaufmann, D.K. Sen, G. Schweikhart, Classification of human placental villi. I. Histology, *Cell Tissue Res.* 200 (1979) 409–423.
- [11] D.K. Sen, P. Kaufmann, G. Schweikhart, Classification of human placental villi. II. Morphometry, *Cell Tissue Res.* 200 (1979) 425–434.
- [12] E. Haussner, A. Buehlmeier, C. Schmitz, F. Edler von Koch, H.-G. Frank, Novel 3D microscopic analysis of human placental villous trees reveals unexpected significance of branching angles, *Sci. Rep.* 4 (2014) 6192.
- [13] B. Ruthensteiner, Soft Part 3D visualization by serial sectioning and computer reconstruction, *Zoosymposia* 1 (2008) 63–100.
- [14] J.L. Fleiss, *The Measurement of Interrater Agreement. Statistical Methods for Rates and Proportions*, John Wiley & Sons, New York, 1981.
- [15] J.L. Fleiss, J. Cohen, The equivalence of weighted kappa and the intraclass correlation coefficient as measures of reliability, *Educ. Psychol. Meas.* 33 (1973) 613–619.
- [16] J.R. Landis, G.G. Koch, The measurement of observer agreement for categorical data, *Biometrics* 33 (1977) 159–174.
- [17] R. Leiser, M. Luckhardt, P. Kaufmann, E. Winterhager, U. Bruns, The fetal vascularisation of term human placental villi. I. Peripheral stem villi, *Anat. Embryol.* 173 (1985) 71–80.
- [18] M. Kadyrov, G. Kosanke, J. Kingdom, P. Kaufmann, Increased fetoplacental angiogenesis during first trimester in anaemic women, *Lancet* 352 (1998) 1747–1749.
- [19] G.J. Burton, The fine structure of the human placental villus as revealed by scanning electron microscopy, *Scanning Microsc.* 1 (1987) 1811–1828.
- [20] S.J. Cantle, P. Kaufmann, M. Luckhardt, G. Schweikhart, Interpretation of syncytial sprouts and bridges in the human placenta, *Placenta* 8 (1987) 221–234.
- [21] G.J. Burton, Intervillous connections in the mature human placenta: instances of syncytial fusion or section artifacts? *J. Anat.* 145 (1986) 13–23.
- [22] W. Küstermann, Über “Proliferationsknoten” und “Syncytialbrücken” der menschlichen Plazenta, *Anat. Anz* 150 (1981) 144–157.
- [23] P. Kaufmann, B. Huppertz, Tenney-Parker changes and apoptotic versus necrotic shedding of trophoblast in normal pregnancy and pre-eclampsia, in: F. Lyall, M. Belfort (Eds.), *Pre-eclampsia: Etiology and Clinical Practice*, Cambridge Univ Press, Cambridge, 2010, pp. 152–163.
- [24] T.M. Mayhew, Morphomics: an integral part of systems biology of the human placenta, *Placenta* 36 (2015) 329–340.
- [25] T.M. Mayhew, G.J. Burton, Stereology and its impact on our understanding of human placental functional morphology, *Microsc. Res. Tech.* 38 (1997) 195–205.
- [26] T.M. Mayhew, Stereology and the placenta: where's the point? – a review, *Placenta* 27 (Suppl A) (2006) S17–S25.
- [27] M.R. Jackson, T.M. Mayhew, P.A. Boyd, Quantitative description of the elaboration and maturation of villi from 10 weeks of gestation to term, *Placenta* 13 (1992) 357–370.
- [28] T.M. Mayhew, et al., Stereological investigation of placental morphology in pregnancies complicated by pre-eclampsia with and without intrauterine growth restriction, *Placenta* 24 (2003) 219–226.
- [29] G.J. Burton, E. Jauniaux, Sonographic, stereological and Doppler flow velocimetric assessments of placental maturity, *BJOG* 102 (1995) 818–825.
- [30] G. Kohnen, S. Kertschanska, R. Demir, P. Kaufmann, Placental villous stroma as a model system for myofibroblast differentiation, *Histochem Cell Biol.* 105 (1996) 415–429.
- [31] M. Gauster, A. Blaschitz, M. Siwetz, B. Huppertz, Keratins in the human trophoblast, *Histol. Histopathol.* 28 (2013) 817–825.
- [32] G. Moser, K. Orendi, M. Gauster, M. Siwetz, C. Helige, B. Huppertz, The art of identification of extravillous trophoblast, *Placenta* 32 (2011) 197–199.
- [33] M. Gauster, M. Siwetz, B. Huppertz, Fusion of villous trophoblast can be visualized by localizing active caspase 8, *Placenta* 30 (2009) 547–550.
- [34] M. Gauster, M. Siwetz, K. Orendi, G. Moser, G. Desoye, B. Huppertz, Caspases rather than calpains mediate remodelling of the fodrin skeleton during human placental trophoblast fusion, *Cell Death Differ.* 17 (2010) 336–345.
- [35] M. Jirkovská, et al., The branching pattern of villous capillaries and structural changes of placental terminal villi in type 1 diabetes mellitus, *Placenta* 33 (2012) 343–351.

Does 2D-Histologic Identification of Villous Types of Human Placentas at Birth Enable Sensitive and Reliable Interpretation of 3D Structure?

Eva Haeussner, Beate Aschauer, Graham J Burton, Berthold Huppertz, Franz Edler von Koch ,
Jens Müller-Starck, Carolyn Salafia, Christoph Schmitz, Hans-Georg Frank

Supplementary Information

Figures

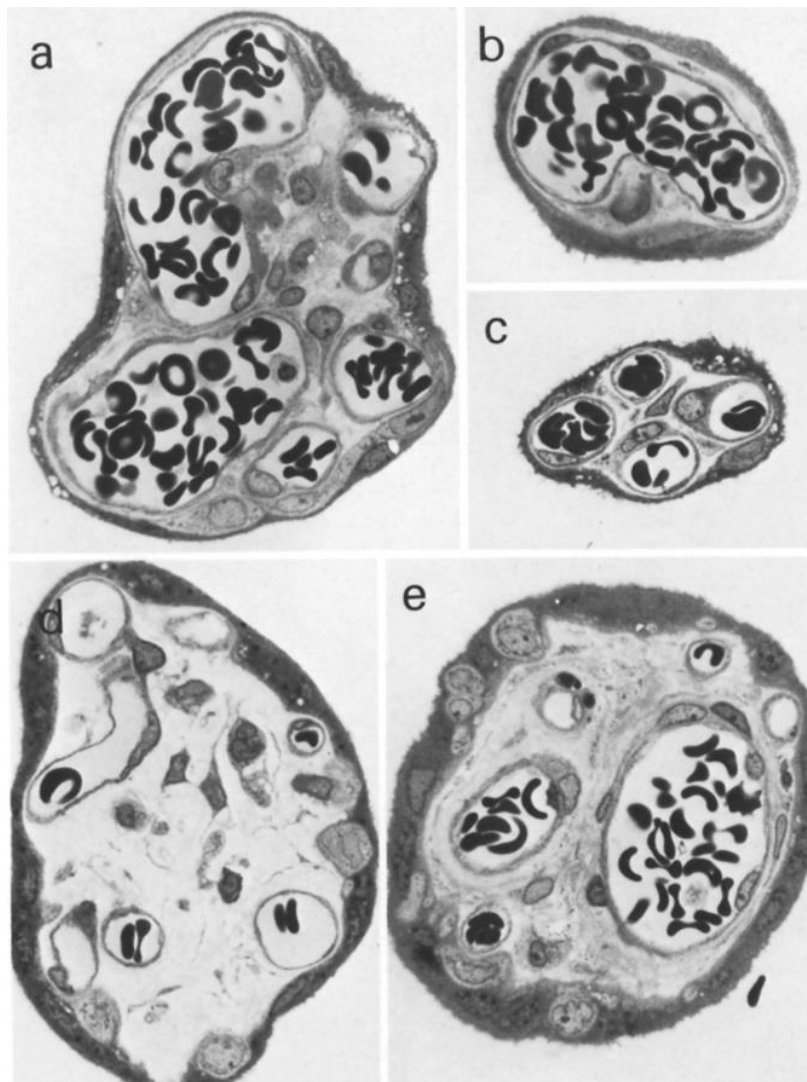


Figure S1 (a-e) Typical cross sections of different parts of the peripheral villous tree. x 1100. (a) Terminal villus containing large sinusoidal capillaries which bulge out the trophoblastic surface forming typical epithelial plates. Connective tissue is poorly developed, (b) Tip of terminal villus with a tangentially sectioned capillary loop. (c) Neck region with four non-dilated capillaries and little connective tissue. (d) Mature intermediate villus with smaller fetal vessels, without a media identifiable light microscopically, and a large amount of loose reticular connective tissue, (e) Small ramulus, with arteriole (showing a conspicuous media), vein and paravascular capillaries. Note condensed fibrous stroma (copy of [10] with permission).

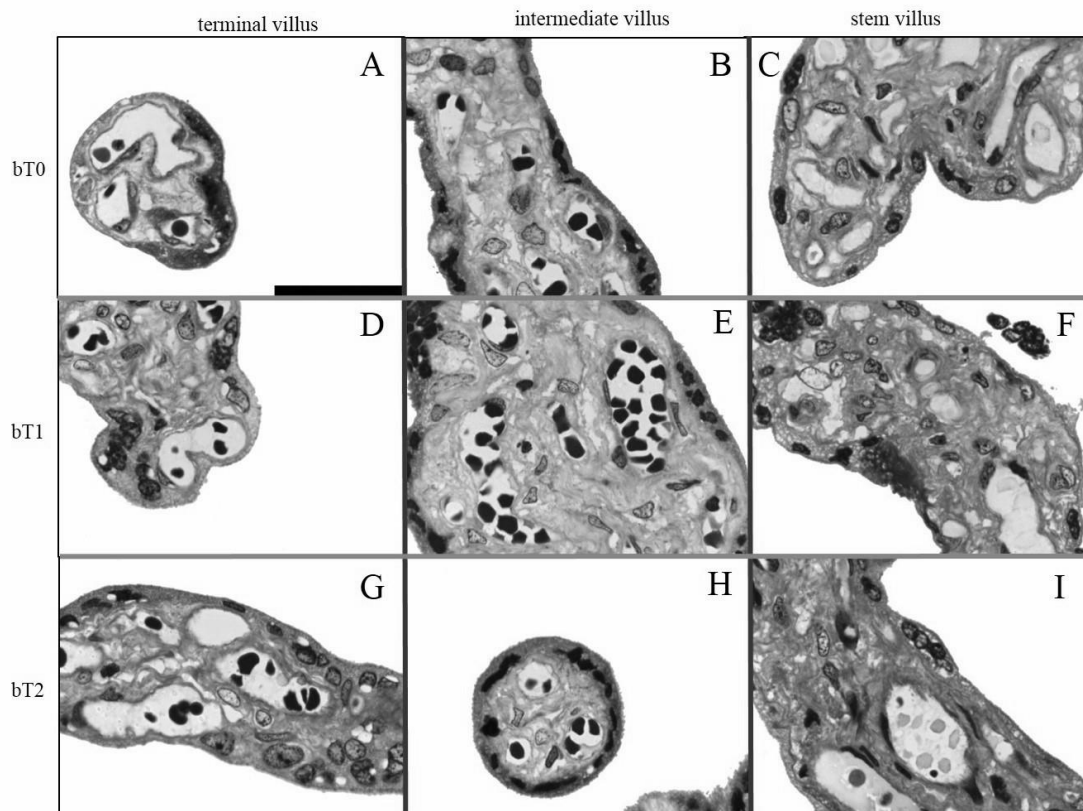


Figure S2 The photomicrographs shown in this figure were selected from the core collection of microphotographs identified by the examiners. The photomicrographs are arranged as visual cross-table with stromal classification (terminal villi, intermediate villi and (small) stem villi) as columns and position of 3D-branches (determined by 3D-Lucida and measured in nodes from the nearest terminal end as bT0 (terminal position), bT1 (one node away from the nearest terminal end), and bT2 (two nodes away from the nearest terminal end) as rows (A-I). A,B and D-I were classified into the respective villous type by at least majority decision of both teams of examiners. C was classified as stem villus by majority decision of team A. The figure shows examples of terminal villi in positions bT0, bT1, and bT2 (A,D,G), of intermediate villi in positions bT0, bT1, and bT2 (B,E,H), and of small stem villi in positions bT0, bT1, and bT2 (C,F,I). The black bar in (A) corresponds to 25µm.

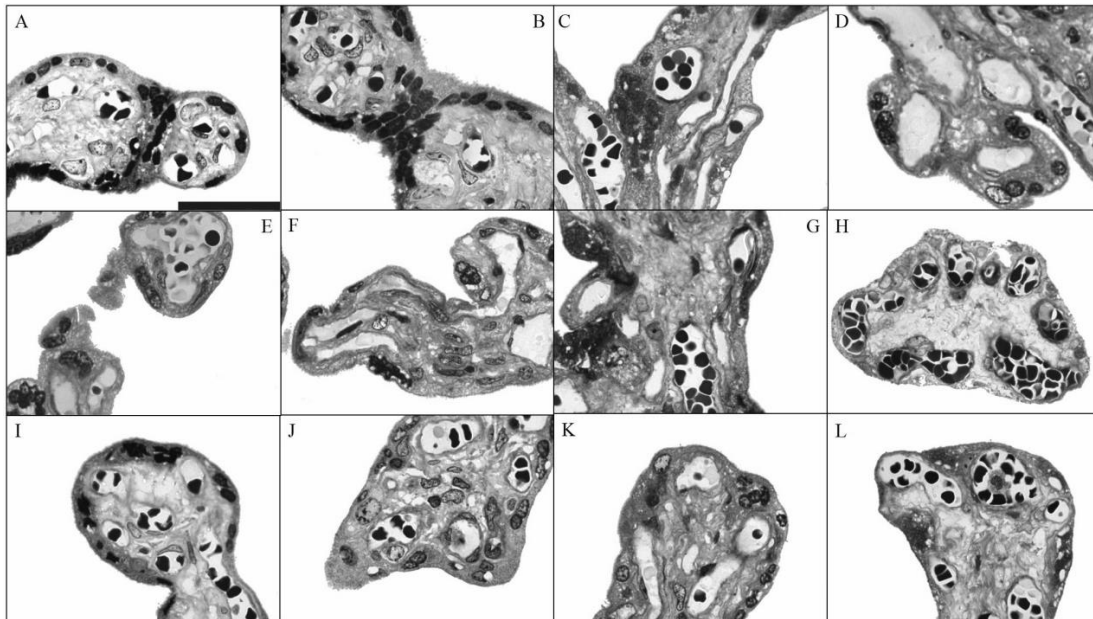


Figure S3 (A-J) Photomicrographs of sections which were from nodes (branching points), but not from internodal regions of the villous trees. These sections were not used for stromal classification by the examiners since nodes were excluded from the interpretation task. That these sections are from nodal regions is known from 3D reconstruction. Without that additional information many of these microphotographs could be interpreted as “villous sections”, too. The proximity to a node is obvious in A and B, but much less obvious in many other tiles. The black bar in (A) corresponds to 25 μ m.

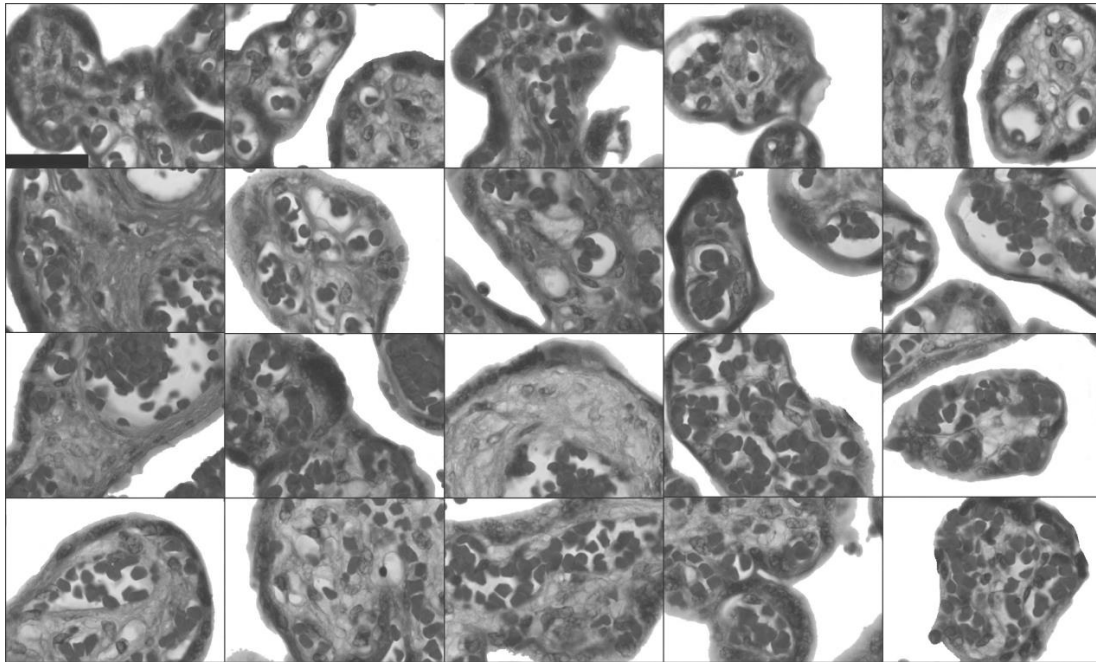


Figure S4 Various examples of sections (at 4 μ m thickness, HE-staining) of archived paraffin-embedded placental tissue. The blocks were taken from the same five placentas from which the five villous trees of the present study were prepared. The quality of structural preservation in these samples is comparable to the sections (at 1 μ m thickness, toluidine blue staining) which were obtained from samples after 3D-Lucida analysis (shown in figures 2-4). The black bar in the upper left tile corresponds to 25 μ m.

Tables

Table S1 Clinical data of the placenta collections used in the present study. Cohort of placentas analyzed by Neurolucida-assisted 3D analysis. The number (n) of placentas, mean and standard deviation of each parameter are given. This table was taken from reference [12].

Parameter	3D Analysis		
	n	mean	SD
delivery mode	50		
— <i>vaginal</i>	21		
— <i>sectio</i>	29		
gestational week	50	39.34	1.08
birth weight [g]	50	3463	589
placenta weight [g]	50	523	121
PW/BW ratio	50	0.150	0.023
thickness [cm]	50	1.73	0.35

Table S2 Branches (b) and villi at the peripheral positions of the villous tree. bT0 designates villous branch in terminal position of the villous tree, bT1 designates villous branch one branching node apart from the nearest terminal end of the villous tree and bT2 designates villous branch which are two nodes apart from the nearest terminal end of the villous tree. The villous types which can theoretically be expected at these positions are listed in the 2nd column of the table. The villous type expected to be the dominant one at this position is labeled in *italic*.

Positional ordering developed by three-dimensional reconstructions	Histologic classification usually used in the literature
bT0	<i>terminal villi</i> ; unbranched intermediate villi; unbranched stem villi
bT1	branched <i>intermediate villi</i> ; branched stem villi
bT2	<i>stem villi</i>

Table S3 Table presenting the data stratified by each individual villous tree 1-5. Data are aggregated as mean \pm standard deviation by histological classification of semi-thin sections (A,C,E,G,I) and Terminal Distance order of the branches (B,D,F;H;J). A,B, data of planar branching angles (angle); C,D, diameter; E,F, length; G,H surface area; I,J volume.

Team A

A	angle terminal villus	angle intermediate villus	angle stem villus
1	70.50 (1)	52.83 \pm 32.24 (11)	(0)
2	56.63 \pm 23.61 (7)	35.65 \pm 16.70 (4)	50.78 \pm 34.54 (13)
3	54.15 \pm 25.05 (4)	51.91 \pm 15.07 (8)	(0)
4	49.58 \pm 31.49 (14)	32.17 \pm 16.15 (7)	72.50 \pm 52.55 (4)
5	63.42 \pm 33.10 (10)	51.37 \pm 21.40 (3)	0 (1)
Σ1-5	55.88 \pm 28.95 (36)	45.60 \pm 23.52 (33)	34.83 \pm 20.05 (18)
B	angle bT0	angle bT1	angle bT2
1	64.89 \pm 33.58 (7)	40.20 \pm 16.90 (4)	24.00 (1)
2	52.75 \pm 30.17 (13)	44.75 \pm 28.24 (10)	45.60 (2)
3	61.82 \pm 19.48 (9)	50.42 \pm 18.02 (6)	54.10 (1)
4	51.40 \pm 29.09 (16)	45.79 \pm 36.28 (10)	12.80 (1)
5	64.31 \pm 36.55 (8)	48.24 \pm 23.39 (6)	56.90 (1)
Σ	57.08 \pm 29.30 (53)	46.05 \pm 27.19 (36)	38.68 \pm 19.38 (6)
C	diameter terminal villus (μ m)	diameter intermediate villus (μ m)	diameter stem villus (μ m)
1	48.00 (1)	52.26 \pm 12.69 (11)	(0)
2	36.50 \pm 7.02 (7)	37.58 \pm 8.34 (4)	47.72 \pm 7.91 (13)
3	31.15 \pm 5.92 (4)	37.13 \pm 3.76 (8)	(0)
4	37.85 \pm 9.22 (14)	46.13 \pm 10.02 (7)	62.23 \pm 8.83 (4)
5	43.94 \pm 5.64 (10)	43.53 \pm 4.61 (3)	48.30 (1)
Σ	38.82 \pm 8.33 (36)	44.72 \pm 11.00 (28)	52.00 \pm 4.32 (18)
D	diameter bT0 (μ m)	diameter bT1 (μ m)	diameter bT2 (μ m)
1	48.93 \pm 13.23 (7)	56.13 \pm 13.11 (4)	59.30 (1)
2	38.12 \pm 8.89 (13)	94.22 \pm 80.16 (10)	10.70 \pm 95.11 (2)
3	32.50 \pm 4.00 (9)	39.28 \pm 4.17 (6)	40.90 (1)
4	39.23 \pm 10.25 (16)	50.22 \pm 14.55 (10)	48.40 (1)
5	43.34 \pm 4.76 (8)	47.02 \pm 5.83 (6)	49.70 (1)
Σ	39.72 \pm 9.87 (53)	45.62 \pm 11.49 (36)	50.15 \pm 5.95 (6)
E	length terminal villus (μ m)	length intermediate villus (μ m)	length stem villus (μ m)
1	62.80 (1)	159.75 \pm 210.78 (11)	(0)
2	63.37 \pm 40.85 (7)	110.28 \pm 87.40 (4)	83.12 \pm 67.05 (13)
3	a. 19.42 (4)	98.21 \pm 92.13 (8)	(0)
4	81.66 \pm 69.44 (14)	108.26 \pm 68.59 (7)	45.48 \pm 18.40 (4)
5	85.14 \pm 70.53 (10)	83.03 \pm 69.63 (3)	46.50 (1)
Σ	73.61 \pm 60.23 (36)	111.61 \pm 132.65 (33)	108.18 \pm 74.27 (18)
F	length bT0 (μ m)	length bT1 (μ m)	length bT2 (μ m)
1	80.17 \pm 83.76 (7)	312.47 \pm 333.08 (4)	208.10 (1)
2	71.41 \pm 43.87 (13)	46.39 \pm 7.43 (10)	52.30 \pm 1.41 (2)
3	57.71 \pm 39.07 (9)	109.68 \pm 102.70 (6)	167.80 (1)
4	81.61 \pm 70.09 (16)	78.91 \pm 57.77 (10)	103.10 (1)

5	69.41 ± 78.11 (8)	94.16 ± 48.78 (6)	73.80 (1)
Σ	73.02 ± 61.64 (53)	109.21 ± 129.28 (36)	118.12 ± 70.75 (6)
G	surface area terminal villus (μm ²)	surface area intermediate villus (μm ²)	surface area stem villus (μm ²)
1	8.96x10 ³ (1)	2.67x10 ⁴ ± 3.73x10 ⁴ (11)	(0)
2	7.08x10 ³ ± 4.64x10 ³ (7)	1.52x10 ⁴ ± 1.23x10 ⁴ (4)	1.21x10 ⁴ ± 1.03x10 ⁴ (13)
3	3.35x10 ³ ± 1.59x10 ³ (4)	1.20x10 ⁴ ± 1.28x10 ⁴ (8)	(0)
4	9.51x10 ³ ± 8.41x10 ³ (14)	1.50x10 ⁴ ± 8.82x10 ³ (7)	8.34x10 ³ ± 2.64x10 ³ (4)
5	1.16x10 ⁴ ± 9.11x10 ³ (10)	1.13x10 ⁴ ± 9.74x10 ³ (3)	7.37x10 ³ (1)
Σ	8.91x10³ ± 7.61x10³ (36)	1.68x10⁴ ± 2.29x10⁴ (33)	1.83x10⁴ ± 1.35x10⁴ (18)
H	surface area bT0 (μm ²)	surface area bT1 (μm ²)	surface area bT2 (μm ²)
1	1.23x10 ⁴ ± 1.16x10 ⁴ (7)	1.52x10 ⁴ ± 5.94x10 ⁴ (4)	3.80x10 ⁴ (1)
2	8.33x10 ³ ± 4.95x10 ³ (13)	1.41x10 ⁴ ± 1.22x10 ⁴ (10)	2.30x10 ⁴ ± 1.50x10 ⁴ (2)
3	5.80x10 ³ ± 4.35x10 ³ (9)	6.88x10 ³ ± 1.45x10 ⁴ (6)	2.17x10 ⁴ (1)
4	9.76x10 ³ ± 8.48x10 ³ (16)	1.14x10 ⁴ ± 7.47x10 ³ (10)	1.71x10 ⁴ (1)
5	8.93x10 ⁴ ± 9.12x10 ⁴ (8)	1.63x10 ⁵ ± 9.45x10 ⁴ (6)	1.45x10 ⁵ (1)
Σ	2.11x10⁴ ± 4.48x10⁴ (53)	1.64x10⁴ ± 2.23x10⁴ (36)	1.89x10⁴ ± 1.21x10⁴ (6)
I	volume terminal villus (μm ³)	volume intermediate villus (μm ³)	volume stem villus (μm ³)
1	9.75x10 ⁴ (1)	3.66x10 ⁵ ± 5.40x10 ⁵ (11)	(0)
2	6.30x10 ⁴ ± 4.32x10 ⁴ (7)	1.70x10 ⁵ ± 1.42x10 ⁵ (4)	1.42x10 ⁵ ± 1.33x10 ⁵ (13)
3	2.40x10 ⁴ ± 1.25x10 ⁴ (4)	1.16x10 ⁵ ± 1.40x10 ⁵ (8)	(0)
4	8.46x10 ⁴ ± 8.14x10 ⁴ (14)	1.61x10 ⁵ ± 9.05x10 ⁴ (7)	1.17x10 ⁵ ± 2.85x10 ⁴ (4)
5	1.24x10 ⁵ ± 1.01x10 ⁵ (10)	1.18x10 ⁵ ± 1.06x10 ⁵ (3)	9.15x10 ⁴ (1)
Σ	8.48x10⁴ ± 7.98x10⁴ (36)	2.05x10⁵ ± 3.25x10⁵ (33)	1.34x10⁵ ± 1.13x10⁵ (18)
J	volume bT0 (μm ³)	volume bT1 (μm ³)	volume bT2 (μm ³)
1	1.46x10 ⁵ ± 1.43x10 ⁵ (7)	2.13x10 ⁵ ± 8.57x10 ⁵ (4)	5.64x10 ⁵ (1)
2	7.92x10 ⁴ ± 5.06x10 ⁴ (13)	1.69x10 ⁵ ± 1.53x10 ⁵ (10)	2.89x10 ⁵ ± 1.88x10 ⁵ (2)
3	4.55x10 ⁴ ± 3.72x10 ⁴ (9)	6.31x10 ⁴ ± 1.60x10 ⁵ (6)	2.23x10 ⁵ (1)
4	8.94x10 ⁴ ± 8.09x10 ⁴ (16)	1.27x10 ⁵ ± 7.92x10 ⁴ (10)	2.06x10 ⁵ (1)
5	6.94x10 ¹ ± 7.81x10 ¹ (8)	1.04x10 ² ± 4.88x10 ¹ (6)	7.38x10 ¹ (1)
Σ	7.34x10⁴ ± 8.24x10⁴ (53)	1.99x10⁵ ± 3.16x10⁵ (36)	2.42x10⁵ ± 5.64x10³ (6)
Team B			
A	angle terminal villus	angle intermediate villus	angle stem villus
1	54.90 (1)	54.39 ± 32.72 (11)	(0)
2	53.54 ± 26.81 (14)	44.06 ± 35.15 (9)	38.40 ± 10.18 (2)
3	54.67 ± 15.78 (10)	63.18 ± 23.88 (6)	(0)
4	48.77 ± 31.35 (17)	46.47 ± 35.07 (10)	(0)
5	58.04 ± 30.81 (15)	(0)	(0)
Σ1-5	52.51 ± 27.76 (57)	45.29 ± 34.25 (36)	38.40 ± 10.18 (2)
B	angle bT0	angle bT1	angle bT2
1	64.89 ± 33.58 (7)	40.20 ± 16.90 (4)	24.00 (1)
2	52.75 ± 30.17 (13)	44.75 ± 28.24 (10)	45.60 (2)
3	61.82 ± 19.48 (9)	50.42 ± 18.02 (6)	54.10 (1)
4	51.40 ± 29.09 (16)	45.79 ± 36.28 (10)	12.80 (1)
5	64.31 ± 36.55 (8)	48.24 ± 23.39 (6)	56.90 (1)
Σ	57.08 ± 29.30 (53)	46.05 ± 27.19 (36)	38.68 ± 19.38 (6)

C	diameter terminal villus (μm)	diameter intermediate villus (μm)	diameter stem villus (μm)
1	42.00 (1)	52.81 \pm 16.11 (11)	(0)
2	42.67 \pm 9.17 (14)	41.13 \pm 10.19 (9)	47.20 \pm 4.38 (2)
3	34.69 \pm 5.51 (10)	35.72 \pm 4.03 (6)	(0)
4	38.62 \pm 9.96 (17)	51.28 \pm 13.09 (10)	(0)
5	44.48 \pm 5.13 (15)	(0)	(0)
Σ	40.53 \pm 8.48 (57)	46.62 \pm 12.64 (36)	47.20 \pm 4.38 (2)
D	diameter bT0 (μm)	diameter bT1 (μm)	diameter bT2 (μm)
1	48.93 \pm 13.23 (7)	56.13 \pm 13.11 (4)	59.30 (1)
2	38.12 \pm 8.89 (13)	94.22 \pm 80.16 (10)	10.70 \pm 95.11 (2)
3	32.50 \pm 4.00 (9)	39.28 \pm 4.17 (6)	40.90 (1)
4	39.23 \pm 10.25 (16)	50.22 \pm 14.55 (10)	48.40 (1)
5	43.34 \pm 4.76 (8)	47.02 \pm 5.83 (6)	49.70 (1)
Σ	39.72 \pm 9.87 (53)	45.62 \pm 11.49 (36)	50.15 \pm 5.95 (6)
E	length terminal villus (μm)	length intermediate villus (μm)	length stem villus (μm)
1	33.80 (1)	162.39 \pm 209.23 (11)	(0)
2	79.51 \pm 54.80 (14)	78.40 \pm 78.53 (9)	103.85 \pm 58.48 (2)
3	73.58 \pm 52.27 (10)	91.60 \pm 103.58 (6)	(0)
4	64.79 \pm 30.10 (17)	110.50 \pm 92.24 (10)	(0)
5	79.76 \pm 63.70 (15)	(0)	(0)
Σ	73.34 \pm 49.80 (57)	115.18 \pm 137.07 (36)	103.85 \pm 58.48 (2)
F	length bT0 (μm)	length bT1 (μm)	length bT2 (μm)
1	80.17 \pm 83.76 (7)	312.47 \pm 333.08 (4)	208.10 (1)
2	71.41 \pm 43.87 (13)	46.39 \pm 7.43 (10)	52.30 \pm 1.41 (2)
3	57.71 \pm 39.07 (9)	109.68 \pm 102.70 (6)	167.80 (1)
4	81.61 \pm 70.09 (16)	78.91 \pm 57.77 (10)	103.10 (1)
5	69.41 \pm 78.11 (8)	94.16 \pm 48.78 (6)	73.80 (1)
Σ	73.02 \pm 61.64 (53)	109.21 \pm 129.28 (36)	118.12 \pm 70.75 (6)
G	surface area terminal villus (μm^2)	surface area intermediate villus (μm^2)	surface area stem villus (μm^2)
1	4.68x10 ³ (1)	2.71x10 ⁴ \pm 3.71x10 ⁴ (11)	(0)
2	1.00x10 ⁴ \pm 6.48x10 ³ (14)	1.14x10 ⁴ \pm 1.30x10 ⁴ (9)	1.57x10 ⁴ \pm 1.04x10 ⁴ (2)
3	8.15x10 ³ \pm 6.66x10 ³ (10)	1.14x10 ⁴ \pm 1.48x10 ⁴ (6)	(0)
4	7.68x10 ³ \pm 3.66x10 ³ (17)	1.55x10 ⁴ \pm 1.07x10 ⁴ (10)	(0)
5	1.10x10 ⁴ \pm 8.30x10 ³ (15)	(0)	(0)
Σ	9.14x10³ \pm 6.34x10³ (57)	1.74x10⁴ \pm 2.32x10⁴ (36)	1.57x10⁴ \pm 1.04x10⁴ (2)
H	surface area bT0 (μm^2)	surface area bT1 (μm^2)	surface area bT2 (μm^2)
1	1.23x10 ⁴ \pm 1.16x10 ⁴ (7)	1.52x10 ⁴ \pm 5.94x10 ⁴ (4)	3.80x10 ⁴ (1)
2	8.33x10 ³ \pm 4.95x10 ³ (13)	1.41x10 ⁴ \pm 1.22x10 ⁴ (10)	2.30x10 ⁴ \pm 1.50x10 ⁴ (2)
3	5.80x10 ³ \pm 4.35x10 ³ (9)	6.88x10 ³ \pm 1.45x10 ⁴ (6)	2.17x10 ⁴ (1)
4	9.76x10 ³ \pm 8.48x10 ³ (16)	1.14x10 ⁴ \pm 7.47x10 ³ (10)	1.71x10 ⁴ (1)
5	8.93x10 ⁴ \pm 9.12x10 ⁴ (8)	1.63x10 ⁵ \pm 9.45x10 ⁴ (6)	1.45x10 ⁵ (1)
Σ	2.11x10⁴ \pm 4.48x10⁴ (53)	1.64x10⁴ \pm 2.23x10⁴ (36)	1.89x10⁴ \pm 1.21x10⁴ (6)
I	volume terminal villus (μm^3)	volume intermediate villus (μm^3)	volume stem villus (μm^3)
1	4.48x10 ⁴ (1)	3.70x10 ⁵ \pm 5.38x10 ⁵ (11)	(0)

2	$1.03 \times 10^5 \pm 7.21 \times 10^4$ (14)	$1.35 \times 10^5 \pm 1.66 \times 10^5$ (9)	$1.88 \times 10^5 \pm 1.43 \times 10^5$ (2)
3	$7.22 \times 10^4 \pm 6.78 \times 10^4$ (10)	$1.12 \times 10^5 \pm 1.64 \times 10^5$ (6)	(0)
4	$7.05 \times 10^4 \pm 4.10 \times 10^4$ (17)	$1.72 \times 10^5 \pm 9.54 \times 10^4$ (10)	(0)
5	$1.18 \times 10^5 \pm 9.13 \times 10^4$ (15)	(0)	(0)
Σ	$9.15 \times 10^4 \pm 7.08 \times 10^4$ (57)	$2.13 \times 10^5 \pm 3.27 \times 10^5$ (36)	$1.88 \times 10^5 \pm 1.43 \times 10^5$ (2)
J	volume bT0 (μm ³)	volume bT1 (μm ³)	volume bT2 (μm ³)
1	$1.46 \times 10^5 \pm 1.43 \times 10^5$ (7)	$2.13 \times 10^5 \pm 8.57 \times 10^5$ (4)	5.64×10^5 (1)
2	$7.92 \times 10^4 \pm 5.06 \times 10^4$ (13)	$1.69 \times 10^5 \pm 1.53 \times 10^5$ (10)	$2.89 \times 10^5 \pm 1.88 \times 10^5$ (2)
3	$4.55 \times 10^4 \pm 3.72 \times 10^4$ (9)	$6.31 \times 10^4 \pm 1.60 \times 10^5$ (6)	2.23×10^5 (1)
4	$8.94 \times 10^4 \pm 8.09 \times 10^4$ (16)	$1.27 \times 10^5 \pm 7.92 \times 10^4$ (10)	2.06×10^5 (1)
5	$6.94 \times 10^1 \pm 7.81 \times 10^1$ (8)	$1.04 \times 10^2 \pm 4.88 \times 10^1$ (6)	7.38×10^1 (1)
Σ	$7.34 \times 10^4 \pm 8.24 \times 10^4$ (53)	$1.99 \times 10^5 \pm 3.16 \times 10^5$ (36)	$2.42 \times 10^5 \pm 5.64 \times 10^3$ (6)

Team A and B

A	angle non-sinusoidal villus	angle sinusoidal villus	
1	36.62 ± 19.94 (8)	24.00 (1)	
2	0 (1)	68.27 ± 39.28 (3)	
3	60.40 ± 17.24 (3)	70.00 (1)	
4	(0)	31.90 ± 6.65 (2)	
5	(0)	67.25 ± 42.78 (3)	
Σ1-5	44.54 ± 2.155 (12)	55.23 ± 31.70 (10)	
B	angle bT0	angle bT1	angle bT2
1	44.00 ± 27.08 (3)	31.85 ± 12.37 (3)	24.00 (3)
2	48.50 (1)	78.15 ± 49.99 (3)	(0)
3	66.17 ± 16.00 (3)	47.20 (2)	54.10 (1)
4	42.50 ± 21.64 (2)	36.60 (1)	(0)
5	67.25 ± 42.78 (2)	0 (1)	(0)
Σ	54.41 ± 23.80 (11)	50.63 ± 31.88 (10)	39.05 ± 21.28 (4)
C	diameter non-sinusoidal villus (μm)	diameter sinusoidal villus (μm)	
1	55.87 ± 15.83 (8)	59.30 (1)	
2	52.30 (1)	47.13 ± 9.91 (3)	
3	37.47 ± 3.04 (3)	29.20 (1)	
4	(0)	39.15 ± 1.91 (2)	
5	(0)	48.00 ± 0.70 (3)	
Σ	49.99 ± 14.74 (12)	45.22 ± 9.21 (10)	
D	diameter bT0 (μm)	diameter bT1 (μm)	diameter bT2 (μm)
1	54.83 ± 17.78 (3)	55.70 ± 24.61 (3)	59.30 (3)
2	45.90 (1)	49.27 ± 10.19 (3)	(0)
3	33.03 ± 3.32 (3)	36.40 (2)	40.90 (1)
4	44.65 ± 9.69 (2)	40.50 (1)	(0)
5	47.85 ± 0.92 (2)	48.30 (1)	(0)
Σ	44.95 ± 12.19 (11)	48.05 ± 12.69 (10)	50.10 ± 13.01 (4)
E	length non-sinusoidal villus (μm)	length sinusoidal villus (μm)	
1	135.58 ± 80.63 (8)	208.10 (1)	
2	10.70 (1)	70.87 ± 28.22 (3)	
3	92.30 ± 65.92 (3)	16.40 (1)	

4	(0)	180.85 ± 162.99 (2)	
5	(0)	47.07 ± 24.95 (3)	
Σ	110.11 ± 78.83 (12)	94.00 ± 89.28 (10)	
F	length bT0 (μm)	length bT1 (μm)	length bT2 (μm)
1	136.70 ± 110.03 (3)	97.65 ± 12.52 (3)	208.10 (3)
2	45.90 (1)	49.27 ± 10.19 (3)	(0)
3	76.87 ± 68.53 (3)	46.20 (2)	167.80 (1)
4	179.15 ± 165.39 (2)	65.60 (1)	(0)
5	47.35 ± 35.28 (2)	46.50 (1)	(0)
Σ	104.84 ± 93.44 (11)	64.68 ± 32.95 (10)	187.95 ± 28.50 (4)
G	surface area non-sinusoidal villus (μm ²)	surface area sinusoidal villus (μm ²)	
1	2.25x10 ⁴ ± 1.28x10 ⁴ (8)	3.80x10 ⁴ (1)	
2	1.80x10 ³ (1)	1.12x10 ⁴ ± 6.70x10 ³ (3)	
3	1.13x10 ⁴ ± 9.02x10 ³ (3)	1.42x10 ³ (1)	
4	(0)	2.23x10 ⁴ ± 1.91x10 ⁴ (2)	
5	(0)	7.26x10 ³ ± 3.64x10 ³ (3)	
Σ	1.71x10⁴ ± 1.29x10⁴ (12)	1.39x10⁴ ± 1.30x10⁴ (10)	
H	surface area bT0 (μm ²)	surface area bT1 (μm ²)	surface area bT2 (μm ²)
1	2.04x10 ⁴ ± 1.48x10 ⁴ (3)	1.79x10 ⁴ ± 9.60x10 ³ (3)	3.80x10 ⁴ (3)
2	8.68x10 ³ (1)	8.87x10 ³ ± 8.82x10 ³ (3)	(0)
3	8.25x10 ³ ± 7.62x10 ³ (3)	5.42x10 ³ (2)	2.17x10 ⁴ (1)
4	2.28x10 ⁴ ± 1.86x10 ⁴ (2)	8.81x10 ³ (1)	(0)
5	7.20x10 ³ ± 5.15x10 ³ (2)	7.37x10 ³ (1)	(0)
Σ	1.40x10⁴ ± 1.19x10⁴ (11)	1.05x10⁴ ± 7.60x10³ (10)	2.99x10⁴ ± 1.15x10⁴ (4)
I	volume non-sinusoidal villus (μm ³)	volume sinusoidal villus (μm ³)	
1	3.10x10 ⁵ ± 1.98x10 ⁵ (8)	5.64x10 ⁵ (1)	
2	2.36x10 ⁴ (1)	1.39x10 ⁵ ± 1.10x10 ⁵ (3)	
3	1.10x10 ⁵ ± 9.78x10 ⁴ (3)	9.65x10 ³ (1)	
4	(0)	2.14x10 ⁵ ± 1.70x10 ⁵ (2)	
5	(0)	8.43x10 ⁴ ± 4.58x10 ⁴ (3)	
Σ	2.21x10⁵ ± 1.94x10⁵ (12)	1.67x10⁵ ± 1.72x10⁵ (10)	
J	volume bT0 (μm ³)	volume bT1 (μm ³)	volume bT2 (μm ³)
1	2.50x10 ⁵ ± 1.75x10 ⁵ (3)	2.73x10 ⁵ ± 2.39x10 ⁵ (3)	5.64x10 ⁵ (3)
2	9.66x10 ⁴ (1)	1.15x10 ⁵ ± 1.30x10 ⁵ (3)	(0)
3	6.79x10 ⁴ ± 6.44x10 ⁴ (3)	4.98x10 ⁴ (2)	2.23x10 ⁵ (1)
4	2.23x10 ⁵ ± 1.57x10 ⁵ (2)	9.39x10 ⁴ (1)	(0)
5	8.08x10 ⁴ ± 6.41x10 ⁴ (2)	9.15x10 ⁴ (1)	(0)
Σ	1.51x10⁵ ± 1.31x10⁵ (11)	1.41x10⁵ ± 1.42x10⁵ (10)	3.93x10⁵ ± 2.41x10⁵ (4)

Table S4 Cross-Table of the data for each branch and the corresponding semi-thin histological section. The data are tabulated by histological classification (columns; terminal villi, intermediate villi, stem villi) and Terminal Distance of branches (rows; bT0, bT1, bT2). Each field of the cross-table contains the number of sections/branches (N), the planar branching angle (pa in degree), the diameter (d in μm), the length (l in μm), the surface area (sa in μm^2), and the volume (v in μm^3). Data are aggregated as means \pm standard deviation, where appropriate. Row data are aggregated across all Terminal Distances in the last row. Column data are aggregated across all data of classified villi in the last column.

Team A		terminal villus	intermediate villus	stem villus	All villi Σ
bT0	N	30	13	5	48
	pa (degree)	53.00 \pm 28.05	60.01 \pm 26.53	63.60 \pm 49.93	56.00 \pm 29.89
	d (μm)	38.36 \pm 8.28	44.02 \pm 11.64	47.06 \pm 11.98	40.80 \pm 10.00
	l (μm)	72.16 \pm 64.16	77.87 \pm 72.73	87.42 \pm 50.45	75.30 \pm 64.27
	sa (μm^2)	8.52x10 ³ \pm 7.80x10 ³	1.03x10 ⁴ \pm 9.92x10 ³	1.13x10 ⁴ \pm 4.19x10 ³	9.29x10 ³ \pm 8.08x10 ³
	v (μm^3)	7.82x10 ⁴ \pm 7.57x10 ⁴	1.09x10 ⁵ \pm 1.18x10 ⁵	1.21x10 ⁵ \pm 3.28x10 ⁴	9.11x10 ⁴ \pm 8.63x10 ⁴
bT1	N	5	18	11	34
	pa (degree)	73.00 \pm 34.62	37.29 \pm 13.67	51.48 \pm 33.98	47.50 \pm 27.48
	d (μm)	39.36 \pm 8.81	44.21 \pm 10.87	52.70 \pm 9.75	46.24 \pm 11.06
	l (μm)	82.24 \pm 42.30	148.19 \pm 168.43	65.09 \pm 62.47	111.61 \pm 132.65
	sa (μm^2)	1.07x10 ⁴ \pm 7.63x10 ³	2.23x10 ⁴ \pm 2.96x10 ⁴	1.06x10 ⁴ \pm 1.02x10 ⁴	1.68x10 ⁴ \pm 2.29x10 ⁴
	v (μm^3)	1.12x10 ⁵ \pm 1.10x10 ⁵	2.74x10 ⁵ \pm 4.25x10 ⁵	1.36x10 ⁵ \pm 1.32x10 ⁵	2.05x10 ⁵ \pm 3.25x10 ⁵
bT2	N	1	2	2	5
	pa (degree)	56.90	18.40 \pm 7.92	45.60	34.83 \pm 20.05
	d (μm)	49.70	53.85 \pm 7.71	51.30 \pm 1.41	52.00 \pm 4.32
	l (μm)	73.80	155.60 \pm 74.25	77.95 \pm 95.11	108.18 \pm 74.27
	sa (μm^2)	1.18x10 ⁴	2.75x10 ⁴ \pm 1.48x10 ⁴	1.24x10 ⁴ \pm 1.50x10 ⁴	1.83x10 ⁴ \pm 1.35x10 ⁴
	v (μm^3)	1.45x10 ⁵	3.85x10 ⁵ \pm 2.53x10 ⁵	1.56x10 ⁵ \pm 1.88x10 ⁵	2.45x10 ⁵ \pm 2.03x10 ⁵
bT0-2 Σ	N	36	33	18	
	pa (degree)	55.88 \pm 28.95	45.60 \pm 23.52	34.83 \pm 20.05	
	d (μm)	38.82 \pm 8.33	44.72 \pm 11.00	52.00 \pm 4.32	
	l (μm)	73.61 \pm 60.23	111.61 \pm 132.65	108.18 \pm 74.27	
	sa (μm^2)	8.91x10 ³ \pm 7.61x10 ³	1.68x10 ⁴ \pm 2.29x10 ⁴	1.83x10 ⁴ \pm 1.35x10 ⁴	
	v (μm^3)	8.48x10 ⁴ \pm 7.98x10 ⁴	2.05x10 ⁵ \pm 3.25x10 ⁵	1.34x10 ⁵ \pm 1.13x10 ⁵	
Team B		terminal villus	intermediate villus	stem villus	All villi Σ
bT0	N	38	15	0	53
	pa (degree)	55.28 \pm 28.09	62.19 \pm 32.94		57.23 \pm 29.39
	d (μm)	38.55 \pm 8.21	43.63 \pm 12.88		39.99 \pm 9.90
	l (μm)	67.13 \pm 49.48	89.57 \pm 84.71		73.48 \pm 61.47
	sa (μm^2)	7.89x10 ³ \pm 5.78x10 ³	1.17x10 ⁴ \pm 1.11x10 ⁴		8.96x10 ³ \pm 7.77x10 ³
	v (μm^3)	7.23x10 ⁴ \pm 5.71x10 ⁴	1.23x10 ⁵ \pm 1.23x10 ⁵		8.68x10 ⁴ \pm 8.33x10 ⁴

	N	17	18	1	36
	pa (degree)	48.84 ± 26.65	44.06 ± 29.10	31.20	44.65 ± 27.93
	d (μm)	44.39 ± 8.08	47.99 ± 13.08	44.10	44.39 ± 8.08
bT1	l (μm)	81.64 ± 47.92	137.84 ± 174.61	62.50	109.21 ± 129.28
	sa (μm ²)	1.11x10 ⁴ ± 6.70x10 ³	2.18x10 ⁴ ± 3.03x10 ⁴	8.35x10 ³	1.64x10⁴ ± 2.23x10⁴
	v (μm ³)	1.21x10 ⁵ ± 8.24x10 ⁴	2.80x10 ⁵ ± 4.31x10 ⁵	8.71x10 ⁴	1.99x10⁵ ± 3.16x10⁵
	N	2	3	1	6
	pa (degree)	55.50 ± 1.98	18.40 ± 7.92	45.60	38.68 ± 19.38
	d (μm)	45.30 ± 6.22	53.33 ± 5.52	50.30	50.15 ± 5.95
bT2	l (μm)	120.80 ± 66.47	107.30 ± 98.77	145.20	118.12 ± 70.75
	sa (μm ²)	1.68x10 ⁴ ± 6.99x10 ³	1.90x10 ⁴ ± 1.82x10 ⁴	2.30x10 ⁴	1.89x10⁴ ± 1.21x10⁴
	v (μm ³)	1.84x10 ⁵ ± 5.50x10 ⁴	2.64x10 ⁵ ± 2.75x10 ⁵	2.89x10 ⁵	2.42x10⁵ ± 5.64x10³
	N	57	36	2	
	pa (degree)	52.51 ± 27.76	45.29 ± 34.25	38.40 ± 10.18	
bT0-2	d (μm)	40.53 ± 8.48	46.62 ± 12.64	47.20 ± 4.38	
Σ	l (μm)	73.34 ± 49.80	115.18 ± 137.07	103.85 ± 58.48	
	sa (μm ²)	9.14x10³ ± 6.34x10³	1.74x10⁴ ± 2.32x10⁴	1.57x10⁴ ± 1.04x10⁴	
	v (μm ³)	9.15x10⁴ ± 7.08x10⁴	2.13x10⁵ ± 3.27x10⁵	1.88x10⁵ ± 1.43x10⁵	

Team A and B		non-sinusoidal villus	sinusoidal villus	All villi Σ
	N	4	5	11
	pa (degree)	52.98 ± 28.48	56.04 ± 28.13	54.41 ± 23.80
	d (μm)	49.90 ± 17.56	41.72 ± 8.15	44.95 ± 12.19
bT0	l (μm)	118.25 ± 97.12	93.34 ± 115.81	104.84 ± 93.44
	sa (μm ²)	1.70x10 ⁴ ± 1.38x10 ⁴	1.21x10 ⁴ ± 1.38x10 ⁴	1.40x10⁴ ± 1.19x10⁴
	v (μm ³)	2.02x10 ⁵ ± 1.72x10 ⁵	1.20x10 ⁵ ± 1.28x10 ⁵	1.51x10⁵ ± 1.31x10⁵
	N	5	4	10
	pa (degree)	36.97 ± 10.17	64.30 ± 42.72	50.63 ± 31.88
	d (μm)	50.03 ± 16.94	46.08 ± 8.86	48.05 ± 12.69
bT1	l (μm)	63.05 ± 43.11	66.30 ± 25.83	64.68 ± 32.95
	sa (μm ²)	1.08x10 ⁴ ± 1.01x10 ⁴	1.02x10 ⁴ ± 5.78x10 ³	1.05x10⁴ ± 7.60x10³
	v (μm ³)	1.55x10 ⁵ ± 1.94x10 ⁵	1.27x10 ⁵ ± 9.30x10 ⁴	1.41x10⁵ ± 1.42x10⁵
	N	3	1	4
	pa (degree)	39.05 ± 21.28	24.00	31.05 ± 21.28
	d (μm)	50.10 ± 13.01	59.30	50.10 ± 13.01
bT2	l (μm)	187.95 ± 28.50	208.10	187.95 ± 28.50
	sa (μm ²)	2.99x10 ⁴ ± 1.15x10 ⁴	3.80x10 ⁴	2.99x10⁴ ± 1.15x10⁴
	v (μm ³)	3.93x10 ⁵ ± 2.41x10 ⁵	5.64x10 ⁵	3.93x10⁵ ± 2.41x10⁵

	N	12	10
	pa (degree)	44.54 ± 2.155	55.23 ± 31.70
bT0-2	d (µm)	49.99 ± 14.74	45.22 ± 9.21
Σ	l (µm)	110.11 ± 78.83	94.00 ± 89.28
	sa (µm ²)	1.71x10 ⁴ ± 1.29x10 ⁴	1.39x10 ⁴ ± 1.30x10 ⁴
	v (µm ³)	2.21x10 ⁵ ± 1.94x10 ⁵	1.67x10 ⁵ ± 1.72x10 ⁵

File

SFile 1 The file shows all microphotographs of the core collection (95 microphotographs, round 1) and the 25 microphotographs used for identification of presence or absence of sinusoidal capillaries (round 2). Each page of the file shows the microphotograph in the upper left part of the page while the 3D position and the outcome of histologic assessments of the examiners are shown at the right part of the page. The histologic assessments are tabulated for all examiners and for teams A and B separately. The pages with the 95 microphotographs of the core collection (round 1) show the dendrogram of the respective villous tree in the lower central part of the page. The position of the branch from which the microphotograph was taken is indicated on each page by a red circle or by a red circle and a red arrow.

3.4 Publication IV

Novel 3D light microscopic analysis of IUGR placentas points to a morphological correlate of compensated ischemic placental disease in humans

Abstract

The villous tree of the human placenta is a complex three-dimensional (3D) structure with branches and nodes at the feto-maternal border in the key area of gas and nutrient exchange. Recently we introduced a novel, computer-assisted 3D light microscopic method that enables 3D topological analysis of branching patterns of the human placental villous tree. In the present study we applied this novel method to the 3D architecture of peripheral villous trees of placentas from patients with intrauterine growth retardation (IUGR placentas), a severe obstetric syndrome. We found that the mean branching angle of branches in terminal positions of the villous trees was significantly different statistically between IUGR placentas and clinically normal placentas. Furthermore, the mean tortuosity of branches of villous trees in directly preterminal positions was significantly different statistically between IUGR placentas and clinically normal placentas. We show that these differences can be interpreted as consequences of morphological adaptation of villous trees between IUGR placentas and clinically normal placentas, and may have important consequences for the understanding of the morphological correlates of the efficiency of the placental villous tree and their influence on fetal development.

Reference

Haeussner E , Schmitz C, Frank HG, Edler von Koch F. - Novel 3D light microscopic analysis of IUGR placentas points to a morphological correlate of compensated ischemic placental disease in humans. Scientific Reports. 2016 April 6:24004

URL Link

<http://www.nature.com/articles/srep24004>

SCIENTIFIC REPORTS

OPEN

Novel 3D light microscopic analysis of IUGR placentas points to a morphological correlate of compensated ischemic placental disease in humans

Received: 17 September 2015

Accepted: 18 March 2016

Published: 05 April 2016

Eva Haeussner¹, Christoph Schmitz¹, Hans-Georg Frank^{1,*} & Franz Edler von Koch^{2,*}

The villous tree of the human placenta is a complex three-dimensional (3D) structure with branches and nodes at the feto-maternal border in the key area of gas and nutrient exchange. Recently we introduced a novel, computer-assisted 3D light microscopic method that enables 3D topological analysis of branching patterns of the human placental villous tree. In the present study we applied this novel method to the 3D architecture of peripheral villous trees of placentas from patients with intrauterine growth retardation (IUGR placentas), a severe obstetric syndrome. We found that the mean branching angle of branches in terminal positions of the villous trees was significantly different statistically between IUGR placentas and clinically normal placentas. Furthermore, the mean tortuosity of branches of villous trees in directly preterminal positions was significantly different statistically between IUGR placentas and clinically normal placentas. We show that these differences can be interpreted as consequences of morphological adaptation of villous trees between IUGR placentas and clinically normal placentas, and may have important consequences for the understanding of the morphological correlates of the efficiency of the placental villous tree and their influence on fetal development.

The villous tree of the human placenta enables feto-maternal exchange. The exchange function of the villous tree is mainly controlled by the trophoblast, an epithelium with an apical, syncytialized layer^{1–4}. The trophoblast is positioned at the surface of a multi-branched villous tree structure which consists of stromal cells and vessels. The villous tree is a three-dimensional (3D) structure with characteristic branching pattern and multiple branching points (nodes), and can be analyzed by tree-specific morphometric assessments similar to those established for other naturally occurring tree structures⁵. Variations in the architecture of branches and nodes of the villous trees have been in focus of microscopic placental research for decades^{3,4}. It has been hypothesized that structural aberrances of the angiogenetically driven branching of villous trees are an essential correlate of pathologic course of pregnancies^{6,7}. A frequent^{4,8} and severe pregnancy disease is intrauterine growth retardation (IUGR;^{1,4,9}) which is an important cause of iatrogenic preterm birth and increases life-long health risks for the child¹⁰. Numerous histological findings (infarction, immaturity, hypermaturity, hyperangiogenesis, etc.^{4,6,11}) were documented for IUGR with conventional, two-dimensional (2D) histology (i.e., by analyzing thin sections of human placentas) but could so far not be consistently translated into quantitative 3D morphological topology of the villous trees.

The 3D topology of the villous tree cannot reliably be analyzed on thin (2D) histological sections because the identification of villi as respectively terminal, intermediate or small peripheral stem villi is not unequivocally possible¹². Furthermore, branching hierarchy, nodes and parameters like branching angles, tortuosity and branch length cannot be determined on thin (2D) histological sections at all^{12,13}.

Recently, we introduced a novel light microscopic method for accurate 3D tracing, reconstruction, visualization and quantitative analysis of the topological position of branches and nodes of human placental villous

¹Department of Anatomy II, LMU Munich, Pettenkoferstr. 11, 80336 Munich, Germany. ²Clinic for Obstetrics and Gynecology Dritter Orden, Menzinger Str. 44, 80638 Munich, Germany. *These authors jointly supervised this work. Correspondence and requests for materials should be addressed to H.-G.F. (email: hans-georg.frank@med.uni-muenchen.de)

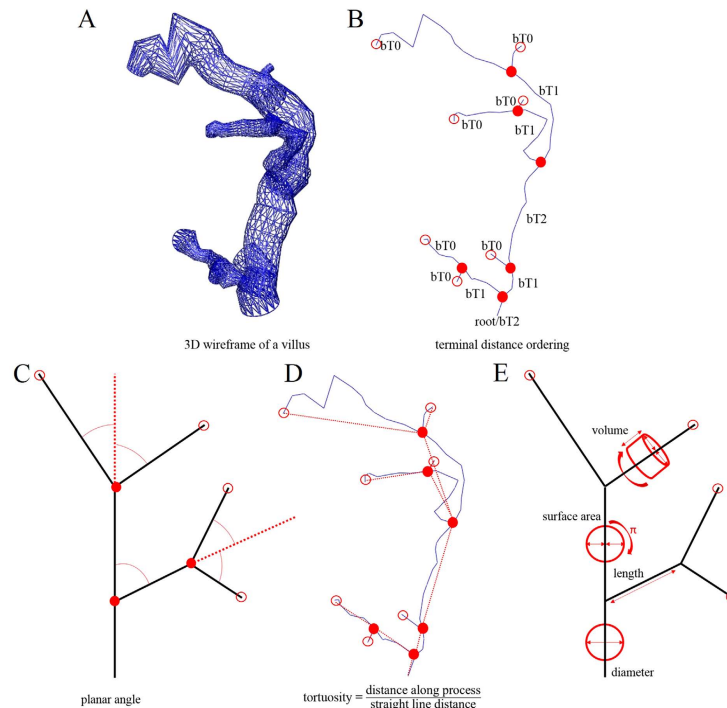


Figure 1. Principles of our novel light microscopic method for accurate 3D microscopic tracing, reconstruction, visualization and quantitative analysis of the topological position of branches and nodes of human placental villous trees. (A,B) two graphs of the same villous tree, obtained by 3D microscopic tracing and reconstruction. The surface of the villous tree is shown as a rendered 3D wireframe (A), whereas (B) shows the skeletonized view of the villous tree. The terminal distance order is given for each branch (abbreviated bT). The number behind bT indicates the number of nodes (filled red dots) to the nearest terminal end of the tree. Accordingly, bT0 indicates villous branches in terminal position of the villous tree, bT1 villous branches in direct preterminal position of the villous tree, and bT2 villous branches that are two nodes apart of the next terminal end. The root gives the start of villous tracing. (C) sketch of a human placental villous tree showing connections between branching nodes (filled red dots) and/or terminal ends (open dots). The planar branching angle of a given branch (black lines) was defined as the change in the direction of the branch with respect to the direction of the branch at the next higher order (red dotted line). The direction of each branch was derived from its endpoint (i.e., a terminal end in case of bT0 or a branching node in case of bT1 and bT2). (D) the same skeletonized view of a human placental villous tree as shown in (B), indicating tortuosity of individual branches. Tortuosity is a measure of how twisted a branch is, and is defined as the ratio between the actual distance in space along a branch (skeleton lines) and the shortest distance in space between the corresponding branching nodes and/or terminal ends (red lines). Thus, a straight line has a tortuosity of 1, and a branch with twists and turns a tortuosity of greater than 1^{42–45}. (E) the same sketch of a human placental villous tree as shown in (C), indicating measurement of the parameters diameter, length, surface area and volume.

trees^{12,13}. This method allows instant determination of topological parameters such as hierarchy of branches, branching angles and length of branches of isolated peripheral villous trees. The principles of this novel method are summarized in Fig. 1. When applied to the analysis of a population of clinically normal placentas this novel method revealed a correlation between the fetoplacental weight ratio at birth and villous branching angles of branches in terminal positions¹³.

In the present study we hypothesized that such advanced 3D microscopic analysis will reveal differences of e.g. branching and length and/or tortuosity of branches in defined topological positions of isolated peripheral villous trees of IUGR placentas as compared to villous trees of clinically normal placentas.

We tested this hypothesis on two collections of human placentas, i.e., $n = 40$ IUGR placentas and $n = 50$ clinically normal placentas. Under careful dissection we prepared and isolated peripheral parts of villous trees and analyzed these tissue samples with the software, NeuroLucida (MBF Bioscience, Williston, VT, USA). We used settings adapted to the requirements of villous branching¹³.

We found that individual mean branching angles of villi in terminal position (i.e., one value per investigated placenta) and individual mean tortuosity of villi in directly preterminal position were significantly different statistically between IUGR placentas and clinically normal placentas.

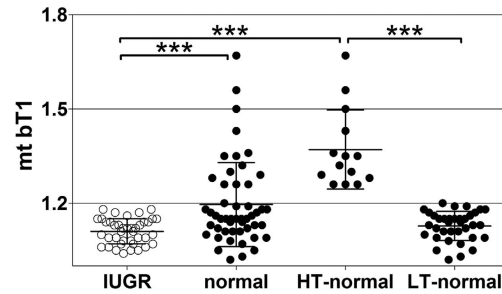


Figure 2. Individual mean tortuosity of villous branches in directly preterminal position of IUGR placentas and clinically normal placentas. The panel shows mean, standard deviation and single values (one per placenta) of the individual mean tortuosity of the branches in directly preterminal position (mt bT1) in IUGR placentas and clinically normal placentas, with the latter split into placentas with either high (HT-normal) or low (LT-normal) tortuosity (details are provided in the main text). The term bT1 is defined in Fig. 1B. Results of statistical analysis (post-hoc Dunn's test for pairwise comparisons after Kruskal-Wallis test; $p < 0.001$) are indicated. * $p < 0.05$; ** $p < 0.01$; *** $p < 0.001$.

Results

Macroscopic analysis for sample validation. No statistically significant differences between the IUGR placentas and the clinically normal placentas were found in the mean fetoplacental weight ratio (i.e., the ratio between placental weight and fetal weight at birth) and the mean roundness of the outer placental rim (Table S1 in Supplementary Information). All other investigated parameters (gestational age, birth weight, placental weight, surface area of the placenta, thickness of the placenta, longest diameter of the placental disk and shortest diameter of the placental disk) were on average significantly smaller statistically in the IUGR placentas compared to the clinically normal placentas (Table S1 in Supplementary Information). These data are in line with results of numerous earlier studies^{14–17} and, thus, validate the present collections of placentas for the purpose of research on IUGR placentas.

Microscopic analysis and branch topology. The individual mean tortuosity of villous branches in directly preterminal position of the villous tree (i.e., at position bT1 according to our new classification¹³; one mean value per investigated placenta) was significantly lower statistically in the IUGR placentas than the clinically normal placentas ($p = 0.0002$; Fig. 2). Detailed analysis revealed that the observed difference between the IUGR placentas and the clinically normal placentas was caused by a subset of clinically normal placentas with individual mean tortuosity of villous branches at position bT1 of more than 1.2, i.e., a higher value than found for any of the investigated IUGR placentas. We therefore divided the clinically normal placentas into two subgroups, i.e., placentas with individual mean tortuosity of villous branches in bT1 of more than 1.2 (henceforth referred to as high tortuosity at position bT1; HT-normal) or less than 1.2 (henceforth referred to as low tortuosity at position bT1; LT-normal), respectively. Accordingly, comparison between the IUGR placentas, the HT-normal placentas and the LT-normal placentas showed statistically significant differences in mean values of the individual mean tortuosity of villous branches at position bT1 between the IUGR placentas and the HT-normal placentas as well as between the HT-normal placentas and the LT-normal placentas, but not between the IUGR placentas and the LT-normal placentas (Fig. 1).

The individual mean planar branching angle of villous branches in terminal position of the villous tree (i.e., at position bT0 according to our new classification¹³; one value per investigated placenta) of the IUGR placentas was significantly larger statistically than in clinically normal placentas ($p = 0.007$; Fig. 3A). When comparing the IUGR placentas with the HT-normal placentas and the LT-normal placentas, the difference between the IUGR placentas and the LT-normal placentas was statistically significant, but neither the difference between the IUGR placentas and the HT-normal placentas nor between the HT-normal placentas and the LT-normal placentas (Fig. 3A). Rose diagrams showed that the distributions of the individual mean planar branching angle of villous branches at position bT0 had two maxima in case of the IUGR placentas (found at 58 and 76 degrees; Fig. 3B), the clinically normal placentas (52 and 66 degrees; Fig. 3B) and the LT-normal placentas (52 and 64 degrees; Fig. 3C). Hartigan's Dip test confirmed non-unimodality of these data. In contrast, the distribution of the individual mean planar branching angle of villous branches at position bT0 of the HT-normal placentas had only one maximum at 67 degree (Fig. 3C).

We found no statistically significant difference in the mean values of the individual mean length of the villous branches at position bT0 between the IUGR placentas, the clinically normal placentas, the HT-normal placentas and the LT-normal placentas (Fig. 4A). Furthermore, the IUGR placentas were not significantly different statistically from the clinically normal placentas with regard to the mean values of the individual mean length of the villous branches at position bT0 (Fig. 4B), the individual mean surface areas of the villous branches at positions bT0 (Fig. 4C) and bT1 (Fig. 4D), and the individual mean volume of the villous branches at positions bT0 (Fig. 4E) and bT1 (Fig. 4F). Furthermore, for none of these parameters statistically significant differences were found between the IUGR placentas and the LT-normal placentas (Fig. 4B–F). In contrast, the HT-normal placentas showed statistically significantly higher mean values for all these parameters than the IUGR placentas and the LT-normal placentas (Fig. 4B–F).

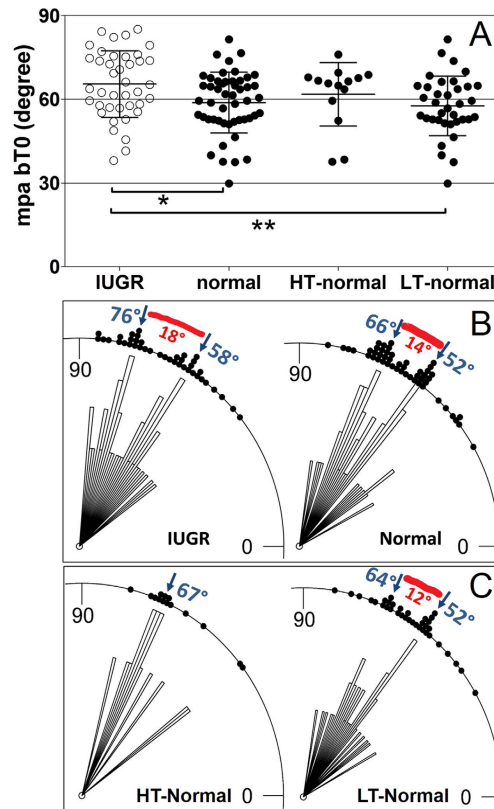


Figure 3. Individual mean planar angles of villous branches in terminal position in IUGR placentas and clinically normal placentas. (A), mean, standard deviation and single values (one per placenta) of the individual mean planar angle of the branches in terminal position (mpa bT0) in IUGR placentas and clinically normal placentas, with the latter split into placentas with either high (HT-normal) or low (LT-normal) tortuosity. The term bT0 is defined in Fig. 1. Results of statistical analysis (post-hoc Dunn's test for pairwise comparisons after Kruskal-Wallis test; $p < 0.0132$) are indicated. * $p < 0.05$; ** $p < 0.01$; *** $p < 0.001$. (B,C) rose diagrams of single values (one per placenta) of the individual mean planar angle of the branches in terminal position (mpa bT0) in IUGR placentas and clinically normal placentas (B), with the latter split into placentas with either high (HT-normal) or low (LT-normal) tortuosity (C). Values that occurred most frequently are labelled with blue arrows. The distance between these maxima is indicated by red segments.

Birth weight, placenta weight and the fetoplacental weight ratio were not significantly different statistically between the LT-normal and HT-normal placentas.

Discussion

The method used in the present study is a novel and innovative approach to analyze the topology of the most peripheral parts of the villous tree in 3D¹³. The most relevant finding of the present study was the statistically significant upward shift of mean planar branching angles of villous branches in terminal position bT0 in IUGR placentas compared to clinically normal placentas (Fig. 3). This result can be interpreted in view of earlier findings that in clinically normal placentas, the mean planar branching angle of branches in position bT0 positively correlated with the fetoplacental weight ratio¹³. This implies that clinically normal placentas with relatively more placental tissue to nourish the fetus tend to have larger branching angles in position bT0. Overall, the upwards shift of angles in position bT0 can be interpreted as a reaction of the placenta to conditions which are present in IUGR, but also in a subpopulation of clinically normal placentas. This novel concept is visualized in Figs 5 and 6 and explained in the following.

The main pathogenetic mechanism associated with IUGR (and other obstetric syndromes like preeclampsia) is insufficient remodeling of uterine spiral arteries by invading trophoblast in early pregnancy (Fig. 5A)^{11,18–22}. Recently, obstetric syndromes associated with this common early pathogenetic event were summarized in a unifying concept named “ischemic placental disease”¹⁸. As placentation proceeds to full hemotrophic nutrition beyond the 12th week, insufficient remodeling of uterine spiral arteries is thought to cause rheologic disturbance (i.e., blood flow disturbances) in the intervillous space and at the surface of the villi (Fig. 5B)²². Higher branching angles in position bT0 can thus potentially be interpreted as a reaction of the constantly growing villous tree to

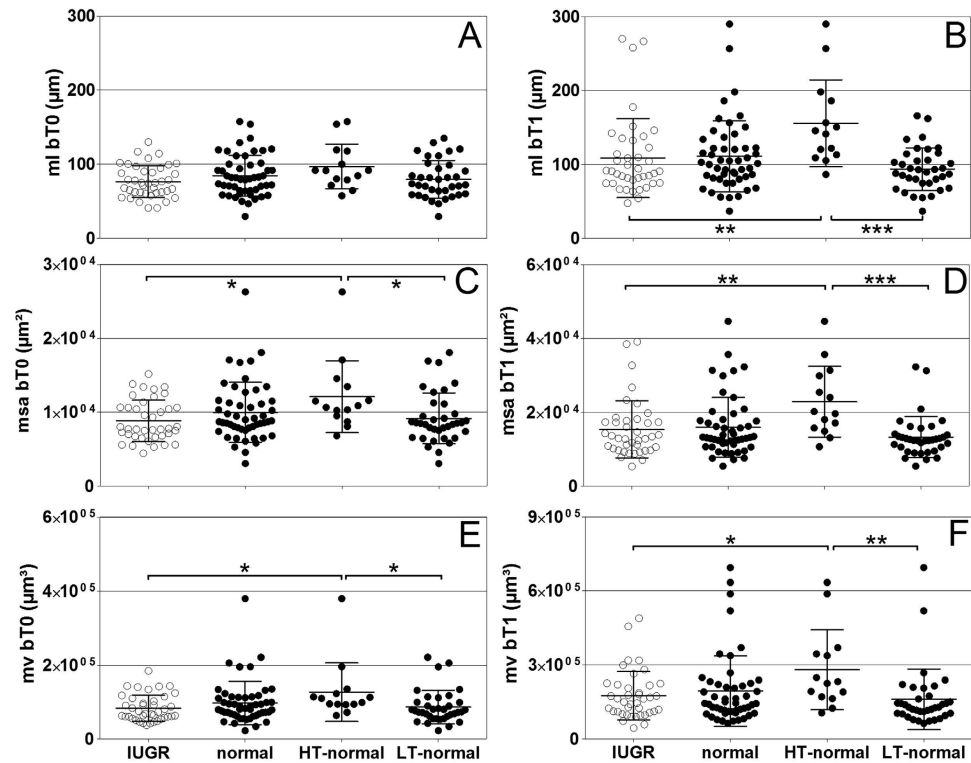


Figure 4. Individual mean length, surface area and volume of villous branches in terminal and directly preterminal position of IUGR placentas and clinically normal placentas. The panels show mean, standard deviation and single values (one per placenta) of the mean length (ml) of the branches at terminal position bT0 (A; ml bT0; result of Kruskal-Wallis test: $p = 0.123$) and directly preterminal position bT1 (B; ml bT1; $p = 0.001$), of the mean surface area (msa) of the branches at positions bT0 (C; msa bT0; $p = 0.027$) and bT1 (D; msa bT1; $p = 0.002$), and of the mean volume (mv) of the branches in bT0 (E; mv bT0; $p = 0.028$) and bT1 (F; mv bT1; $p = 0.008$) in IUGR placentas and clinically normal placentas, with the latter split into placentas with either high (HT-normal) or low (LT-normal) tortuosity in bT1 as defined in Fig. 2. The terms bT0 and bT1 are defined in Fig. 1B. Results of statistical analysis (post-hoc Dunn's tests for pairwise comparisons after Kruskal-Wallis test with $p < 0.05$) are indicated. * $p < 0.05$; ** $p < 0.01$; *** $p < 0.001$.

modified intervillous blood flow (Figs 5C and 6B,C). Such reaction of villous branching to modified blood flow environment could be initiated by direct mechanical force on the villous tree, driving branching into higher angles (Fig. 6B). However, data in favor of such a directly flow-mechanical impact have not yet been published. Another option would be that the modified blood flow environment is recognized by mechanotransduction and signaled to angiogenically active cells inside the villi. Angiogenesis (especially non-branching angiogenesis in the late phase of pregnancy) is thought to be the main mechanism driving villous branching⁴. Differences in branching angles can thus be interpreted as signs of differences of villous angiogenesis. Indeed, branching angles in vascular beds can be influenced by the mechanism of angiogenesis. An angiogenic mechanism which is known to modify vascular branching angles (and thus possibly also villous branching as consequence of angiogenic branching) is intussusceptive angiogenesis^{23–25}. This type of angiogenesis modifies branching angles and is also known to be a fast-response mechanism to mechanical stress^{26,27}. Intussusceptive angiogenesis would be able to respond to e.g. modifications of rheology in the intervillous space. Thus far, to our knowledge, data on the occurrence and relevance of intussusceptive angiogenesis in villous trees of complicated pregnancies are not available.

With the data currently available, it cannot be clarified whether the observations of the present study on branching angles in position bT0 in IUGR placentas and HT-normal placentas reveal a reactive symptom or (in case of IUGR) a cause of growth retardation (Figs 5 and 6). Since the early invasive processes leading to remodeling of uterine spiral arteries are very specific to the human species²², animal models with a different type of early placentation and particularly the absence of villous trees are in principle not helpful to move this field forward.

The present study shows for the first time that tortuosity of branches in the directly preterminal position bT1 significantly differs statistically between IUGR placentas and clinically normal placentas (Fig. 2; note that tortuosity as defined in the present study is not identical to the increased formation of knots and syncytial folds at the villous surface which were reported in earlier studies on severe early onset IUGR placentas¹¹).

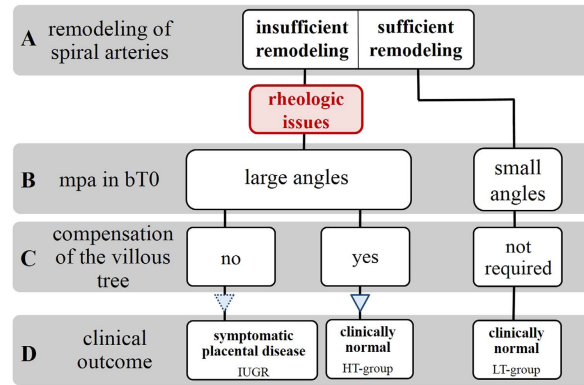


Figure 5. Scheme illustrating our novel hypothesis on pathophysiological interpretation of branching angles and tortuosity of villous branches in positions bT0 and bT1 of human placentas. The proposal starts with the widely accepted early origin of IUGR as insufficient remodeling of uterine spiral arteries (A). Due to rheologic disturbance caused by this insufficient remodeling of uterine spiral arteries, branching angles (mpa) in position bT0 become larger (B; c.f. Fig. 6). For reasons that are currently unknown some placentas cannot compensate this rheologic disturbance and develop into IUGR placentas. In contrast, other placentas with insufficient remodeling of uterine spiral arteries (and, thus, rheologic disturbance and large branching angles at position bT0) develop highly tortuous branches in position bT1 as morphological correlate of successful compensation of rheologic disturbance (C). As a result this subset of placentas (i) shares some morphological characteristics with IUGR placentas (i.e., large branching angles in position bT0; c.f. Fig. 3) and (ii) shows certain morphological characteristics that were neither found in IUGR placentas nor in placentas with sufficient remodeling of uterine spiral arteries (i.e., higher mean tortuosity of the branches in position bT1, higher length of the branches in position bT1 as well as higher mean surface area and higher mean volume of the branches in positions bT0 and bT; c.f. Fig. 4). Because of this successful compensation of rheologic disturbance these placentas present as clinically normal, but are morphologically distinct from other clinically normal placentas in which no insufficient remodeling of uterine spiral arteries occurred.

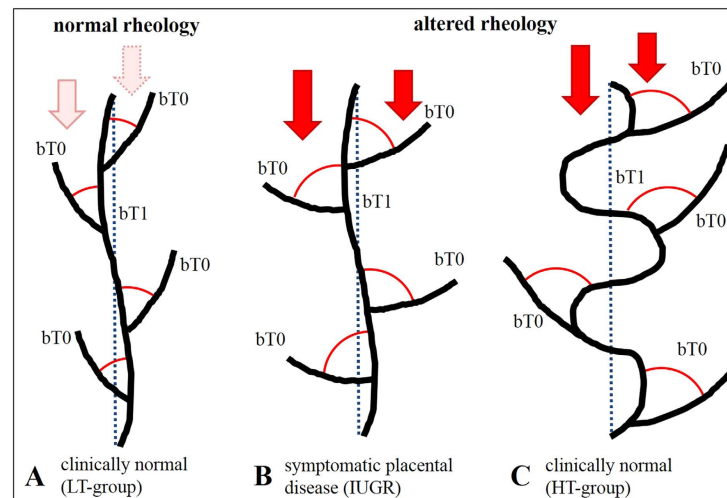


Figure 6. Scheme of hypothesized reactions of the placental villous tree to altered rheology in the intervillous space. (A) without altered rheology in the intervillous space branching angles of villi in position bT0 and tortuosity of villi in position bT1 are small. These placentas present as clinically normal. (B) altered rheologic properties of the blood flow in the intervillous space are indicated by red arrows. The branching angles of branches in position bT0 increase (red circular arcs). Without compensation these placentas develop into IUGR placentas. (C) in a subgroup of placentas exposed to altered rheologic properties of the blood flow in the intervillous space highly tortuous (and, thus, longer) branches in position bT1 appear (tortuosity indicated by increased deviation from the straight blue dotted line; not to scale). These placentas develop into clinically normal placentas (C).

The changes of tortuosity concerned the branch generations in position bT1 and thus the peripheral region of placental villous trees which is considered the main exchange region of the placenta^{4,28}. A relation to placental function is likely for modifications of tortuosity of branches in this region. All tortuosity values in position bT1 of the villous trees from IUGR placentas were below a threshold value of 1.2. In contrast, the tortuosity values in position bT1 of villous trees of 14 out of 50 (28%) investigated clinically normal placentas were substantially higher than this threshold (HT-normal; Fig. 2). Further detailed analysis revealed that the branches in position bT1 of the HT-normal group of the clinically normal placentas were on average longer and had on average a greater surface area and a larger mean volume of branches in positions bT0 and bT1 compared to branches of the LT-normal group of the clinically normal placentas (Fig. 4). They have thus properties which can be expected for structures that were formed to compensate for a possible deficit in maternofetal exchange (Fig. 5). In the IUGR group we could not detect a single case with such highly tortuous branches in bT1. Basically, this could be indicative of a higher flexibility of a subset of placentas to respond to rheologic challenges by adaptation of the structure of villous trees, resulting in clinically normal placentas with certain morphological alterations compared to other clinically normal placentas (outlined in detail in Figs 5D and 6C).

If this hypothesis is correct, the HT-normal group of placentas identified for the first time in the present study represents a subgroup of clinically normal placentas with successful compensation of rheologic disturbance. Without this structural adaptation of villous trees the development of symptomatic disease may be unavoidable (Figs 5D and 6B). Accordingly, for the first time, the present study points to a morphological correlate of compensated “ischemic placental disease”^{18–22,29}. That placentas could be able to evade the rheologic disturbance caused by insufficient remodeling of uterine spiral arteries is a novel aspect. This view is not only important for basic research^{18–22,29} and prenatal programming, but if confirmed in future studies will open a totally new paradigm which could in the future be therapeutically instrumentalized to minimize the fraction of patients with ischemic placental disease which becomes clinically symptomatic.

However, it must be kept in mind that many aspects remain open at this stage. For instance, we do not know whether the degree of remodeling of uterine spiral arteries and severity of rheologic disturbance have to be below a critical threshold to allow compensation by the villous tree. Another option can be that certain placentas are intrinsically (by genetic or other reasons) not able to adapt to the modified blood flow in the intervillous space.

The clinical and macroscopic findings of the present study were in line with earlier findings in the literature^{1,4}, demonstrating that placentas of pregnancies with IUGR were statistically significantly smaller and younger than clinically normal placentas (Table S1). The fetoplacental weight ratio and the roundness of the outer rim of IUGR placentas were not significantly different statistically between IUGR placentas and clinically normal placentas (Table S1). This can be interpreted such that the size of the placenta and fetal weight are strictly coupled to each other^{1,4}, irrespective of the difference of gestational ages between IUGR placentas and clinically normal placentas in the present study and the presence or absence of symptomatic obstetric disease. The hypothesis that variability of placental form might be associated with IUGR^{30–33} is not supported by the data of the present study.

Finally it should be mentioned that the novel 3D light microscopic method used in the present study has some limitations. Although the novel 3D microscopic analysis provides unique access to branching topology (including branching angles, length, tortuosity and nodes), the analysis of villous stroma and angiogenesis is not possible because no histological sectioning is involved. The latter also leads to the limitation that only the most peripheral branches of the placental villous tree can be examined, whereas data on larger stem villi and anchoring villi cannot be obtained because they cannot be investigated at the light microscopic level without histological sectioning.

Conclusion

The 3D microscopic architecture of villous trees of IUGR placentas and clinically normal placentas differs in two main aspects: (i) the branching angles of branches at terminal positions bT0 are on average larger in IUGR, and (ii) villous trees of IUGR placentas do not show a remarkable population of longer and more tortuous villi in the directly preterminal part (bT1) of the villous trees of clinically normal placentas. The shift to larger angles in position bT0 can be indicative of rheologic disturbance caused by insufficient remodeling of uterine spiral arteries. The highly tortuous population of villous branches in position bT1 in a subgroup of clinically normal placentas can be interpreted as morphological correlate of functional compensation of insufficient uterine spiral arterial remodeling. In this subgroup of clinically normal placentas, symptomatic development of IUGR could thus possibly be avoided though signs of rheologic disturbances (indicated by higher branching angles in position bT0) were present.

Materials and Methods

Study design. The present study used two collections of placental tissue. We included 40 placentas from patients with intrauterine growth retardation (IUGR placentas) and 50 placentas from clinically normal pregnancies (clinically normal placentas). Both cohorts of placentas were collected at the Department of Obstetrics and Gynecology of the hospital “Dritter Orden”, Munich, Germany. The collection of clinically normal villous trees was used in a previous study¹³ and served as control group for the collection of IUGR placentas. The course of each pregnancy was assessed by obstetricians based on clinical information regarding the pregnancy and delivery. An IUGR was diagnosed if the growth data of the fetus determined by ultrasound (e.g. femur length, abdomen and head circumferences, etc.) were above the 10th growth percentile during the first two trimesters and then dropped below the 10th growth percentile. Patients with a combination of IUGR and symptoms of preeclampsia were not included.

Placentas were collected after informed consent of the mothers/parents was obtained. Placentas were excluded when (i) no informed consent of the mothers/parents could be obtained, (ii) the language skills of the mothers/parents limited the understanding of information concerning the study, or (iii) psychiatric problems or any other condition caused doubts regarding the mothers/parents ability to independently decide. All work was

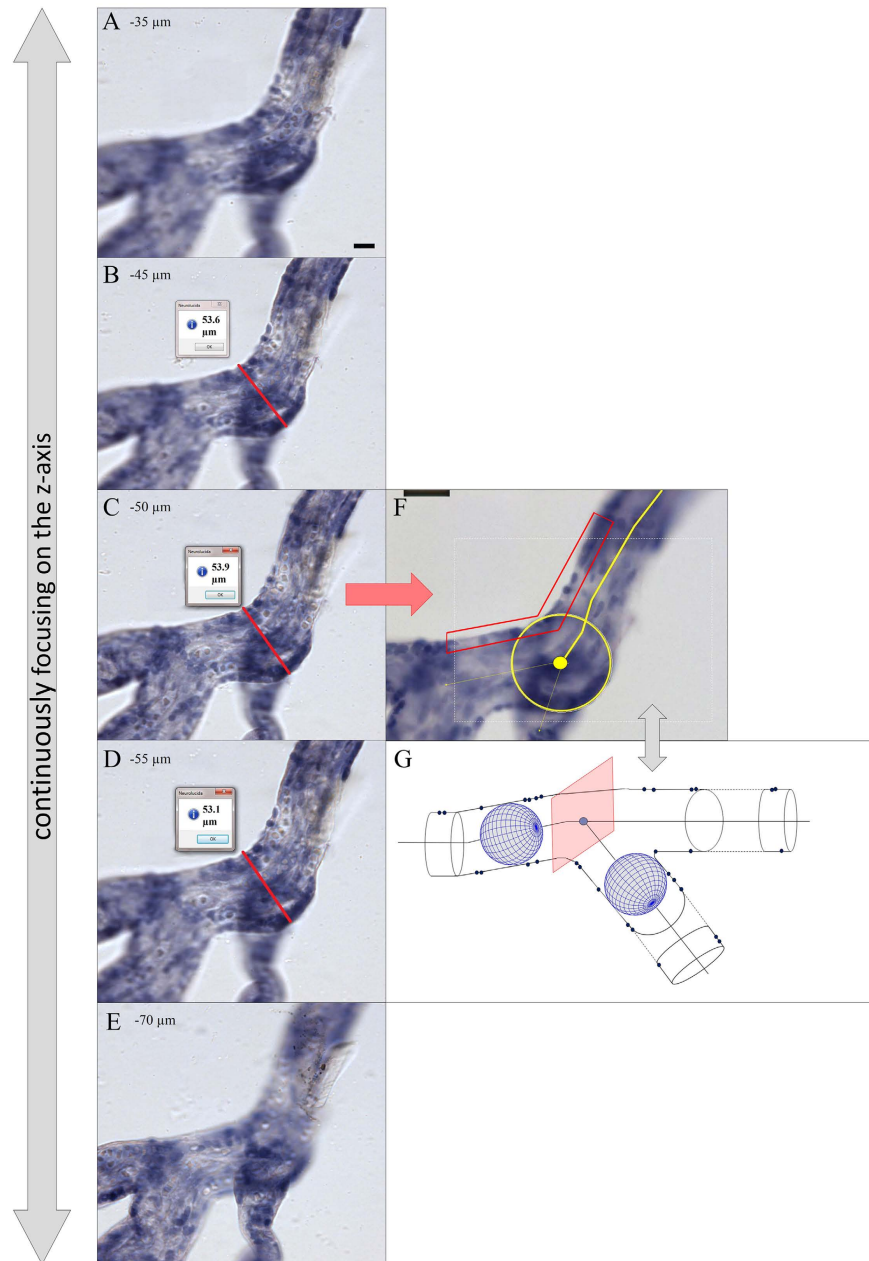


Figure 7. Identification of center lines and branching points of human placental villous segments with 3D light microscopy. (A–E) Selected screenshots of the same microscopic field-of-view taken at various focus depths during an analysis session of a villous tree using NeuroLucida software (MBF Bioscience) through a distance of 35 μm in Z direction (starting at $-35\ \mu\text{m}$ in A through $-70\ \mu\text{m}$ in E). The procedure of positioning the center point at a node is illustrated. The center point was positioned at the Z position at which the investigated villous segment had its maximum diameter (found in panel C; red lines in panels B–D represent the “quick measure line” function of the NeuroLucida software). At a focus depth of $-50\ \mu\text{m}$ (panel C) the largest diameter of the investigated villous segment was in focus. (F,G) illustrates how the center point of the investigated villous segment at the shown XY position was identified with the NeuroLucida software. At the Z position with the largest diameter in focus (panel C) a circle was opened which defined the center point (red arrow from C to F). Note that the marginal cell nuclei of trophoblast were in focus at this Z position (red rectangular label in F) which was used as additional criterion for correct positioning of the center point at the selected Z position. (G) NeuroLucida’s approach is comparable to software algorithms of 3D analysis which are based on “virtual rolling balls” to define center lines and branching points. The scale bar in (A) represents 25 μm in (A–E), and the scale bar in (F) 25 μm in (F).

conducted according to relevant guidelines and regulations. This study was approved by the ethics committee of the Ludwig-Maximilians-University of Munich (Munich, Germany) under the numbers **084-11** and **478-12**. All data were anonymized. The thickness of the placentas was determined by ultrasound. The placental weight (PW) was measured prior to tissue sampling and processing without the umbilical cord but with membranes^{1,4,34}. The birth weight (BW) was determined immediately after birth, and the feto-placental weight ratio (PW/BW) was calculated (Supplementary Table S1). The cohort of clinically normal placentas was collected between February 2012 and April 2013¹³, and the cohort of IUGR placentas between January 2013 and August 2014.

Procedure of tissue sampling and preparation. All placentas were cooled at 4 °C immediately after birth and processed for histology at the Department of Anatomy II of Ludwig-Maximilians-University (Munich, Germany) as described earlier¹³.

For the preparation of single, isolated peripheral parts of villous trees, a sample (edge length, 2–3 cm) was collected. The sampling site was determined using a systematic and random sampling scheme based on the projection of a point pattern onto the chorionic surface of the placenta³⁰. Six sampling sites were taken for routine paraffin embedding and histology; the sampling of the isolated peripheral villous trees was done from the remaining unfixed placental tissue at the midpoint between sampling sites 3 and 4³⁰, a spot that turned out to be not more than 5 cm distant from the insertion of the umbilical cord in all cases. The sample was excised and transferred to physiological saline at 4 °C as previously described¹³. The preparation of peripheral villous trees began within one hour after sampling for histology. Free bushes of peripheral villi were identified, removed using small scissors, and fixed in 4.5% formaldehyde. After washing and bleaching the villous trees were stained with Mayer's hematoxylin. After dehydration in a graded series of ethanol, the probes were mounted in DPX on a concave slide. These preparations have a true 3D character and are free from oppressing contact with the concave slide or cover glass¹³.

3D analysis of villous trees. All peripheral villous trees were traced with Neurolucida^{35–37} (version 10.54; MBF Bioscience) under a light microscope using a 20x objective lens with the working direction from the proximal toward the terminal end of the peripheral villous tree as previously described (Fig. 1)¹³. The diameter of branches was determined continuously as a frustum around the center point. To position the center point correctly in 3D, the diameter was determined in the focus plane showing the largest diameter of the branch. In case of doubt, the “quick measure line” function of the software Neurolucida was used to determine the correct focus plane (Fig. 7). In addition, the trophoblast nuclei of the branch surface should be visible at the margin (Fig. 7) in the same plane. Using these two criteria, the center points were correctly positioned in 3D and the center line connecting them provided an accurate 3D skeleton for determination of branching points and branching angles (Fig. 1). Tree ordering for measurements was set to “Terminal Distance Ordering” in Neurolucida because the terminal end was the biologically defined end of the isolated peripheral villous trees (Fig. 1). Terminal Distance Ordering classifies branches according to their distance in nodes from the terminal end of the villous tree. The measuring system generated a digital 3D replica of the peripheral villous tree under investigation in parallel to the process of tracing (Fig. 1). These data were analyzed with Neurolucida Explorer software (MBF Bioscience) using the option “branching structure analysis”.

We used two microscope systems: (i) an Axioskop (Zeiss, Goettingen, Germany) with a motorized XYZ specimen stage (Maerzhaeuser, Wetzlar, Germany), LEP MAC6000 XYZ 3-axis stage controller (Ludl), focus encoder (Type MT 1271; Heidenhain), and color digital camera (3/40 CCD chip 1,92 MP, 1600 × 1200 pixel, MBF Bioscience; and (ii) a BX50 (Olympus, Tokyo, Japan) with motorized XYZ specimen stage (MBF Bioscience), LEP MAC6000 XYZ 3-axis stage controller (Ludl), focus encoder (Type MT 1271; Heidenhain) and color digital camera (1/20 CCD chip, 1392 × 1040 pixel, MBF Bioscience). The parts of villi connecting two nodes or connecting a terminal end with a node were named branches (b). Branches were further classified by their distance to the nearest terminal end (bT, with the T indicating classification by terminal distance). The distance was measured by the number of nodes to the nearest terminal end, i.e., bT0 (terminal end), bT1 (one node apart of the next terminal end) and bT2 (two nodes apart of the next terminal end)¹³.

Furthermore, we collected data regarding the planar branching angle, diameter, length, surface area and volume of each individual branch. These data were aggregated by the terminal distances of branches for each villous tree (Fig. 1). Of 50 peripheral villous trees of clinically normal placentas, 11 did not show bT2 branches. Of the remaining 39 bT2 branches the planar branching angle of bT2 branches could not be determined for six samples due to a missing previous branch (n = 33 for mpa bT2)¹³. Of the 40 peripheral villous trees of IUGR placentas, 18 did not show bT2 branches (n = 22 for bT2).

Statistical analysis. For all investigated parameters, the mean and standard deviation (SD) were calculated using SPSS software (Version 23; IBM, Armonk, NY, USA)³⁸. Student's t-test and Kruskal-Wallis test with Dunn's comparison test³⁸ were performed with GraphPad Prism software (Version 5; GraphPad, San Diego, CA, USA). A post-hoc statistical analysis was carried out to explore properties of two subpopulations selected from clinically normal villous trees. The two subpopulations distinguished one group with high tortuosity in bT1 (HT-normal) and another group with low tortuosity in bT1 (LT-normal). Rose diagrams of the data on branching angles were prepared with the function rose.diag using the software R³⁹ and the R package CircStats⁴⁰. Unimodal/multimodal distribution of the data on branching angles was tested with Hartigan's Dip Test⁴¹ using the software R³⁹.

References

1. Boyd, J. D. & Hamilton, W. J. *The human placenta*. (Heffer, Cambridge, 1970).
2. Kaufmann, P. Development and differentiation of the human placental villous tree. *Bibl. Anat.* **22**, 29–39 (1982).
3. Kingdom, J., Huppertz, B., Seaward, G. & Kaufmann, P. Development of the placental villous tree and its consequences for fetal growth. *Eur. J. Obstet. Gynecol. Reprod. Biol.* **92**, 35–43 (2000).
4. Benirschke, K., Burton, G. & Baergen, R. N. *Pathology of the human placenta*. (Springer, Berlin and London, 2012).

5. Barker, S. B., Cumming, G. & Horsfield, K. Quantitative morphometry of the branching structure of trees. *J. Theor. Biol.* **40**, 33–43 (1973).
6. Kaufmann, P., Mayhew, T. M. & Charnock-Jones, D. S. Aspects of human fetoplacental vasculogenesis and angiogenesis. II. Changes during normal pregnancy. *Placenta* **25**, 114–26 (2004).
7. Mayhew, T. M., Charnock-Jones, D. S. & Kaufmann, P. Aspects of human fetoplacental vasculogenesis and angiogenesis. III. Changes in complicated pregnancies. *Placenta* **25**, 127–39 (2004).
8. Chaddha, V., Viero, S., Huppertz, B. & Kingdom, J. Developmental biology of the placenta and the origin of placental insufficiency. *Semin. Fetal Neonatal Med.* **9**, 357–69 (2004).
9. Rath, W. *Geburtshilfe und Perinatalogie*. (Thieme, Stuttgart, 2010).
10. Gaudineau, A. Prevalence, risk factors, maternal and fetal morbidity and mortality of intrauterine growth restriction and small-for-gestational age. *J. Gynecol. Obstet. Biol. Reprod.* **42**, 895–910 (2013).
11. Kingdom, J. C., Walker, M., Drewlo, S. & Keating, S. In: *Fetal therapy: Scientific basis and critical appraisal of clinical benefits*, (eds Kilby M., Johnson A., Oepkes, D.) Ch. 18.1, 341–54 (Cambridge University Press, Cambridge, 2013).
12. Haeussner, E. *et al.* Does 2D-histologic identification of villous types of human placentas at birth enable sensitive and reliable interpretation of 3D structure? *Placenta* **36**(12), 1425–1432 (2015).
13. Haeussner, E., Buehlmeier, A., Schmitz, C., Edler von Koch, F. & Frank, H. G. Novel 3D microscopic analysis of human placental villous trees reveals unexpected significance of branching angles. *Sci. Rep.* **4**, 6192 (2014).
14. Burkhardt, T., Schaffer, L., Schneider, C., Zimmermann, R. & Kurmanavicius, J. Reference values for the weight of freshly delivered term placentas and for placental weight-birth weight ratios. *Eur J Obstet Gynecol Reprod Biol* **128**(1–2), 248–52 (2006).
15. Tomas, S. Z., Roje, D., Prusac, I. K., Tadin, I. & Capkun, V. Morphological characteristics of placentas associated with idiopathic intrauterine growth retardation: a clinicopathologic study. *Eur J Obstet Gynecol Reprod Biol* **152**(1), 39–43 (2010).
16. Almog, B. *et al.* Placenta weight percentile curves for singleton and twins deliveries. *Placenta* **32**(1), 58–62 (2011).
17. Almasry, S. M. & Elfayomy, A. K. Morphometric analysis of terminal villi and gross morphological changes in the placentae of term idiopathic intrauterine growth restriction. *Tissue Cell* **44**(4), 214–19 (2012).
18. Ananth, C. V. Ischemic placental disease: A unifying concept for preeclampsia, intrauterine growth restriction, and placental abruption. Ischemic placental disease. *Semin. Perinatol* **38**, 131–132 (2014).
19. Pijnenborg, R., Borsens, I. & Romero R. *Placental bed vascular disorders. Basic science and its translation to obstetrics* (Cambridge University Press, Cambridge, 2010).
20. Bakker, P. & van Geijn H. P. Uterine activity: implications for the condition of the fetus. *J. Perinat. Med.* **36**, 30–7 (2008).
21. Pijnenborg, R., Vercruysse, L. & Hanssens, M. Fetal-maternal conflict, trophoblast invasion, preeclampsia, and the red queen. *Hypertens. Pregnancy* **27**, 183–96 (2008).
22. Burton, G. J., Woods, A. W., Jauniaux, E. & Kingdom, J. C. P. Rheological and Physiological Consequences of Conversion of the Maternal Spiral Arteries for Uteroplacental Blood Flow during Human Pregnancy. *Placenta* **30**, 473–82 (2009).
23. Belle, J. *et al.* Stretch-induced Intussusceptive and Sprouting Angiogenesis in the Chick Chorionallantoic Membrane. *Microvasc. Res.* **95**, 60–67 (2014).
24. Ackermann, M., Tsuda, A., Secomb, T. W., Mentzer, S. J. & Konerding, M. A. Intussusceptive remodeling of vascular branch angles in chemically-induced murine colitis. *Microvasc. Res.* **87**, 75–82 (2013).
25. Burri, P. H., Hlushchuk, R. & Djonov, V. Intussusceptive angiogenesis: its emergence, its characteristics, and its significance. *Dev. Dyn.* **231**, 474–488 (2004).
26. Secomb, T. W., Alberding, J. P., Hsu, R., Dewhirst, M. W. & Pries, A. R. Angiogenesis: an adaptive dynamic biological patterning problem. *PLoS Comput. Biol.* **9**, e1002983 (2013).
27. Kurz, H., Burri, P. H. & Djonov, V. G. Angiogenesis and Vascular Remodeling by Intussusception: From Form to Function. *Physiology* **18**, 65–70 (2003).
28. Charnock-Jones, D. S., Kaufmann, P. & Mayhew, T. M. Aspects of human fetoplacental vasculogenesis and angiogenesis. I. Molecular regulation. *Placenta* **25**, 103–13 (2004).
29. Ananth, C. V. & Friedman, A. M. Ischemic placental disease and risks of perinatal mortality and morbidity and neurodevelopmental outcomes. *Semin. Perinatol.* **38**, 151–158 (2014).
30. Salafia, C. M., Vintzileos, A. M., Silberman, L., Bantham, K. F. & Vogel, C. A. Placental pathology of idiopathic intrauterine growth retardation at term. *Am. J. Perinatol.* **9**, 179–84 (1992).
31. Salafia, C. M., Ernst, L. M., Pezzullo, J. C., Wolf, E. J., Rosenkrantz, T. S. & Vintzileos, A. M. The very low birthweight infant: maternal complications leading to preterm birth, placental lesions, and intrauterine growth. *Am. J. Perinatol.* **12**, 106–10 (1995).
32. Salafia, C. M., Misra, D. P., Yampolsky, M., Charles, A. K. & Miller, R. K. Allometric metabolic scaling and fetal and placental weight. *Placenta* **30**, 355–60 (2009).
33. Salafia, C. M. & Yampolsky, M. Metabolic scaling law for fetus and placenta. *Placenta* **30**, 468–71 (2009).
34. Haeussner, E., Schmitz, C., Edler von Koch, F. & Frank, H. G. Birth Weight correlates with Size but not Shape of the Normal Human Placenta. *Placenta* **34**, 574–82 (2013).
35. Aguiar, P., Sousa, M. & Szucs, P. Versatile morphometric analysis and visualization of the three-dimensional structure of neurons. *Neuroinformatics* **11**, 393–403 (2013).
36. Halavi, M., Hamilton, K. A., Parekh, R. & Ascoli, G. A. Digital reconstructions of neuronal morphology: three decades of research trends. *Front. Neurosci.* **6**, 49–61 (2012).
37. Glaser, J. & Glaser, E. Neuron imaging with Neurolucida—A PC-based system for image combining microscopy. *Comput. Med. Imag. Grap.* **14**, 307–317 (1990).
38. Bronstein, I. N. & Semendjajew, K. A. *Taschenbuch der Mathematik*. (Deutsch, Thun, 2001).
39. R. Core Team. R: A language and environment for statistical computing. R Foundation for Statistical Computing, Vienna, Austria (2015). Available at: <http://www.R-project.org>. (Accessed: 8th January 2016).
40. S-plus original by Ulric Lund and R port by Claudio Agostinelli. CircStats: Circular Statistics, from “Topics in circular Statistics” (2001). R package version 0.2-4. (2012) Available at: <http://CRAN.R-project.org/package=CircStats>. (Accessed: 8th January 2016).
41. diptest: Hartigan's Dip Test Statistic for Unimodality—Corrected. R package version 0.75-7 (2015) Available at: <http://CRAN.R-project.org/package=dipetest>. (Accessed: 8th January 2016).
42. Benhamou, S. How to reliably estimate the tortuosity of an animal's path: straightness, sinuosity, or fractal dimension? *J. Theor. Biol.* **229**, 209–220 (2004).
43. Franken, R. *et al.* Increased aortic tortuosity indicates a more severe aortic phenotype in adults with Marfan syndrome. *Int. J. Cardiol.* **194**, 7–12 (2015).
44. Dursun, I. *et al.* Effects of early postnatal exposure to ethanol on retinal ganglion cell morphology and numbers of neurons in the dorsolateral geniculate in mice. *Alcohol Clin. Exp. Res.* **35**, 2063–2074 (2011).
45. Coombs, J., van der List, D., Wang, G. Y. & Chalupa, L. M. Morphological properties of mouse retinal ganglion cells. *Neuroscience* **140**, 123–136 (2006).

Acknowledgements

The authors acknowledge the skillful technical assistance and diligent work of the entire team of technicians at the Department of Anatomy II at LMU Munich, namely A. Baltruschat, U. Fazekas, S. Kerling, C. Stanglmair, B. Mosler and S. Tost. We would also like to express our thanks to the obstetricians, midwives, and nurses of the Dritter Orden hospital (Munich, Germany) who enabled the clinical work of this study with great care and engagement. Results are part of the doctoral thesis of EH.

Author Contributions

E.H. and H.-G.F. performed the analysis. E.H., C.S., F.v.K. and H.-G.F. designed the study. F.v.K. was responsible for obstetrical tasks. E.H. and H.-G.F. prepared figures and tables. H.-G.F., C.S., F.v.K. and E.H. wrote the manuscript.

Additional Information

Supplementary information accompanies this paper at <http://www.nature.com/srep>

Competing financial interests: No organization sponsored the research described in the present study. C.S. serves as paid consultant for and receives benefits from MBF Bioscience, the manufacturer and distributor of the software, Neurolucida. However, MBF Bioscience had no any role in study design, data collection and analysis, decision to publish, or preparation of this manuscript. Furthermore, C.S. has not received any honoraria or consultancy fee in writing this manuscript. No other potential conflicts of interest relevant to this article were reported.

How to cite this article: Haeussner, E. *et al.* Novel 3D light microscopic analysis of IUGR placentas points to a morphological correlate of compensated ischemic placental disease in humans. *Sci. Rep.* **6**, 24004; doi: 10.1038/srep24004 (2016).



This work is licensed under a Creative Commons Attribution 4.0 International License. The images or other third party material in this article are included in the article's Creative Commons license, unless indicated otherwise in the credit line; if the material is not included under the Creative Commons license, users will need to obtain permission from the license holder to reproduce the material. To view a copy of this license, visit <http://creativecommons.org/licenses/by/4.0/>

Novel 3D light microscopic analysis of IUGR placentas points to a morphological correlate of compensated ischemic placental disease in humans

Eva Haeussner, Christoph Schmitz, Hans-Georg Frank, Franz Edler von Koch

Supplementary Information

Table S1 Descriptive statistic of macroscopic parameters (gestational age (GA), birth weight (BW), placental weight (PW), feto-placental weight ratio (PW/BW), surface area (surface), roundness of placental disc (roundness), thickness of placental disc (thickness), longest diameter of placental disc (LD), shortest diameter of placental disc (SD)) of intrauterine growth restriction (IUGR) and clinically normal placentas is shown. The number (n), mean and standard deviation (SD) is given per case. The p-value of the Student's t-test between IUGR and clinically normal placentas is given in the last column.

IUGR	n	mean	SD	clinically normal	n	mean	SD	t-Test p-value
GA (weeks)	40	37.53	2.72	GA (weeks)	50	39.29	1.03	p < 0.001
BW (g)	40	2273.10	498.96	BW (g)	50	3456.98	583.09	p < 0.001
PW (g)	40	350.40	85.66	PW (g)	50	524.06	121.69	p < 0.001
PW/BW ratio	40	0.160	0.049	PW/BW ratio	50	0.150	0.023	ns
surface area (cm ²)	40	915.50	244.43	surface area (cm ²)	50	1143.70	243.43	p < 0.001
roundness	40	1.21	0.15	roundness	50	1.19	0.16	ns
thickness (cm)	40	1.51	0.35	thickness (cm)	50	1.75	0.37	p < 0.01
LD (cm)	40	18.54	2.56	LD (cm)	50	20.71	2.83	p < 0.001
SD (cm)	40	15.50	2.41	SD (cm)	50	17.45	1.97	p < 0.001

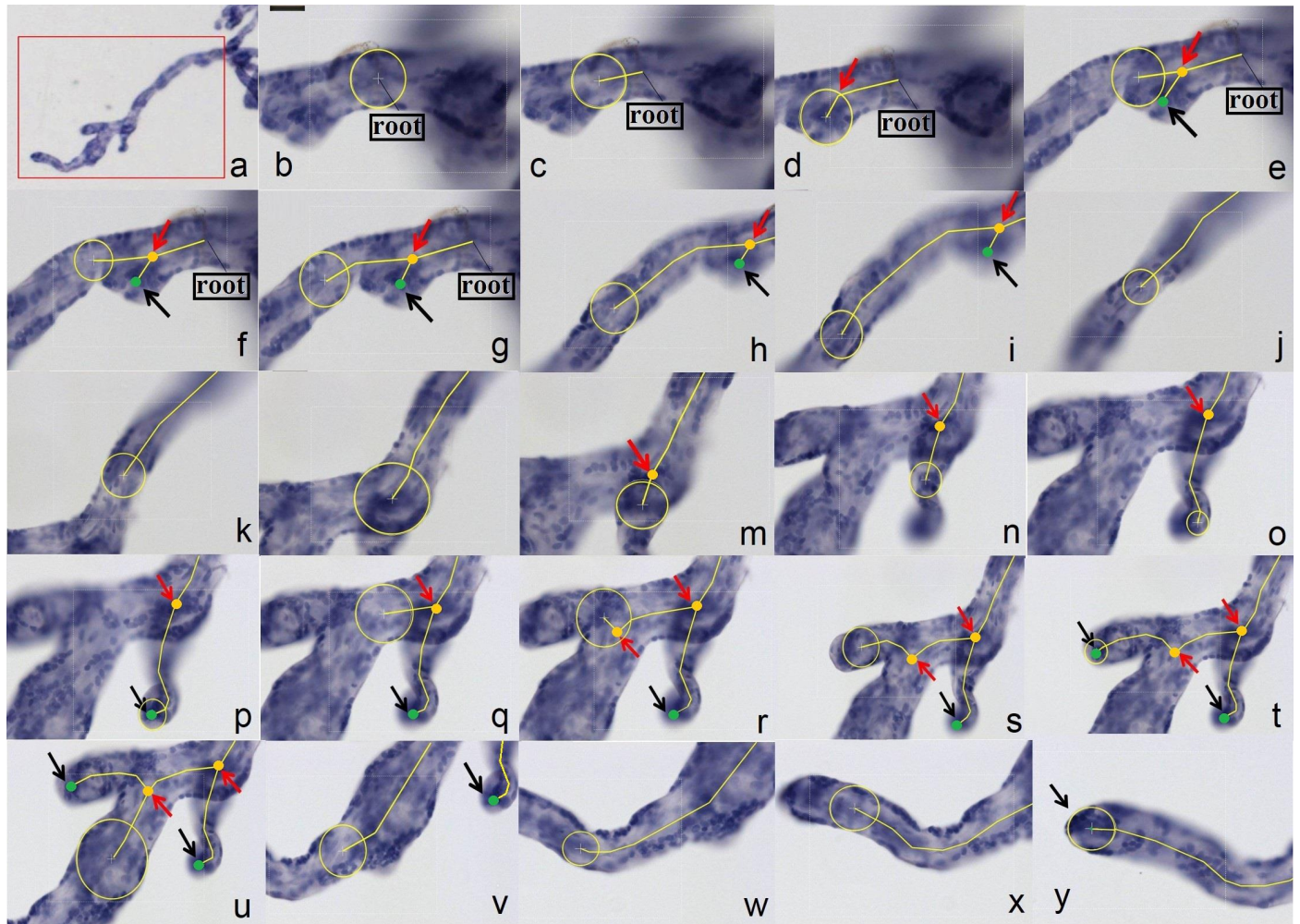


Figure S1 Computer-assisted viewing generates a quantitative digital three-dimensional (3D) replica of villous trees of the human placenta. (a–y) Example illustrating the procedure by which the Neurolucida software assisted in generating a digital and quantitative 3D replica of a whole-mount preparation of an isolated villous tree of a human placenta. The entire instrument and software setup was calibrated such that the software recorded 3Dcoordinates of all positions and mouse functions. Measurement and 3D-reconstruction were simultaneous processes. (a) shows an overview at low magnification (2x objective). The red box in (a) delineates the region of interest. The region of interest is larger than a single microscopic field-of-view at working magnification (20x objective). (b–y) Screenshots taken at working magnification (20x objective; scale bar in (b) 25 μ m on the top is equal for each tile) while the tracing of the villous tree in the region of interest was in progress. The coordinates of the centerpoint of the yellow circle and the diameter of this circle were recorded while the villous tree was traced in x,y, and z. The work flow started with the most proximal point of the region of interest (root point of the model, (b)). The yellow circle shown could be adjusted to the diameter of the villus in focus using the mouse wheel function. Its moving center defined the center line (yellow line) of each branch. Branching points (nodes; shown as yellow dots with associated red arrows) were placed by clicking functions. Similarly, terminal ends were defined using the mouse wheel function and are shown as green dots with associated black arrows (copy of reference 13 with permission).

4 Discussion

4.1 A perspective: The interpretation of placental shape

The present study shows [49] that placental shape is an independent parameter and can be determined independent of placental size and weight by the placenta-specific implementation of geometric morphometry [49]. The novel shape parameter defined here could be determined independently and behaves independently of the placental size and weight (summarized as form). Because form parameters are influenced directly by gestational age [51–53, 55, 56, 58], the non-correlation of placental shape with gestational age highlights the uniqueness of shape among the other macroscopic measures.

One of the most important objectives of shape analysis by geometric morphometry is the determination of shape-divergent groups within larger populations of, e.g., one species. In paleoanthropology, this determination has frequently been used to identify species transitions or evolutionary pressures acting on populations [68, 70, 71]. Although the novel placental shape parameters used in the present study revealed substantial variability, it was not possible to detect shape-divergent groups within the general and clinically normal population. This substantial variability of placental shapes considered to be "round shapes" (the outer rim) and/or "triangle shapes" (the connection of the outer rim of the placenta with the position of umbilical cord insertion) can thus be considered part of the normal morphological features of human placentas [49]. High variability and absent convergence to a common and potential functionally relevant placental shape (for shape-divergent subpopulations) makes it unlikely that an evolutionary pressure toward a specific placental shape exists [68, 70, 71].

These findings suggest that many possible factors could determine the placental shape variability. Clearly, placental shape can vary substantially among similar outcomes of functional and clinical measures, such as placental weight or birth weight. Therefore,

what is reflected by the placental shape? One possibility could be that placental shape evolves early during the first trimester as a direct consequence of adaptive placentation and thus precedes the phase of massive placental growth (size) during the second half of the pregnancy [49]. This interpretation considers placental shape to result from the interaction of early placental development with uterine factors, the uterine habitat.

The uterine habitat can be understood in various ways, e.g., as the morphological region-specific curvature of the uterine surface at the site of implantation (round at the top (*fundus*), with two long side walls, and shorter flat back and front walls), as a consequence of variable numbers of spiral arteries at the placentation site, or residuals of previous pregnancies (e.g., uterine cesarean section scars) (Figure 4.1) [49].

Additionally, the placental shape parameter determined in the present study could also reflect early morphological events, which is supported by knowledge about the determination of the insertion point of the umbilical cord. The umbilical cord insertion is determined early in gestation, during the first trimester [60, 74]. After the implantation of the blastocyst in the uterus and the formation of the allantoic stalk, the position of the umbilical cord is defined [60, 74]. All following placental formations occur around the umbilical cord insertion on the placentation site, more or less concentric about this point. Because the shape parameter explicitly refers to the landmark of the insertion point and the outer contour of the placenta, these early morphological formations can be expected to be reflected.

These considerations also imply that placental shape analysis would allow investigating earlier events in pregnancy than placental size analysis. In the latter, enlargements of the placental size and weight predominantly occur beyond the 20th week of gestation to meet the increasing nutritional needs of the simultaneously and rapidly growing fetus. Form parameters are influenced by both processes and take an intermediate position between the shape and size of the placenta (Figure 4.1).

Overall, the placental shape can be interpreted in this context as the outcome of peri-implantative embryo-uterine interactions, which are somewhat analogous to ecological adaptation processes toward the optimal occupation of a given niche [49]. A wide variety of placental shapes can thus provide an appropriate basis for the size expansion of the placenta in late pregnancy.

Because the present study determined the placental shapes of clinically normal placentas only, the placentas of patients with IUGR and/or PE could show other types of shape variability. A failure to adapt to the uterine environment can lead to, e.g., spontaneous abortion or the occurrence of complicated pregnancies involving, for example, IUGR and

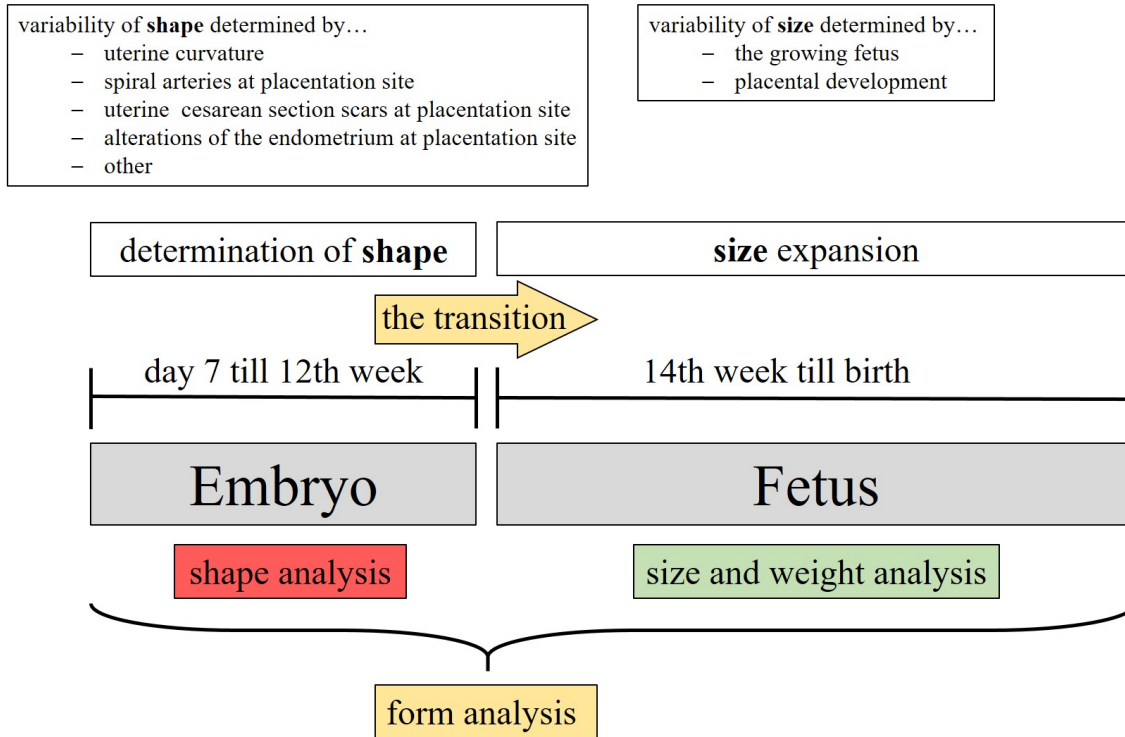


Figure 4.1 The time line of pregnancy and the origin of placental measures. Placental shape may be determined early in gestation (1st trimester) and is likely influenced by maternal factors, such as the uterus surface or the environment of the placentation site. The placental size and weight reflect the normal size expansion of the fetus and placenta during late gestation (2nd and 3th trimesters). Placental form parameters exist between the placental shape and size/weight.

PE [26,133–135]. The influence of early placentation on the course of pregnancy is supported by experiences from *in-vitro*-fertilization (IVF). Here, implantation in the posterior part (*fundus*) of the uterus was demonstrated to help avoid pregnancy complications [136]. The predefined positioning of the fertilized ovum at an in-ovulation is performed to select the best possible implantation spot. Thus, it can be expected that normal, natural pregnancies are also influenced by the position of placentation (as one aspect of the uterine habitat). An important next step in shape analysis will thus be the shape analysis of placentas from patients with IUGR/PE and those after IVF-based pregnancy initiation. Moreover, if shape analysis becomes established as a tool than can facilitate the morphological analysis of events during the first trimester, it may also reflect information about early issues associated with ischemic placental disease and so the roots of the pathogenetic chain of IUGR and/or PE.

Overall, a wide field of research has developed and is now investigating the shape analysis of human placentas. The placental shape data of the present study thus constitute an ideal basis for subsequent studies and a solid reference dataset.

4.2 Defining the progress achieved by the novel and advanced 3D microscopic analysis of villous trees

The present study shows that 3D reconstruction of the villous tree using a computer-assisted camera lucida technique is feasible and generates reliable data about villous branches, their branching points and their topology [123]. The computer-assisted camera lucida technique is a straightforward method [122] that enables to objects be visualized and drawn simultaneously in 3D.

Compared to conventional 2D histological sectioning, considerable differences exist in tissue pretreatment and processing for 3D microscopy. These differences represent both strengths and weaknesses of the microscopic analysis of human placental villous trees.

Conventional 2D histological analysis of villous trees utilizes tissue sectioning to visualize and examine the villous stroma, including, for example, the connective tissue and villous capillaries. Moreover, histological sectioning of villous trees allows the examination of all parts of the villous trees under the microscope, not only the most peripheral parts, as with the novel 3D microscopy. Because of this sectioning, however, the 3D orientation is lost, and previous attempts to overcome this issue by allocating the properties of the stroma to positions in the tree have been problematic [137]. In contrast, 3D microscopic analysis generates the topological relations of various branches of the villous tree easily and in an observer-independent and direct manner. To date, it remains difficult to interpret the stromal architecture of villi in 3D, but future work and additional studies could solve this problem by, e.g., special immunohistochemical staining of the stromal cells of transparent villi.

These different microscopic analysis approaches to villous trees enable examining different aspects of the villous tree and complement each other. The uncertain association of the topological positions of sectioned villous trees in 2D histology can be resolved using 3D microscopy. In contrast, stromal analysis is not yet feasible with 3D microscopy but can be achieved using 2D histology.

To simplify and clearly delineate these two microscopic approaches, the present study introduced a special nomenclature system for the 3D reconstructions of villous trees. This

system relies on the hierarchical nomenclature of branches, and not villi, ordered by their position on the villous tree downward from the terminal end. The hierarchy is determined by a number which indicates the branch category (terminal branches, e.g., are **b** branches in terminal position **0** (short: bT0)) [123]. Thus, peripheral villous branches can be automatically and observer-independently classified.

The focus on peripheral branches only is not necessarily a disadvantage because the functionally relevant units of the villous tree are the terminal and preterminal peripheral branches. These parts of the villous tree are essentially responsible for nutrient exchange during late pregnancy. Thus, structural and anatomical variations in the peripheral parts of the villous tree could directly correspond to the course of pregnancy [98,138].

One objective of the present study was to validate the current histological concept of villous topology against the novel 3D microscopy technique implemented here.

The current histological approach to the villous tree was challenged successfully

The current histological concept based on the stromal classification of villous types of sectioned villi evolved in the 2nd half of the 20th century [101]. To date, it was considered to be the gold standard method of developmental pathology and was reviewed frequently and even described at the textbook level [20]. The stromal structures were allocated to villous types, and these villous types were named by their type-associated topological positions (e.g., intermediate villi or terminal villi). This topological analysis of villous positions based on 2D histology can thus be interpreted as an indirect 3D method and was especially frequently used to classify placental developmental disorders in placental research [20]. For example, the volumes of different villous types were determined to reveal disturbances in placental development [139,140].

The validation of this approach against the direct 3D topological allocations of branches, using the novel 3D microscopy technique, revealed a number of difficulties with regard to the reliability and validity of indirect 3D interpretations derived from 2D sections [137]. This validation showed that a considerable observer influence on the classification of villous types exists. Moreover, the level of histological experience in placental morphology did not substantially minimize observer dependence. The interobserver variability only reached the level of “fair agreement”, which indicates that the reliability of this technique is quite low. Furthermore, a substantial mismatch between the real 3D positions of branches and the section-derived indirect 3D interpretation of the same villous structure was found. The histological outcomes were, e.g., unbranched stem villi in the terminal position or terminal

4.2 Defining the progress achieved by the novel and advanced 3D microscopic analysis of villous trees 95

villi distant from the real terminal ends of the villous trees. These combinations should not be possible according to the histological classification of villi (Figure 4.2) [137].

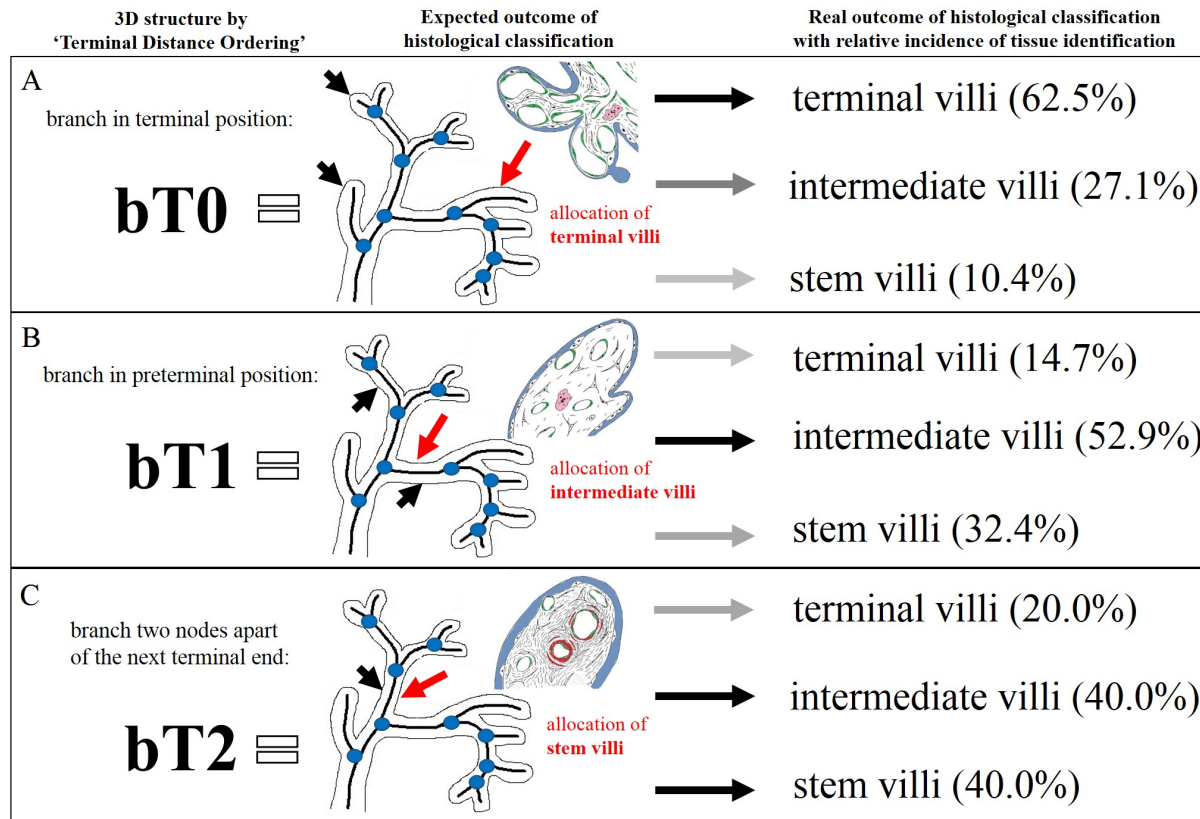


Figure 4.2 Terminal position ordering versus histological classification of a villous tree. Schematic describing the mismatch between the terminal distance ordering and the histological classification of villous trees (for more detail regarding the allocation of villous sections, see Figure 1.4). Branching nodes (blue dots) bifurcating branches are marked in the skeletonized villous tree. The terminal distance ordering was measured in terms of the number of nodes to the nearest terminal end. Thus, "0" encodes a branch in the terminal position, and "1" encodes a branch one node from the nearest terminal position (preterminal); thus, in general, "X" encodes a branch X nodes from the nearest terminal end. (A) It was expected that the branches at the terminal position (bT0) would contain only terminal villi; however, but all villous types were observed in bT0. (B) It was expected that branches at preterminal positions (bT1) would consist only of intermediate villi, and (C) that branches two nodes from the nearest next terminal end (bT2) would include only stem villi. However, all villous types were observed in bT1 and bT2. Calculation of the relative incidence of tissue identification based on publication III [137], Table 3, Team A (modified from [28] and Neurolucida Explorer software (version 10.54, MBF Bioscience, Williston, VT, USA)).

Another and still widely underestimated issue is the determination of branching points (nodes) in sectioned villous trees. Currently, 2D histology has no consistent nomenclature or structural concept to handle and classify nodes that appear in sections. However, it is estimated that one third of sectioned villi are actually not sections of free villous branches but instead are sections that traverse through a branching point [123]. This was deduced from the relationship between the branch diameter and the internodal distance determined using 3D microscopy. Some studies have attempted to identify nodes to interpret syncytial nodes/bridges [141,142], which exhibit some of the important aspects of branching nodes in placental research. These studies constitute an example of an effort to develop a taxonomic system to classify nodes in placental histological sections, but their results have not been reliably validated [141].

This inconsistent nomenclature for branching nodes may have contributed significantly to the high interobserver variability in the classification of villous types. However, the determination of villous branching nodes is not an issue for the novel 3D microscopy technique. Indeed, in 3D, these nodes are easily recognized and can be observer independently labeled and topologically allocated by software algorithms, which represents a very important advantage of this method [137].

In addition to analyzing branching nodes, this novel 3D microscopic method instantly records the lengths, diameters, surface areas, volumes and branching angles of the branches of villous trees. The visibility of nodes, branch lengths and branching angles in 3D provides direct and quantitative access to the branching structure, which is impossible using 2D histology. As outlined above, 2D histological analysis can only be used with great caution for topological allocations, and achieving quantitative results is substantially more difficult than when using 3D microscopy [123].

Design-based stereology is a quantitative approach to determine certain 3D parameters using 2D sections [143,144]. This approach uses 2D histological sectioning and inherits all the advantages and disadvantages of the 2D histological approach. It applies a mathematical-statistical perspective to histological sampling and sectioning and interprets sampling and sectioning as statistical procedures [143,144]. If samples were systematically selected randomly to ensure that every part of the placenta has the same chance of being analyzed, the quantitative results of 2D histology can be extrapolated to the 3D space. The Cavalieri method is the most used stereological approach to quantify tissue volumes from sectioned villous trees in placental research (for a review, see [143]). The Cavalieri method is essentially a point-counting system (volume estimation) using 2D sections on a

microscopic level [144]. Retrospectively, this volume estimation technique can be used to calculate the estimated cell or structure volume in the whole placenta [143]. Design-based stereology is a strategy that allows quantitative conclusions regarding large 3D structures to be drawn using small 2D sections as probes.

If design-based stereology is used to determine the parameters of structures that can be unequivocally identified in histology, the results of correctly implemented stereological measurements will be valid. Determining the whole volume of the villous tree relative to the volume of the intervillous space, thus, is readily achieved. If volumes or other stereological estimates are assigned to villous types, the uncertainties of histological classification will be imported into the design-based stereology. However, because topology is non-statistical in nature, design-based stereology can not provide specific information regarding the nature of the structure (topology) per se. Moreover, the statistical nature of design-based stereology is independent of the 3D structure to be analyzed, and whether the 3D structure is a tree or a cube, the outcome is not affected. Thus, design-based stereology and the 3D microscopic analysis of villous trees are complementary techniques for 3D analysis.

Thus, the major progress achieved by the novel 3D microscopical method applied here relates to the ease and reliability by which the topological structures of peripheral villous trees can now be determined. Because the classical topological analysis relies upon the allocation of villous types was insufficiently reliable, topological analysis is now a unique feature of 3D microscopy. This development is important because the branching patterns of villous trees constitute a major topic among histopathological concepts. These concepts describe alterations in the villous trees of placentas derived from pregnancies complicated by obstetric disease (especially IUGR and PE).

The whole field analyzing the branching of villous trees and its role in health and disease now has access to a quantitative topological analysis technique. Thus, new light should be cast on established concepts of (patho-)mechanisms of villous branching. Additionally, new concepts and/or extend current concepts relating to the developmental pathology of villous trees may emerge.

4.3 The relevance of 3D microscopic analysis of branching patterns

Are the branching angles of villous trees involved in angiogenesis?

The paragraph above outlined the specific area in which the 3D microscopic analysis of villous trees delivers unique topological data. This quantitative topological analysis of 3D villous trees identified functionally relevant and previously unidentified 3D microscopic structural features of human placentas as follows: (i) by analyzing villous trees from clinically normal human placentas [123] and (ii) by comparing the villous trees isolated from clinically normal placentas and those of the pregnancies of patients with IUGR [145].

One important outcome produced by this novel 3D microscopy was the statistically significant correlation between the branching angles and the fetal-placental weight (PW/BW) ratio [123]. In previous research relating to prenatal programming, it was impossible to detect any parameter on a microscopic level that was significantly correlated with the PW/BW ratio. The PW/BW ratio is a widely used clinical parameter that describes the relationship between placental weight and fetal weight [27] and, thus, serves as an estimate of placental efficiency. Moreover, the gestational age influences the PW/BW ratio, which decreases toward term (time of delivery). Fetal and placental weight seem to be closely linked [27]. Accordingly, birth weight and placental weight are significantly smaller in IUGR pregnancies than in clinically normal pregnancies, whereas the PW/BW ratio does not differ [27, 145].

This correlation essentially indicates that the branching angles of the terminal branches (bT0) of clinically normal placentas tend to be smaller in placentas with a higher PW/BW ratio [123]. Although the interpretation of the PW/BW ratio is fairly simple, that of the decreasing branching angles of terminal branches is challenging. Moreover, the interpretation of the functional relevance of branching angles appears to be highly important because the terminal branching angles are significantly larger in IUGR placentas than in clinically normal placentas [145].

Based on the current concept of villous branching, the branching angles of terminal branches are interpreted as resulting from non-branching angiogenesis (Figure 4.3), which dominating parts of the second and third trimesters [93]. Non-branching angiogenesis is the transformation of an immature villous tree into a mature villous tree via the formation of longer capillaries. In this process, terminal villi bulge out of the villous tree and mainly consist of capillary loops with some segmental order (Figure 1.5)

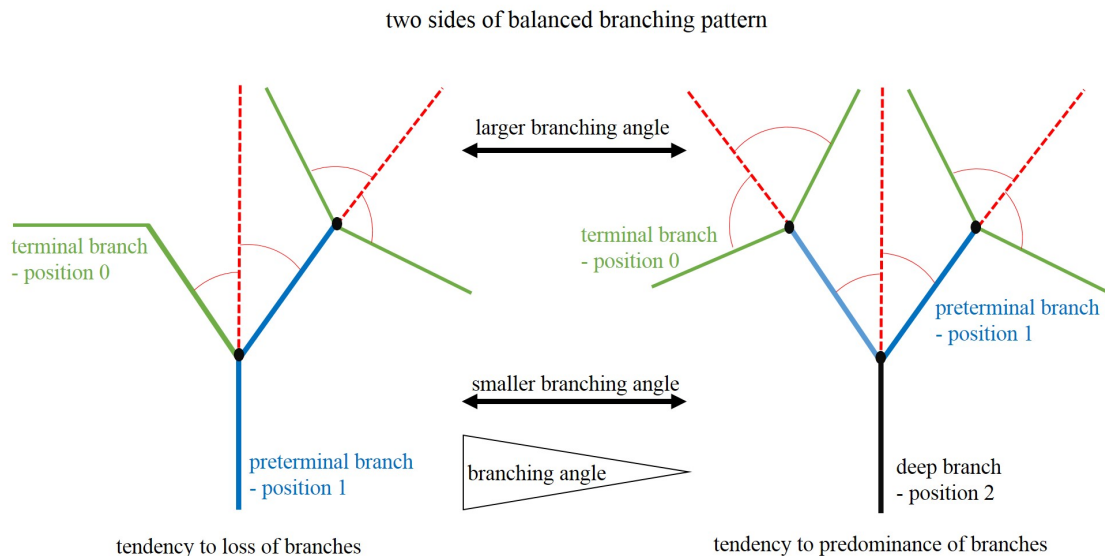


Figure 4.3 Variation of branching angles in the villous tree. Schematic representations of branching villous trees with color-coding indicating the positions of villous segments (green: terminal position (bT0); blue: preterminal position (bT1); black: deep branch position (bT2)). The branching angles of single villous segments are indicated (angle field in red). The variability of normal branching increases from left to right. The loss of nodes (black dots) in the periphery of the trees induces the progressive inclusion of villous types with smaller branching angles into the population of villous segments in the terminal position. As a result, the mean planar branching angle at the terminal position decreases.

Furthermore, it is assumed that the rheological conditions in the intervillous space (IVS) differ between IUGR and clinically normal pregnancies [86] and that the rheological conditions could influence the villous tree [29]. Thus, it can be hypothesized that the different mechanisms that regulate angiogenesis inside the villous tree (e.g., VEGF and PlGF) and/or altered rheological conditions outside the villous tree could cause the average branching angle in IUGR pregnancies to increase [145].

Angiogenic processes within villous trees determine their branching patterns [93, 94, 105], including, e.g., the occurrence of hyper- or hypocapillarization [95, 138, 146]. It is assumed that these alterations in the branching pattern correspond to, e.g., fetal hypoxic stress, and result in malnutrition during pregnancy [111, 147]. To confirm or exclude hypotheses relating to these mechanisms, additional studies, such as the determination of growth factor profiles (e.g., VEGF or PlGF) and modeling of the rheological conditions in the IVS, will be needed to search for the sites and mechanisms of the mechanotransduction of intervillous rheological atypia. Although such studies are both promising and necessary, they are

outside of the scope of this work. Instead, they will be the topics of follow-up studies. Because of the current results regarding the appearance of smaller branching angles in terminal branches with high PW/BW ratios in clinically normal pregnancies, an additional hypothesis can be formulated. In general, branching angles decrease toward the terminal ends of villous trees (Figure 4.3) [123]. Thus, smaller branching angles of branches in the terminal position can indicate that these branches are actual preterminal branches that have slid into the terminal position such that one branch hierarchy is missing. If this is true, the average branching angle of branches in the terminal position should decrease. Thus, changes in terminal branching angles should indicate less branching and higher abundances of branches of higher hierarchy levels in the terminal position (Figure 1.6).

Although this study could not confirm this hypothesis, follow-up studies focusing on immunohistochemical investigations would enable observing, for example, stem villi using immunohistochemical marker molecules (e.g., gamma smooth muscle action [96]), which facilitate clarifying such shifts in villous maturation in 3D.

The present study not only implemented a new 3D method and validated it against current standards but also produced novel data supporting novel mechanistic hypotheses, which could be verified in subsequent experiments. These experiments could include applications of the actual method or further improvements (e.g., immunohistochemical protocols) of 3D topological analysis. This hypothesis, as discussed above, is also supported by another feature of the structural variations of the villous tree that was discovered in placentas from clinically normal pregnancies, as discussed in the next chapter 4.4.

4.4 Adaptation of the villous tree to rheological issues

In addition to the increased branching angles in IUGR villous trees, the tortuosity of the preterminal branches also differs significantly between IUGR and clinically normal villous trees [145]. Branches in the preterminal position (bT1) are very long and tortuous (highly tortuous (HT)) in villous trees of clinically normal placentas. Moreover, branching angles associated with these HT branches do not exhibit a bimodal distribution and are generally higher than those of branches with low tortuosity (LT) [145]. This relationship was interpreted as indicating compensatory adaptations because the HT branches were not present in IUGR. Indeed, in IUGR pregnancies, only LT branches were found in the preterminal position of villous trees [145]. Analyzing the main differences between the HT and LT branches of villous trees from clinically normal pregnancies revealed that HT

branches exhibit substantially different structures (e.g., volumes) than LT branches [145]. This difference may suggest that clinically normal villous trees can adapt more flexibly to conditions during pregnancy or, in contrast, that flexible adaptations support clinically normal pregnancies. This type of compensation reaction or flexibility in the architecture of the villous tree regarding the conditions during pregnancy seems to be missing in IUGR. The disturbed differentiation of the villous tree in IUGR placentas could be responsible for the mismatch between fetomaternal exchange and placental adaptation beyond the second trimester (Figure 4.4).

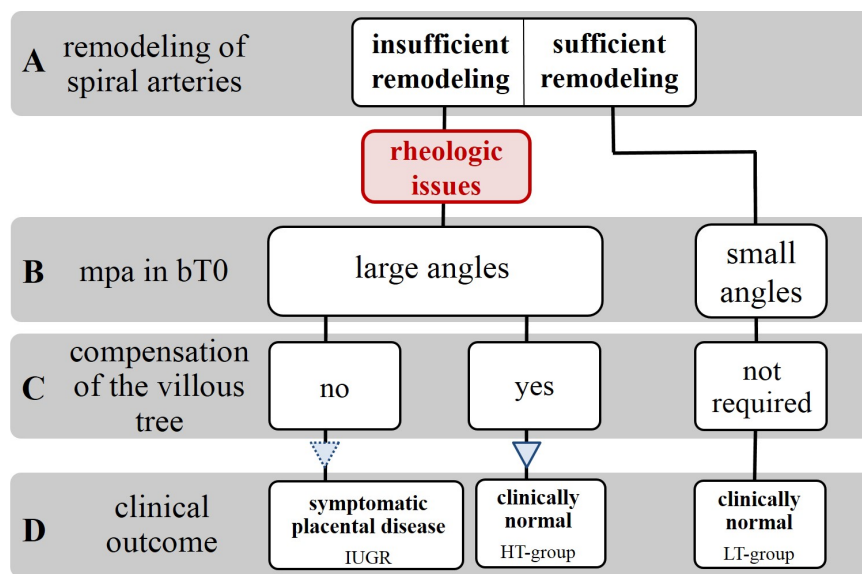


Figure 4.4 Schematic of a proposed pathophysiological interpretation of the data on angles and tortuosity. The proposed interpretation is based on the widely accepted early origin of IUGR: insufficient remodeling of spiral arteries (A). Because of the rheological consequences of insufficient modeling, branching angles in bT0 increase (B). In a subset of clinically normal placentas, highly tortuous branches occur in bT1 (C), which are interpreted as morphological correlate of successful compensation for rheological disturbance (D) [145].

This villous adaptation mechanism integrates smoothly with the concept of ischemic placental disease [29]. It can be reasoned that the insufficient remodeling of spiral arteries and high maternal blood pressure cause mechanotransduction, which increases the branching angles of the villous tree. Higher branching angles could interfere with placental function in a variety of ways [145]: (i) Higher branching angles could modify the IVS and its boundaries such that the normal rheology of this space shifts toward a more unfavorable situation. (ii) Higher branching angles could be symptomatic of a shift in the angiogenic mechanisms that

control the branching of villi during the second half of pregnancy [92, 94, 148]. (iii) The appearance of higher branching angles could indicate prenatal maturation of the villous trees and thus signal a mismatch with developmental gestational age.

Based on other research fields, modified tortuosity may be associated with various diseases, including, for example, microvascular complications in diabetes [149] or cardiovascular diseases [150].

The hypothesis that HT branches indicate compensated ischemic placental disease will be analyzed in follow-up studies. Nevertheless, the present study identified discrete morphological subgroups at the microscopic scale within clinically normal pregnancies. Thus, 3D microscopy has the potential to be more sensitive for placental structural alterations than clinical observations. Therefore, the hope that such novel morphological tools will allow the refinement of clinical syndromes by post-partum placental analysis is justified.

If confirmed, the method described in the present study could be used to identify morphologically defined subgroups within clinically normal pregnancies and reveal features that differentiate patient subgroups that were previously invisible to clinicians. Thus, one important objective for follow-up studies on this topic is to further subdivide clinically predefined patient groups by microscopic analysis. The hypothesis that these highly tortuous branches signal compensated ischemic placental disease is supported by the fact that the PW/BW ratios of the placentas with HT branches in the preterminal position were slightly higher than those in other clinically normal pregnancies without HT branches. This difference was not significant but could become so in an adequately powered follow-up study including a larger number of placentas.

Bibliography

- [1] Barker D. In utero programming of chronic disease. *Clinical science*. 1998;95:115–128.
- [2] Aihie-Sayer A, Cooper C, Barker D. Is lifespan determined in utero? *Archives of diseases in childhood fetal neonatal*. 1997;77:162–164.
- [3] Barker D. Fetal origins of coronary heart disease. *British medical journal*. 1995;311:171–174.
- [4] Barker D, Osmond C, Law C. The intrauterine and early postnatal origins of cardiovascular disease and chronic bronchitis. *Journal of epidemiology and community health*. 1989;43:237–240.
- [5] Barker D, Larsen G, Osmond C, Thornburg K, Kajantie E, Eriksson J. The placental origins of sudden cardiac death. *International journal of epidemiology*. 2012;41:1394–1399.
- [6] Nehring I, Chmitorz A, Reulen H, von Kries R, Ensenauer R. Gestational diabetes predicts the risk of childhood overweight and abdominal circumference independent of maternal obesity. *Diabetic medicine*. 2013;30:1449–1456.
- [7] Kim S, England L, Sharma A, Njoroge T. Gestational diabetes mellitus and risk of childhood overweight and obesity in offspring: A systematic review. *Experimental diabetes research*. 2011;2011:541308.
- [8] Gillman M, Ludwig D. How early should obesity prevention start? *The new england journal of medicine*. 369;2013:2173–2175.
- [9] Frias A, Grove K. Obesity: A transgenerational problem linked to nutrition during pregnancy. *Seminars in reproductive medicine*. 2012;30:472–478.

- [10] Kemp M, Kallapur S, Jobe A, Newnham J. Obesity and the developmental origins of health and disease. *Journal of paediatrics and child health*. 2012;48:86–90.
- [11] Spinillo A, Gardella B, Preti E, Zanchi S, Tzialla C, Stronati M. Preeclampsia and brain damage among preterm infants: A changed panorama in a 20-year analysis. *American journal of perinatology*. 2007;24:101–106.
- [12] Barker D, Winter P, Osmond C, Phillips D, Sultan H. Weight gain in infancy and cancer of the ovary. *Lancet*. 1995;345:1087–1088.
- [13] Gardener H, Spiegelman D, Buka S. Perinatal and neonatal risk factors for autism: A comprehensive meta-analysis. *Pediatrics*. 2011;128:344–355.
- [14] Susser E, Lin S. Schizophrenia after prenatal exposure to the Dutch Hunger Winter of 1944-1945. *Archives of general psychiatry*. 1992;49:983–988.
- [15] Silva D, Colvin L, Hagemann E, Bower C. Environmental risk factors by gender associated with attention-deficit/hyperactivity disorder. *Pediatrics*. 2014;133:e14–22.
- [16] Barker D, Osmond C, Forsén T, Kajantie E, Eriksson J. Trajectories of growth among children who have coronary events as adults. *The new england journal of medicine*. 2005;353:1802–1809.
- [17] Savchev S, Sanz-Cortes M, Cruz-Martinez R, Arranz A, Botet F, Gratacos E, et al. Neurodevelopmental outcome of full-term small-for-gestational-age infants with normal placental function. *Ultrasound in obstetrics and gynecology*. 2013;42:201–206.
- [18] Baschat A. Neurodevelopment following fetal growth restriction and its relationship with antepartum parameters of placental dysfunction. *Ultrasound in obstetrics and gynecology*. 2011;37:501–514.
- [19] Longtine M, Nelson M. Placental dysfunction and fetal programming: The importance of placental size, shape, histopathology, and molecular composition. *Seminars in reproductive medicine*. 2011;29:187–196.
- [20] Benirschke K, Burton G, Beargen R. *Pathology of the human placenta*. vol. 6. Berlin, London: Springer; 2012.
- [21] Rath W. *Geburtshilfe und Perinatologie*. vol. 2. Stuttgart: Thieme; 2010.

-
- [22] Heffer L. Advanced maternal age—how old is too old? *The new england journal of medicine*. 2004;351:1927–1929.
- [23] St-Pierre J, Laurent L, King S, Vaillancourt C. Effects of prenatal maternal stress on serotonin and fetal development. *Placenta*. 2015;S0143-4004:30094–1.
- [24] Roberts K, Riley S, Reynolds R, Barr S, Evans M, Statham A, et al. Placental structure and inflammation in pregnancies associated with obesity. *Placenta*. 2011;32:247–254.
- [25] Pötzsch O, Weinmann J, Haustein T. *Geburtentrends und Familiensituation in Deutschland*. Wiesbaden: Statistisches Bundesamt; 2012.
- [26] Freitag L, von Kaisenberg C, Kreipe H, Hussein K. Evaluierung des intrauterinen Fruchttods: Stellenwert der Untersuchung fetaler, plazentarer und maternaler Faktoren. *Der Pathologe*. 2014;35:77–82.
- [27] Boyd J, Hamilton W. *The human placenta*. Cambridge: Heffer; 1970.
- [28] Polin R, Fox W, Abman S. *Fetal and neonatal physiology*. vol. 3. Philadelphia: Saunders; 2004.
- [29] Ananth C. Ischemic placental disease: A unifying concept for preeclampsia, intrauterine growth restriction, and placental abruption. *Seminars in perinatology*. 2014;38:131–132.
- [30] Dennis A, Castro J. Hypertension and haemodynamics in pregnant women—is a unified theory for pre-eclampsia possible? *Anaesthesia*. 2014;69:1183–1189.
- [31] Wagner M. An epidemiologic analysis of dysmaturity. *Biologia neonatorum, Neo-natal studies*. 1964;6:164–172.
- [32] Wagner M. Observation on the newborn dysmature infant and his development during the first 9 months. *The journal of pediatrics*. 1963;63:335–338.
- [33] Warkany J, Monroe B, Sutherland B. Intrauterine growth retardation. *American journal of diseases of children*. 1961;102:149–279.
- [34] Irving F. A study of five hundred consecutive cases of pre-eclampsia. *Canadian medical association journal*. 1939;40:137–140.

- [35] Bolehovská P, Sehnal B, Driák D, Halaška M, Magner M, Novotný J, et al. Changes in placental angiogenesis and their correlation with foetal intrauterine restriction. *Ceská gynekologie*. 2015;80:144–150.
- [36] Dean K, Murray R. Environmental risk factors for psychosis. *Dialogues in clinical neuroscience*. 2005;7:69–80.
- [37] Washburn L, Nixon P, Russell G, Snively B, O'Shea T. Adiposity in adolescent offspring born prematurely to mothers with preeclampsia. *The Journal of pediatrics*. 2013;162:912–917.
- [38] Barker D. The long-term outcome of retarded fetal growth. *Clinical obstetrics and gynecology*. 1997;40:853–863.
- [39] The world health report 2001 - Mental Health: New Understanding, New Hope; 2001.
- [40] Diabetes die Krankheit - Zahlen;. Accessed: 21-01-2016. <http://www.dzd-ev.de/diabetes-die-krankheit/zahlen/>.
- [41] Unwin N, Whiting D, Gan D, Jacqmain O, Ghyoot G. Diabetes Atlas. vol. 4. Brussels: International diabetes federation; 2009.
- [42] Guttmacher A, Maddox Y, Spong C. The Human Placenta Project: Placental structure, development, and function in real time. *Placenta*. 2014;35:303–304.
- [43] The Human Placenta Project;. Accessed: 25-01-2016. <https://www.nichd.nih.gov/research/hpp/Pages/default.aspx>.
- [44] Guttmacher A, Spong C. The Human Placenta Project: It's time for real time. *American journal of obstetrics and gynecology*. 2015;213:S3–S5.
- [45] Sadovsky Y, Clifton V, Burton G. Invigorating placental research through the 'Human Placenta Project'. *Placenta*. 2014;35:527.
- [46] Romero R, Dey S, Fisher S. Preterm labor: One syndrome, many causes. *Science*. 2014;345:760–765.
- [47] Jauniaux E, Oppenraaij RV, Burton G. Obstetric outcome after early placental complications. *Current opinion in obstetrics and gynecology*. 2010;22:452–457.

- [48] Kingdom J, Kaufmann P. Oxygen and placental villous development: Origins of fetal hypoxia. *Placenta*. 1997;18:613–621.
- [49] Haeussner E, Schmitz C, von Koch FE, Frank HG. Birth weight correlates with size but not shape of the normal human placenta. *Placenta*. 2013;34:574–585.
- [50] Almog B, Shehata F, Aljabri S, Levin I, Shalom-Paz E, Shrim A. Placenta weight percentile curves for singleton and twins deliveries. *Placenta*. 2011;32:58–62.
- [51] Thompson J, Irgens L, Skjaerven R, Rasmussen S. Placenta weight percentile curves for singleton deliveries. *BJOG : an international journal of obstetrics and gynaecology*. 2007;114:715–720.
- [52] Dombrowski M, Berry S, Hurd W, Saleh A, Chik L, Sokol R. A gestational-age-independent model of birth weight based on placental size. *Biology of the neonate*. 1994;66:56–64.
- [53] Dombrowski M, Berry S, Johnson M, Saleh A, Sokol R. Birth weight-length ratios, ponderal indexes, placental weights, and birth weight-placenta ratios in a large population. *Archives of pediatrics and adolescent medicine*. 1994;148:508–512.
- [54] Alwasel S, Abotalib Z, Aljarallah J, Osmond C, Omar SA, Harrath A, et al. The breadth of the placental surface but not the length is associated with body size at birth. *Placenta*. 2012;33:619–622.
- [55] Hutcheon J, McNamara H, Platt R, Benjamin A, Kramer M. Placental weight for gestational age and adverse perinatal outcomes. *Obstetrics and gynecology*. 2012;119:1251–1258.
- [56] Imada S, Takagi K, Kikuchi A, Ishikawa K, Tamaru S, Horikoshi T, et al. Birthweight placental weight ratio of appropriate-for-dates and light-for-dates infants in preterm delivery. *The journal of obstetrics and gynaecology research*. 2012;38:122–129.
- [57] Barker D, Osmond C, Thornburg K, Kajantie E, Eriksson J. The lifespan of men and the shape of their placental surface at birth. *Placenta*. 2011;32:783–787.
- [58] Shehata F, Levin I, Shrima A, Ata B, Weisz B, Gamzu R, et al. Placentabirthweight ratio and perinatal outcome: A retrospective cohort analysis. *British journal of obstetrics and gynaecology*. 2011;118:741–747.

- [59] Yampolsky M, Salafia C, Shlakhter O. Probability distributions of placental morphological measurements and origins of variability of placental shapes. *Placenta*. 2013;34:493–496.
- [60] Salafia C, Yampolsky M, Shlakhter A, Mandel D, Schwartz N. Variety in placental shape: When does it originate? *Placenta*. 2012;33:164–170.
- [61] Zelditch M, Swiderski D, Sheets D, Fink W. Geometric morphometrics for biologists. vol. 1. Academic press; 2004.
- [62] Bookstein F. Landmark methods for forms without landmarks: Morphometrics of group differences in outline shape. *Medical image analysis*. 1997;1:225–243.
- [63] Bookstein F. Morphometric tools for landmark data: Geometry and Biology. Cambridge: Cambridge University Press; 1997.
- [64] Goodall C. Procrustes methods in the statistical analysis of shape. *Journal of the royal statistical society*. 1991;53:285–339.
- [65] Bookstein F. The measurement of biological shape and shape change - Lecture notes in biomathematics. Berlin: Springer; 1978.
- [66] Gill J, Woods M, Salafia C, Vvedensky D. Probability distributions for measures of placental shape and morphology. *Physiological measurements*. 2014;35:483–500.
- [67] Salafia C, Yampolsky M, Misra D, Shlakhter O, Haas D, Eucker B, et al. Placental surface shape, function, and effects of maternal and fetal vascular pathology. *Placenta*. 2010;31:958–962.
- [68] Gunz P, Neubauer S, Golovanova L, Doronichev V, Maureille B, Hublin JJ. A uniquely modern human pattern of endocranial development. Insights from a new cranial reconstruction of the Neandertal newborn from Mezmaiskaya. *Journal of human evolution*. 2012;62:300–313.
- [69] Mitteroecker P, Gunz P, Neubauer S, Müller G. How to explore morphological integration in human evolution and development? *Evolutionary biology*. 2012;39:536–533.

- [70] Singh N, Harvati K, Hublin JJ, Klingenberg C. Morphological evolution through integration: A quantitative study of cranial integration in Homo, Pan, Gorilla and Pongo. *Journal of human evolution*. 2012;62:155–164.
- [71] Neubauer S, Gunz P, Hublin JJ. Endocranial shape changes during growth in chimpanzees and humans: A morphometric analysis of unique and shared aspects. *Journal of human evolution*. 2010;59:555–566.
- [72] Barker D, Thornburg K. Placental programming of chronic diseases, cancer and lifespan: A review. *Placenta*. 2013;34:841–845.
- [73] Barker D, Lampl M, Roseboom T, Winder N. Resource allocation in utero and health in later life. *Placenta*. 2012;33:e30–34.
- [74] Burton G, Barker D, Moffett A, Thornburg K. The placenta and human developmental programming. Cambridge: Cambridge University Press; 2011.
- [75] Schmitz C, Frank H. Discrete placental dysfunction - The overlooked player in prenatal roots of neuropsychiatric diseases? *Neuroembryology*. 2002;1:169–175.
- [76] Pijnenborg R, Brosens I, Romero R. Placental bed vascular disorders. Cambridge, New York: Cambridge University Press; 2010.
- [77] Pijnenborg R, Vercruysse L, Hanssens M. Fetal-maternal conflict, trophoblast invasion, preeclampsia, and the red queen. *Hypertension in pregnancy*. 2008;27:183–196.
- [78] Ramsey E, Harris J. Comparison of the uteroplacental vasculature and circulation in the rhesus monkey and man. *Contributions to embryology*. 1966;261:61–70.
- [79] Martin C, McGaughey H, Kaiser I, Donner M, Ramsey E. Intermittent functioning of the uteroplacental arteries. *American journal of obstetrics and gynecology*. 1964;90:819–823.
- [80] Ramsey E, Corner G, Donner M. Serial and cineradioangiographic visualization of maternal circulation in the primate (hemochorial) placenta. *American journal of obstetrics and gynecology*. 1963;86:213–225.
- [81] Burton G, Jauniaux E, Charnock-Jones D. The influence of the intrauterine environment on human placental development. *The International journal of developmental biology*. 2010;54:303–312.

- [82] Jauniaux E, Poston L, Burton G. Placental-related diseases of pregnancy: Involvement of oxidative stress and implications in human evolution. *Human reproduction update*. 2006;12:747–755.
- [83] Jauniaux E, Burton G. Pathophysiology of histological changes in early pregnancy loss. *Placenta*. 2005;26:114–123.
- [84] Zhang L. Uteroplacental circulation and maternal/fetal health. *Current vascular pharmacology*. 2013;11:543.
- [85] Brosens I, Pijnenborg R, Vercruysse L, Romero R. The "Great Obstetrical Syndromes" are associated with disorders of deep placentation. *American journal of obstetrics and gynecology*. 2011;204:193–201.
- [86] Burton G, Woods A, Jauniaux E, Kingdom J. Rheological and physiological consequences of conversion of the maternal spiral arteries for uteroplacental blood flow during human pregnancy. *Placenta*. 2009;30:473–482.
- [87] Conti N, Torricelli M, Voltolini C, Vannuccini S, Clifton V, Bloise E, et al. Term histologic chorioamnionitis: A heterogeneous condition. *European journal of obstetrics, gynecology, and reproductive biology*. 2015;188:34–38.
- [88] Labarrere C, Hardin J, Haas D, Kassab G. Chronic villitis of unknown etiology and massive chronic intervillitis have similar immune cell composition. *Placenta*. 2015;36:681–686.
- [89] Bulmer J, Johnson P, Sasagawa M, Takeuchi S. Immunohistochemical studies of fetal trophoblast and maternal decidua in hydatidiform mole and choriocarcinoma. *Placenta*. 1988;9:183–200.
- [90] Mayhew T, Sampson C. Maternal diabetes mellitus is associated with altered deposition of fibrin-type fibrinoid at the villous surface in term placentae. *Placenta*. 2003;24:524–531.
- [91] Mifsud W, Sebire N. Placental pathology in early-onset and late-onset fetal growth restriction. *Fetal diagnosis and therapy*. 2014;36:117–128.
- [92] Charnock-Jones D, Kaufmann P, Mayhew T. Aspects of human fetoplacental vasculogenesis and angiogenesis. I. Molecular regulation. *Placenta*. 2004;25:103–113.

- [93] Kaufmann P, Mayhew T, Charnock-Jones D. Aspects of human fetoplacental vasculogenesis and angiogenesis. II. Changes during normal pregnancy. *Placenta*. 2004;25:114–126.
- [94] Mayhew T, Charnock-Jones D, Kaufmann P. Aspects of human fetoplacental vasculogenesis and angiogenesis. III. Changes in complicated pregnancies. *Placenta*. 2004;25:127–139.
- [95] Kingdom J, Huppertz B, Seaward G, Kaufmann P. Development of the placental villous tree and its consequences for fetal growth. *European journal of obstetrics, gynecology, and reproductive biology*. 2000;92:35–43.
- [96] Demir R, Kosanke G, Kohnen G, Kertschanska S, Kaufmann P. Classification of human placental stem villi: Review of structural and functional aspects. *Microscopy research and technique*. 1997;38:29–41.
- [97] Leiser R, Luckhardt M, Kaufmann P, Winterhager E, Bruns U. The fetal vascularisation of term human placental villi. I. Peripheral stem villi. *Anatomy and embryology*. 1985;173:71–80.
- [98] Kaufmann P, Bruns U, Leiser R, Luckhardt M, Winterhager E. The fetal vascularisation of term human placental villi. II. Intermediate and terminal villi. *Anatomy and embryology*. 1985;173:203–214.
- [99] Kaufmann P. Development and differentiation of the human placental villous tree. *Bibliotheca anatomica*. 1982;22:29–39.
- [100] Sen D, Kaufmann P, Schweikhart G. Classification of human placental villi. II. Morphometry. *Cell and tissue research*. 1979;200:425–434.
- [101] Kaufmann P, Sen D, Schweikhart G. Classification of human placental villi. I. Histology. *Cell and tissue research*. 1979;200:409–423.
- [102] Graf R, Matejevic D, Schuppan D, Neudeck H, Shakibaei M, Vetter K. Molecular anatomy of the perivascular sheath in human placental stem villi: The contractile apparatus and its association to the extracellular matrix. *Cell and tissue research*. 1997;290:601–607.

- [103] Graf R, Neudeck H, Gossrau R, Vetter K. Elastic fibres are an essential component of human placental stem villous stroma and an integrated part of the perivascular contractile sheath. *Cell and tissue research*. 1995;283:133–141.
- [104] Graf R, Langer J, Schonfelder G, Oney T, Hartel-Schenk S, Reutter W, et al. The extravascular contractile system in the human placenta. Morphological and immunocytochemical investigations. *Anatomy and embryology*. 1994;190:541–548.
- [105] Burton G, Charnock-Jones D, Jauniaux E. Regulation of vascular growth and function in the human placenta. *Reproduction*. 2009;138:895–902.
- [106] Castellucci M, Kosanke G, Verdenelli F, Huppertz B, Kaufmann P. Villous sprouting: Fundamental mechanisms of human placental development. *Human reproduction update*. 2000;6:485–494.
- [107] Castellucci M, Celona A, Bartels H, Steininger B, Benedetto V, Kaufmann P. Mitosis of the Hofbauer cell: Possible implications for a fetal macrophage. *Placenta*. 1987;8:65–76.
- [108] Castellucci M, Schweikhart G, Kaufmann P, Zaccheo D. The stromal architecture of the immature intermediate villus of the human placenta. Functional and clinical implications. *Gynecologic and obstetric investigation*. 1984;18:95–99.
- [109] Huppertz B, Gauster M. Trophoblast fusion. *Advances in experimental medicine and biology*. 2011;713:81–95.
- [110] Kadyrov M, Kosanke G, Kingdom J, Kaufmann P. Increased fetoplacental angiogenesis during first trimester in anaemic women. *Lancet*. 1998;352:1747–1749.
- [111] Mayhew T. A stereological perspective on placental morphology in normal and complicated pregnancies. *Journal of anatomy*. 2009;215:77–90.
- [112] Mayhew T, Ohadike C, Baker P, Crocker I, Mitchell C, Ong S. Stereological investigation of placental morphology in pregnancies complicated by pre-eclampsia with and without intrauterine growth restriction. *Placenta*. 2003;24:219–226.
- [113] Oberlaender M, de Kock C, Bruno R, Ramirez A, Meyer H, Dercksen V, et al. Cell type-specific three-dimensional structure of thalamocortical circuits in a column of rat vibrissal cortex. *Cerebral cortex*. 2012;22:2375–2391.

- [114] Oberlaender M, Boudewijns Z, Kleele T, Mansvelder H, Sakmann B, de Kock C. Three-dimensional axon morphologies of individual layer 5 neurons indicate cell type-specific intracortical pathways for whisker motion and touch. *Proceedings of the national academy of sciences*. 2011;108:4188–4193.
- [115] Helmstaedter M, Sakmann B, Feldmeyer D. The relation between dendritic geometry, electrical excitability, and axonal projections of L2/3 interneurons in rat barrel cortex. *Cerebral cortex*. 2009;19:938–950.
- [116] Aguiar P, Sousa M, Szucs P. Versatile morphometric analysis and visualization of the three-dimensional structure of neurons. *Neuroinformatics*. 2013;11:393–403.
- [117] Földy C, Malenka R, Südhof T. Autism-associated neuroligin-3 mutations commonly disrupt tonic endocannabinoid signaling. *Neuron*. 2013;78:498–509.
- [118] Sholl D. Dendritic organization in the neurons of the visual and motor cortices of the cat. *Journal of anatomy*. 1953;87:387–406.
- [119] Milosević N, Ristanović D. The sholl analysis of neuronal cell images: Semi-log or log-log method? *Journal of theoretical biology*. 2007;245:130–140.
- [120] Glaser J, Glaser E. Neuron imaging with neurolucida — A PC-based system for image combining microscopy. *Computerized medical imaging and graphics*. 1990;14:307–317.
- [121] Halavi M, Hamilton K, Parekh R, Ascoli G. Digital reconstructions of neuronal morphology: Three decades of research trends. *Frontiers in neuroscience*. 2012;6:49–61.
- [122] Wollaston WH. Description of the camera lucida. *Philosophical magazine*. 1807;27:343–347.
- [123] Haeussner E, Buehlmeyer A, Schmitz C, von Koch FE, Frank HG. Novel 3D microscopic analysis of human placental villous trees reveals unexpected significance of branching angles. *Scientific reports*. 2014;4:6192.
- [124] Chaouat G, Clark D. Are animal models useful or confusing in understanding the human feto-maternal relationship? A debate. *Journal of reproductive immunology*. 2015;108:56–64.

- [125] Gundling W, Wildman D. A review of inter- and intraspecific variation in the eutherian placenta. *Philosophical transactions of the Royal Society of London, Series B, Biological sciences*. 2015;370:20140072.
- [126] Burton G, Moffett A, Keverne B. Human evolution: Brain, birthweight and the immune system. *Philosophical transactions of the Royal Society of London, Series B, Biological sciences*. 2015;370:20140061.
- [127] Carter A, Enders A, Pijnenborg R. The role of invasive trophoblast in implantation and placentation of primates. *Philosophical transactions of the Royal Society of London, Series B, Biological sciences*. 2015;370:20140070.
- [128] Wooding P, Burton G. *Comparative placentation*. Berlin, Heidelberg: Springer; 2008.
- [129] Iriyama T, Sun K, Parchim N, Li J, Zhao C, Song A, et al. Elevated placental adenosine signaling contributes to the pathogenesis of preeclampsia. *Circulation*. 2015;131:730–741.
- [130] Carnevale D, Pallante F, Fardella V, Fardella S, Iacobucci R, Federici M, et al. The angiogenic factor PlGF mediates a neuroimmune interaction in the spleen to allow the onset of hypertension. *Immunity*. 2014;41:737–752.
- [131] Dilworth M, Sibley C. Review: Transport across the placenta of mice and women. *Placenta*. 2013;34 Suppl:S34–39.
- [132] Bonagura T, Babischkin J, Aberdeen G, Pepe G, Albrecht E. Prematurely elevating estradiol in early baboon pregnancy suppresses uterine artery remodeling and expression of extravillous placental vascular. *Endocrinology*. 2012;153:2897–2906.
- [133] Parker S, Werler M. Epidemiology of ischemic placental disease: A focus on preterm gestations. *Seminars in perinatology*. 2014;38:133–138.
- [134] Vintzileos A, Ananth C. First trimester prediction of ischemic placental disease. *Seminars in perinatology*. 2014;38:159–166.
- [135] Ananth C, Vintzileos A. Ischemic placental disease: Epidemiology and risk factors. *European journal of obstetrics, gynecology, and reproductive biology*. 2011;159:77–82.

- [136] Coroleu B, Barri P, Carreras O, Martínez F, Parriego M, Hereter L, et al. The influence of the depth of embryo replacement into the uterine cavity on implantation rates after IVF: A controlled, ultrasound-guided study. *Human reproduction*. 2002;17:341–346.
- [137] Haeussner E, Aschauer B, Burton G, Huppertz B, von Koch FE, Mueller-Starck J, et al. Does 2D-histologic identification of villous types of human placentas at birth enable sensitive and reliable interpretation of 3D structure? *Placenta*. 2015;36:1425–1432.
- [138] Ali K, Burton G, Morad N, Ali M. Does hypercapillarization influence the branching pattern of terminal villi in the human placenta at high altitude? *Placenta*. 1996;17:677–682.
- [139] Almasry S, Eldomiaty M, Elfayomy A, Habib F, Safwat M. Structural analysis of human placental stem and terminal villi from normal and idiopathic growth restricted pregnancies. *Journal of molecular histology*. 2012;43:263–271.
- [140] Almasry S, Elfayomy A. Morphometric analysis of terminal villi and gross morphological changes in the placentae of term idiopathic intrauterine growth restriction. *Tissue cell*. 2012;44:214–219.
- [141] Cantle S, Kaufmann P, Luckhardt M, Schweikhart G. Interpretation of syncytial sprouts and bridges in the human placenta. *Placenta*. 1987;8:221–234.
- [142] Burton G. Intervillous connections in the mature human placenta: Instances of syncytial fusion or section artifacts? *Journal of anatomy*. 1986;145:13–23.
- [143] Mayhew T. Morphomics: An integral part of systems biology of the human placenta. *Placenta*. 2015;36:329–340.
- [144] Howard C, Reed M. Unbiased stereology. Three-dimensional measurement in microscopy. vol. 1. New York: Springer; 1998.
- [145] Haeussner E, Schmitz C, Frank H, von Koch FE. Novel 3D light microscopic analysis of IUGR placentas points to a morphological correlate of compensated ischemic placental disease in humans. *Scientific reports*. 2016;6:24004.
- [146] Demir R, Kaufmann P, Castellucci M, Erben T, Kotowski A. Fetal vasculogenesis and angiogenesis in human placental villi. *Acta anatomica*. 1989;136:190–203.

- [147] Mayhew T. Estimating oxygen diffusive conductances of gas-exchange systems: A stereological approach illustrated with the human placenta. *Annals of anatomy.* 2014;196:34–40.
- [148] Barker S, Cumming G, Horsfield K. Quantitative morphometry of the branching structure of trees. *Journal of theoretical biology.* 1973;40:33–43.
- [149] Ikram M, Kamran C, Carol Y, Lorenzi M, Klein R, Jones T, et al. Retinal vascular caliber as a biomarker for diabetes microvascular complications. *Diabetes care.* 2013;36:750–759.
- [150] Franken R, Morabit AE, de Waard V, Scholte JTA, van den Berg M, Marquering H, et al. Increased aortic tortuosity indicates a more severe aortic phenotype in adults with Marfan syndrome. *International journal of cardiology.* 2015;194:7–12.

List of Figures

1.1	Gross morphological placental measurements.	5
1.2	Geometric morphometric analysis in placental research.	8
1.3	Ischemic placental disease.	10
1.4	Allocation of villous sections of human placentas.	13
1.5	Fetal capillaries in the villous tree.	14
1.6	Developmental pathology of the villous tree.	16
1.7	The microscopic villous tree of human placentas.	18
4.1	The origin of placental measures.	92
4.2	Terminal position ordering versus histological classification of a villous tree.	95
4.3	Variation of branching angles in the villous tree.	99
4.4	Pathophysiological interpretation of angles and tortuosity.	101

Appendix

List of publications and declaration of contributions to individual manuscripts

Haeussner E, Schmitz C, Edler von Koch F, Frank HG. - Birth weight correlates with size but not shape of the normal human placenta. Placenta. 2013 July 34(7):574-82. (Publication I)

Eva Häußner performed the analysis, interpreted the data, and wrote most of the manuscript.

Haeussner E, Buehlmeier A, Schmitz C, Edler von Koch F, Frank HG. - Novel 3D microscopic analysis of human placental villous trees reveals unexpected significance of branching angles. Scientific Reports. 2014 August 4:6192. (Publication II)

Eva Häußner performed the 3D reconstructions, analyzed and interpreted the data, and wrote most of the manuscript.

Poster presentation at IFPA - International Federation of Placenta Association, in Paris (France) September 2014: Haeussner E, Schmitz C, Edler von Koch F, Frank HG - Novel and Efficient 3D Microscopic Analysis of Isolated Villous Trees of Human Placentas. Placenta. 2014 September 35(9):A12. (Publication II)

Haeussner E, Aschauer B, Burton GJ, Huppertz B, Edler von Koch F, Müller-Starck J, Salafia C, Schmitz C, Frank HG. - Does 2D-histologic identification of villous types of human placentas at birth enable sensitive and reliable interpretation of 3D structure? Placenta. 2015 December 36(12):1425-32. (Publication III)

Eva Häußner performed the experiment, analyzed and interpreted the data, and wrote the manuscript.

Haeussner E, Schmitz C, Frank HG, Edler von Koch F. - Novel 3D light microscopic analysis of IUGR placentas points to a morphological correlate of compensated ischemic placental disease in humans. Scientific Reports. 2016 April 6:24004. (Publication IV)

Eva Häußner performed the 3D reconstructions, analyzed and interpreted the data, and wrote the manuscript.

.....
Unterschrift, Eva Häußner

.....
Unterschrift, Prof. Dr. Hans-Georg Frank

Acknowledgment

First, I would like to thank Prof. Dr. Christoph Schmitz and Prof. Dr. Hans-Georg Frank for giving me the opportunity to conduct my doctoral thesis.

Next, I owe a very special thank you to PD Dr. Annette Müller-Taubenberger for supporting my doctoral thesis.

I acknowledge the skillful technical assistance and diligent work of the entire team of technicians of the Department of Anatomy II at LMU Munich.

I would also like to express my thanks to the obstetricians, midwives, and nurses of the Dritter Orden Hospital who enabled the clinical work of this study with great care and engagement.

A special thank you is extended to Dr. Katharina Sternecker for proofreading this thesis and for providing many explanatory notes.

Finally, I would like to thank my family, my boyfriend Matthias, and all of my friends who provided constant support for me and listened to all my worries.

Curriculum Vitae

Eva Maria Häußner

Pettenkoferstrasse 11

D-80336 München

Tel.: +49 89 2180 72655

Fax: +49 89 2180 72683

email eva.haeussner@med.uni-muenchen.de

Personal Data

Date of birth: 27.01.1985

Place of birth: Offenbach am Main

Doctoral Thesis

May 2011 to present – scientific assistant, Department of Anatomy II, Ludwig-Maximilians-University, Munich

Study (Diploma)

October 2004 to August 2010 – studying bioscience at Goethe University, Frankfurt at Main, final degree

March 2007 to June 2007 – studying earth science at University of Vienna, Austria; ERASMUS exchange student

Internship During Study

April 2006 to January 2007 – student research assistant at Senckenberg Research Institute, Department of Paleoanthropology, "Ruwenzori-Projekt in Uganda", Frankfurt at Main

April 2005 to March 2006 – internship at the Senckenberg Research Institute, Department of Paleoanthropology, Frankfurt at Main

August 2005 to September 2005 – geological-paleontological dig in Eppelsheim (Rheinland-Pfalz), organized by the Museum of Natural History Mainz

School

August 1991 to June 2004 – final graduation from the Theodor-Heuss-School, Offenbach am Main